

Design and Synthesis of Three-Dimensional Pyrrolidine Fragments

Ngai Shing Chan

MSc by Research

University of York

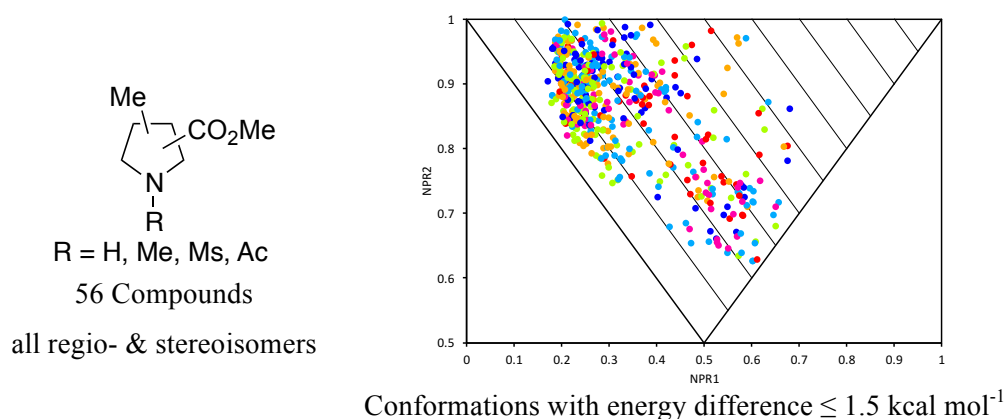
Chemistry

December 2016

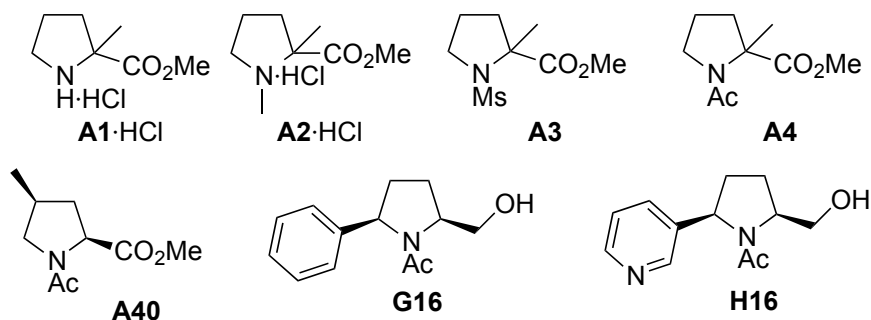
Abstract

The research described in this thesis concerns the design and synthesis of three-dimensional pyrrolidine fragments for use in fragment-based drug discovery. Chapter 1 provides an overview of fragment-based drug discovery and highlights the importance of three-dimensionality in drugs and fragments.

In Chapter 2, a principal moments of inertia (PMI) analysis of the three-dimensional shape of pyrrolidine fragments is described. The PMI plot that was used to select pyrrolidine fragments with methyl and methyl ester groups and four different nitrogen substituents (NH, NMe, NMs, NAc) is shown below.



In Chapter 3, the synthetic efforts towards some of the three-dimensional pyrrolidine fragments are described. The synthesis of **A1**·HCl, **A2**·HCl, **A3-4** and **A40** was successful, but problems were found in the synthesis of **H16** and **G16**.



List of Contents

Abstract	2
List of Contents	3
List of Tables	4
Acknowledgments	5
Author's Declaration	6
Chapter 1: Introduction	7
1.1 <i>Fragment-Based Drug Discovery</i>	7
1.2 <i>Screening of Fragment Libraries</i>	12
1.3 <i>Case Studies of FBDD</i>	13
1.4 <i>Three Dimensionality in Drug and Fragments</i>	18
1.5 <i>Three-Dimensionality in Fragment Libraries</i>	32
1.6 <i>Project Outline</i>	42
Chapter 2: Computational Analysis and Selection of Three-Dimensional Pyrrolidine Fragments	43
2.1 <i>Introduction to Computational Protocol and Analysis of a Maybridge Fragment Library</i>	44
2.2 <i>Fragment Design and Overview of Our Enumeration and Selection Approach</i>	50
2.3 <i>Comparison of the Three-dimensionality of Pyrrolidine Fragments with Different Substituents</i>	57
2.4 <i>Conclusions</i>	70
Chapter 3: Synthesis of Three-Dimensional Pyrrolidine Fragments	71
3.1 <i>Model Studies on N-functionalisation of Pyrrolidine Fragments</i>	72
3.2 <i>Synthesis of 2,2-Disubstituted Pyrrolidine Fragments</i>	75
3.3 <i>Synthesis of a cis-2,4-Disubstituted Pyrrolidine Fragment</i>	88
3.4 <i>Attempted Synthesis of 2,5-cis-Disubstituted Pyrrolidine Fragments</i>	101
3.5 <i>Conclusions and Future Work</i>	112
Chapter 4: Experimental	115
4.1 <i>General Procedures</i>	115
4.2 <i>Experimental Procedures and Characterisation Data</i>	118
Abbreviations	155
References	159

List of Tables

Table 1.1: The comparison between 'rule of three' and 'rule of five'.	10
Table 1.2: Mean aromatic ring count in compounds in the GlaxoSmithKline pipeline.	20
Table 1.3: Number of aromatic ring in a molecule and its activity with different bioassays.	22
Table 1.4: Example of fragments from this study and the mean of physicochemical properties of their fragments with Chembridge and Maybridge commercial libraries.	38
Table 2.1: Number of conformations and percentage in each PMI category with conformational energy difference ≤ 1.5 kcal mol⁻¹.	48
Table 2.2: Predicted average physicochemical properties of a Maybridge fragment library using Pipeline Pilot 8.5.	49
Table 2.3: Number of conformations and percentage in each PMI category with conformational energy difference ≤ 1.5 kcal mol⁻¹.	53
Table 2.4: Number of fragments and percentage in each PMI category with conformational energy difference ≤ 1.5 kcal mol⁻¹.	53
Table 2.5: Analysis of ΣNPRs values to select a suitable number of fragments for synthesis.	54
Table 2.6: Predicted average physicochemical properties of 14 selected fragment from Pipeline Pilot 8.5.	56
Table 2.7: ΣNPRs ≥ 1.4 with conformational energy difference ≤ 1.5 kcal mol⁻¹.	60
Table 2.8: ΣNPRs ≥ 1.4 with conformational energy ≤ 1.5 kcal mol⁻¹.	63
Table 2.9: ΣNPRs ≥ 1.4 with conformational energy difference energy conformations ≤ 1.5 kcal mol⁻¹.	67
Table 2.10: The predicated average physicochemical properties of the 11 selected fragment from Pipeline Pilot 8.5.	69
Table 3.11: Effect of scale on the yield of the enolate alkylation.	78
Table 3.12: Conditions trialled to optimise the hydrogenation.	97

Acknowledgments

Special appreciation and thanks must go to my supervisor Professor Peter O'Brien. Without his help, suggestions and encouragement the research presented in this thesis would have not been possible. My sincere thanks go to my second supervisor Professor Roderick Hubbard for his invaluable suggestions. I would also like to thank Dr Martin Fascione for his assistance and guidance as my independent panel member. Moreover, I would like to give a massive thank you to Masakazu for his help and suggestions on my experimental works.

In addition, I would like to thank Heather for the help with VT NMRs and Karl for the mass spectrometry service. Also, I would like to thank Paul Bond from YSBL for his help and assistance with the computational experiments.

I would like to thank all the members of the POB group, past and present, for good discussions, laughs and support during my journey: Peter, Masakazu, James, Mary, Sarah, Adam, Mickey, Will, Paul, Tom and Alice; it has been a pleasure to work with you all.

Finally, none of this would have been possible without the love and support from my mum, dad and sister Irene. Thank you so much!

Author's Declaration

I declare that this thesis is a presentation of original work and I am the sole author. This work has not previously been presented for an award at this, or any other, University. All sources are acknowledged as References.

Chapter 1: Introduction

1.1 Fragment-Based Drug Discovery

1.1.1 Introduction to Fragment-Based Drug Discovery

Over the last two decades, fragment-based drug discovery (FBDD), also known as fragment-based lead discovery (FBLD), has become an established alternative approach for identifying new drugs. The approach is different to the conventional high-throughput screening (HTS) approach.¹⁻⁴ There are already two FDA approved drugs, Vemurafenib^{4,5} and Venetoclax^{4,6} (Figure 1.1), and many more clinical drug candidates that have been developed from using the FBDD approach. Vemurafenib was developed by Plexxicon for the treatment of late-stage melanoma, whereas Venetoclax was developed by AbbVie and Genentech for the treatment of chronic lymphocytic leukaemia.⁴⁻⁶

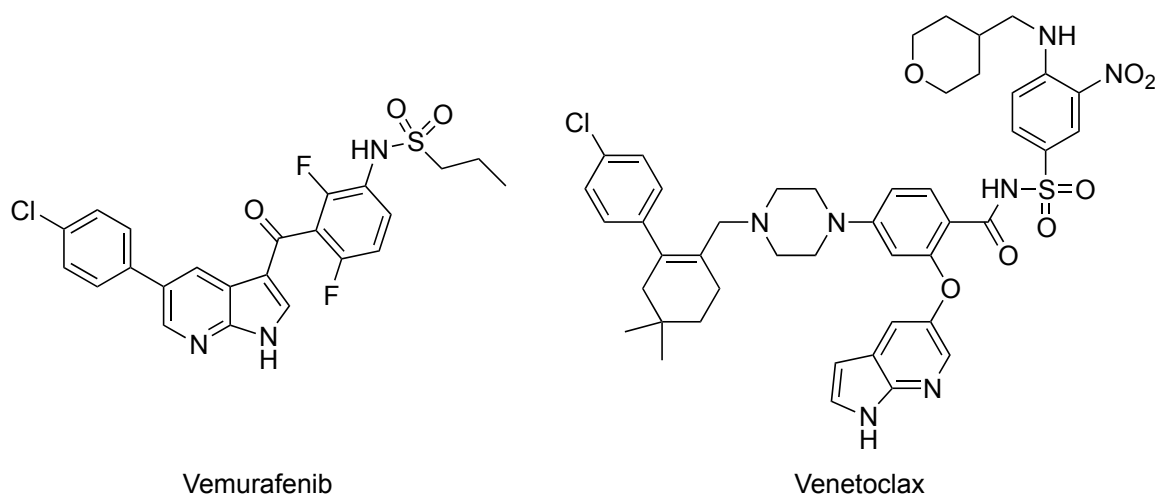


Figure 1.1: The Structure of Vemurafenib and Venetoclax

In comparison to HTS, fragment-based screening starts from compounds with a much lower molecular weight (250 Da) and smaller heavy atom count (HAC no more than

20). Some typical fragments **1–4** are shown in Figure 1.2. Fragments **1** and **2** were identified from screening against choline kinase α (ChoK α) and could be further developed into antitumour agents.⁷ Indole fragment **3** was developed into an inhibitor of Matrix metalloproteases-13 (MMP-13) which is a protein for arthritic diseases medication.⁸ Bicyclic thiazine **4** was a fragment hit and was developed into a BACE1 inhibitor for potential treatment of Alzheimer's disease.⁹

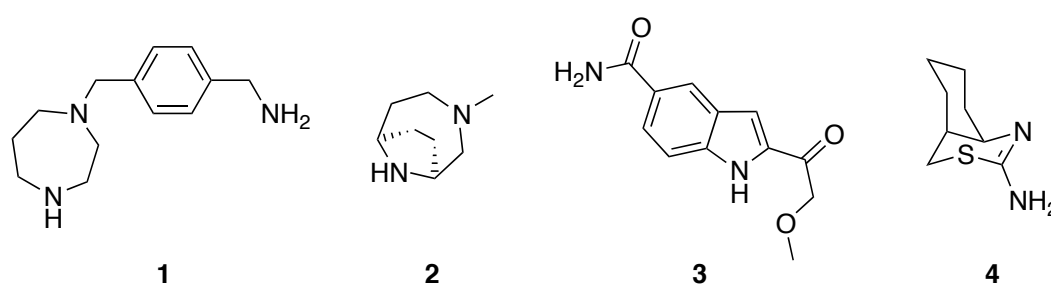


Figure 1.2: Examples of fragments from FBDD programmes.

There are several advantages of using a fragment-based screening method over HTS methods in drug discovery programmes. One of the advantages is that fragments have a wider chemical space coverage. This was statistically quantified by Hann *et al.*^{10,11} and Reymond *et al.*¹² In the study, they estimated the total number of possible compounds in the universe to be near to 10^{60} . Thus, with a large screening library which typically has 10^6 compounds, it can barely touch the surface of the chemical space of all the compounds in the universe. However, for fragment space, it was estimated that there are 14 million compounds that have molecular weight below 160. Hence a fragment screening library of 10 000 compounds can significantly cover the available chemical space. Therefore, their result suggests that FBDD covers a much greater area of chemical space than traditional HTS methods. Another benefit of

developing lead compounds from fragments is that it can give a straightforward chemical optimisation in the later stages of drug discovery.¹³ Moreover, starting from a higher ligand efficiency (LE), a small fragment could lead to a final optimised ligand that is relatively low in molecular weight (MW < 500 Da). Another advantage of FBDD is that the structure-activity relationships (SAR) can be obtained more quickly since analogues can be easily obtained synthetically or from commercial sources. Overall, FBDD tends to be less resource dependent than HTS and a summary of the two approaches is shown in Figure 1.3. However, the key feature of FBDD is also a drawback as small fragments give weaker binding affinities in the millimolar or micromolar region. This means that highly sensitive biophysical screening methods are required instead of bioassays.¹⁴

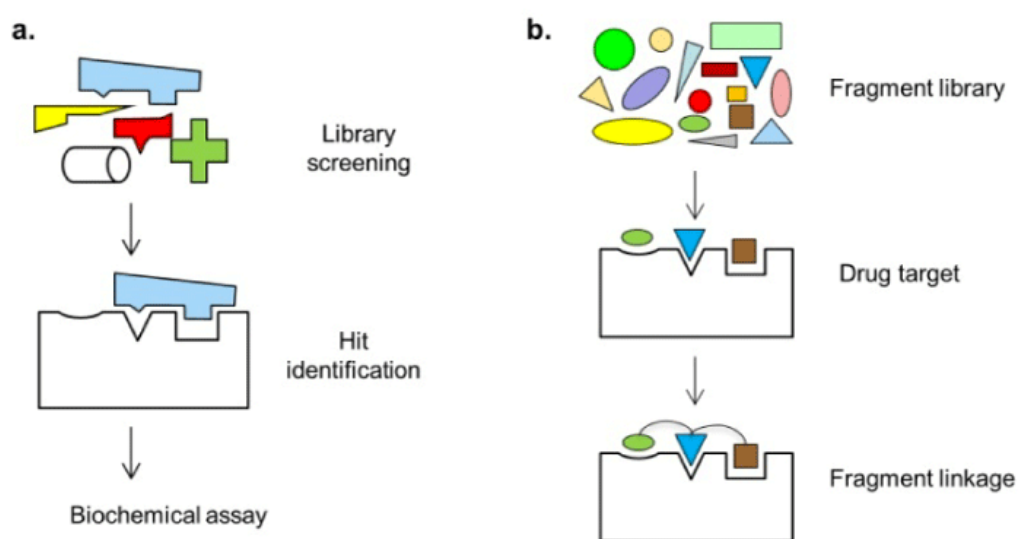


Figure 1.3: Comparison of HTS and FBDD approaches. (Figure adapted from reference 15)

1.1.2. Properties of Fragment Libraries

Similar to the ‘rule of five’, which was promoted by Lipinski *et al.*¹⁶ in 1997 to define drug-like properties, fragments adhere to a ‘rule of three’. The ‘rule of three’ properties

are: molecular weight (MW) < 300 Da (i.e. HAC ≤ 20), total number of hydrogen bond donors (HBD) and acceptors (HBA) ≤ 3, ClogP ≤ 3, number of rotatable bonds (NROT) ≤ 3 and a polar surface area (PSA) ≤ 60 (Table 1.1).^{13,17}

Table 1.1: The comparison between 'rule of three' and 'rule of five'.

<i>Rule of Three</i>	<i>Molecular Descriptors</i>	<i>Rule of Five</i>
Less than 300 Da	Molecular Weight	Less than 500 Da
No more than 3	Hydrogen-bond Donors	No more than 5
No more than 3	Hydrogen-bond Acceptors	No more than 10
Less than 3	ClogP	Less than 5

It is also advisable that fragment libraries avoid structures that do not behave well in screening. Such compounds include pan-assay interference compounds (PAINS), a la assay to detect reactive molecules (ALARM) and 'Shoichet' aggregators. Avoiding these compounds in the fragment selection process will promote a higher hit rate and prevent false results at later stages in a drug discovery programme.^{13,17-22} Examples of typical PAINS are shown in Figure 1.4.

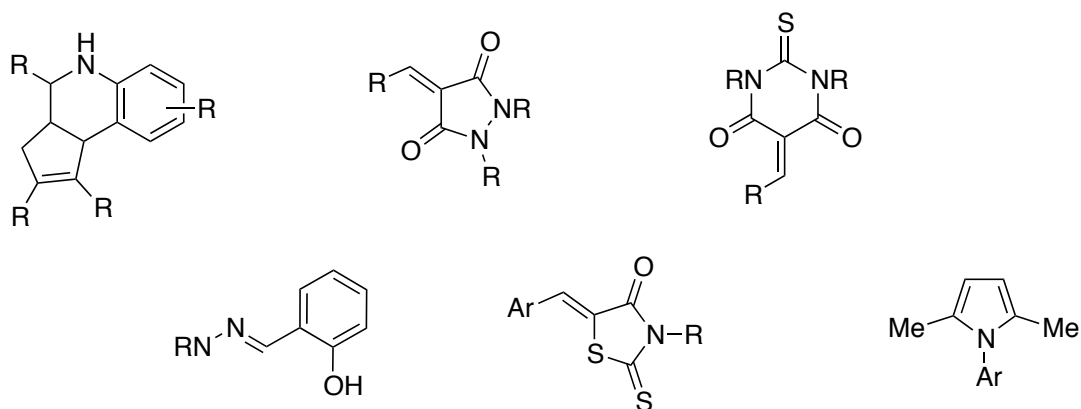


Figure 1.4: Examples of PAINS motifs.

1.1.3 Management of Fragment Libraries

Another key aspect of a successful fragment-based drug discovery project is to maintain the integrity of the fragment collections, as impure samples can then compromise the generation of fragment hits. It is thus necessary to ensure that the library stocks are chemically stable over a long period of time. Library fragments should be stored as dry powders or in solvent (e.g. DMSO) and their qualities should be monitored by ^1H NMR spectroscopy and/or LC-MS repeatedly over months.²⁰

1.2 Screening of Fragment Libraries

The first step of a HTS drug discovery programme for SAR studies starts with bioassays. In this approach, screening of a very large collection (typically 10^6 – 10^7) of drug-like molecules is often carried out and hits can have good potency. These studies might provide an early indication of relevant activity. In contrast, with FBDD, the detection of the weak fragment binding using bioassays has proven to be difficult. Therefore, fragment-based screening (FBS) in FBDD projects is carried with much more sensitive biophysical techniques. Nuclear magnetic resonance-based screening, surface plasmon resonance (SPR) and X-ray crystallography are the most common techniques for fragment screening.

1.3. Case Studies of FBDD

1.3.1 Vemurafenib – The First FDA-approved Drug

The late-stage melanoma medication, Vemurafenib, was approved for clinical use in August 2011. It was developed by Plexxicon and it is the first marketed drug developed using the FBDD strategy.^{5,23,24}

This discovery of Vemurafenib began with screening a library of 20 000 fragment-like compounds with molecular weight between 150–350 Da at a concentration of 200 μ M. Five different kinases were screened and there were 238 compounds that inhibited at least three kinases (PIM1, p38, and CSK) over 30% of their activity. After being confirmed with co-crystallisation, over 100 compounds were found to be bound with at least one of the three kinases and exclusively with PIM1 for low affinity compounds. Figure 1.5 shows the lead generation of Vemurafenib. One of the ATP site binders in the PIM1 co-structure 7-azaindole, was selected for further development to give 3-aminophenyl-7-azaindole. This compound had improved potency with PIM1 and had only one binding mode. Upon further coupling with a 3-methoxybenzyl moiety, the potency improved significantly with FGFR1, which is likely due to the additional hydrogen bond interaction between the methoxy group and the protein. Additional modification of the 3-(*m*-methoxybenzyl)-7-azaindole around the 7-azaindole core identified PLX4720. This compound had an excellent potency with B-Raf and was subsequently developed into Vemurafenib.

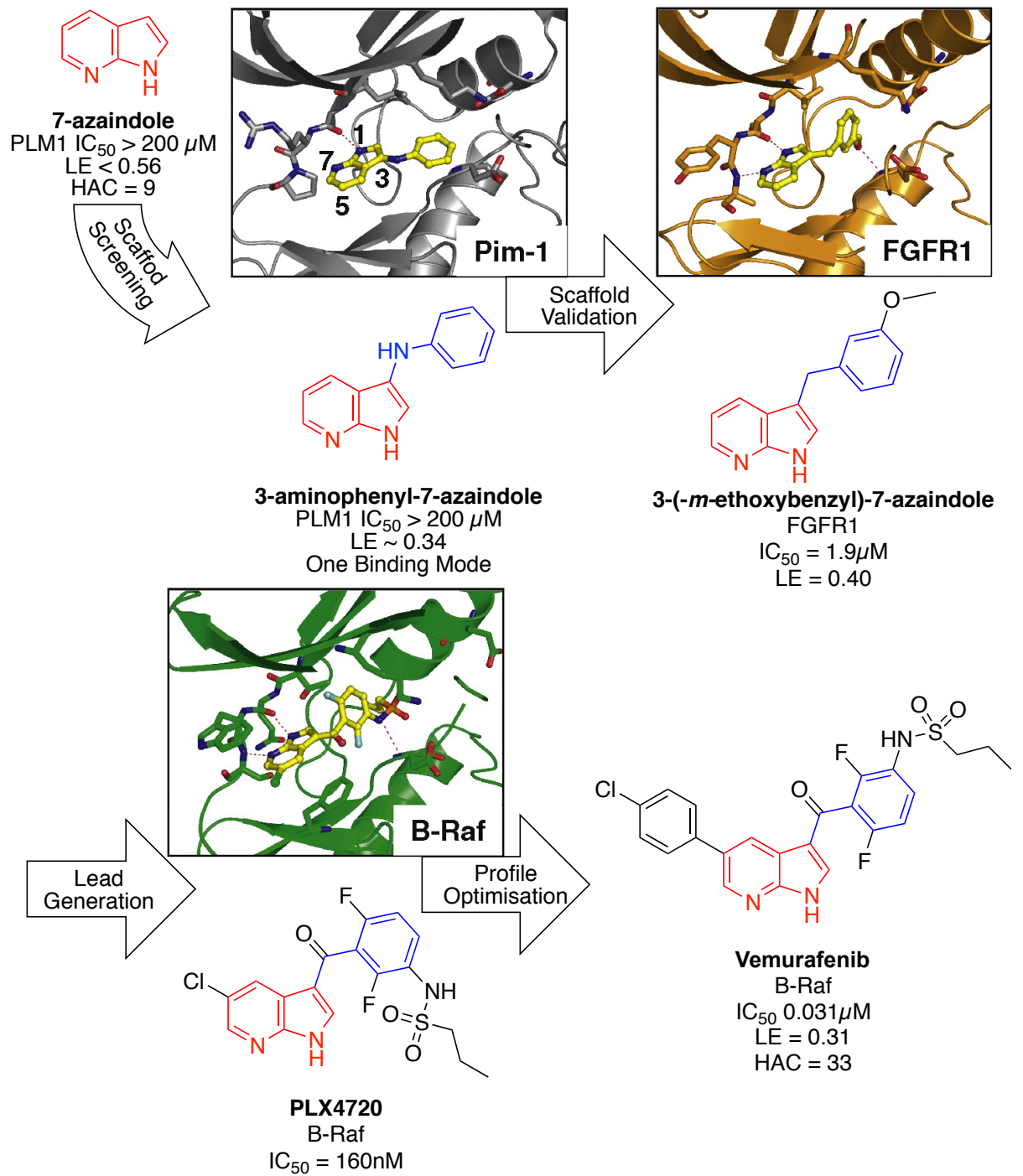


Figure 1.5: The FBDD process in the development of Vemurafenib. (Figure adapted from reference 24)

1.3.2 ASTX660 – Phase I Clinical Trial Candidate for Cancer Treatment

The Astex Phase I candidate, ASTX660, is a dual inhibitor of apoptosis (IAP). This is another example of FBDD used in the development of a cancer therapy. ASTX660 is a novel non-peptidomimetic inhibitor that targeted both XIAP and cIAP1 *in vivo*. XIAP and cIAP1 belong to the family of IAP which has a role to block programmed cell death.

This discovery of ASTX660 began with a virtual screening of 100 fragments against XIAP-BIR3 and piperazine amide **5** was selected (Figure 1.6). Fragment **5** had a rather weak affinity, but it had balanced activity at the targets. In order to improve affinity, a methyl group was added to the piperazine to fill a small hydrophobic pocket that is normally occupied by the alanine side chain. Also, the piperidine was replaced by a pyrrolidine to yield fragment **6** that had significantly improved activity.

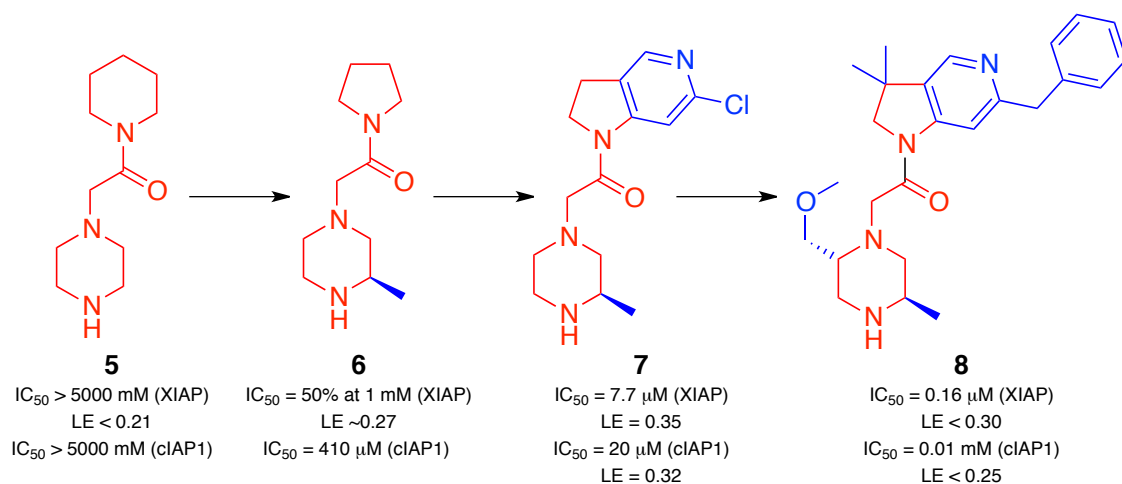


Figure 1.6: The FBDD of ASTX660.

Next, the pyrrolidine group was changed to a fused-ring as in fragment **7** which afforded better binding to the target. The next steps in the lead generation were introduction of the phenyl group, and modification on the indoline and the piperazine. This gave the lead compound **8** with nanomolar potency against both XIAP-BIR3. After profile optimisation, **8** was then further developed into the clinical trial candidate ASTX660 for cancer treatment.²⁵

1.3.3 Small Molecule Choline Kinase α (ChoK α) Inhibitor

A novel small molecule which inhibits Choline Kinase α (ChoK α) was developed by ARIAD Pharmaceuticals *via* a FBDD method. The ChoK α inhibitor showed potentially useful antitumour properties. The project began with the structure-guided hit exploration by virtual screening against ChoK α to identify compound **9** (Figure 1.7). Then, SAR of the initial fragment hit **9** was used to search for commercially available analogues by docking studies with the binding site in the target. The results showed that compound **10** gave the highest potency and exhibited the best interaction with the target. Further fragment optimisation and elaboration, by addition of the phenyl and piperazine group to give **12**, gave a significant improvement of potency. Finally, optimisation to a biphenyl system gave lead compound **13**. The X-ray crystallography showed that lead compound **13** bound in the pocket of the ChoK α protein and the water molecule displaced in the co-structure gave hydrogen bonding interactions.⁷

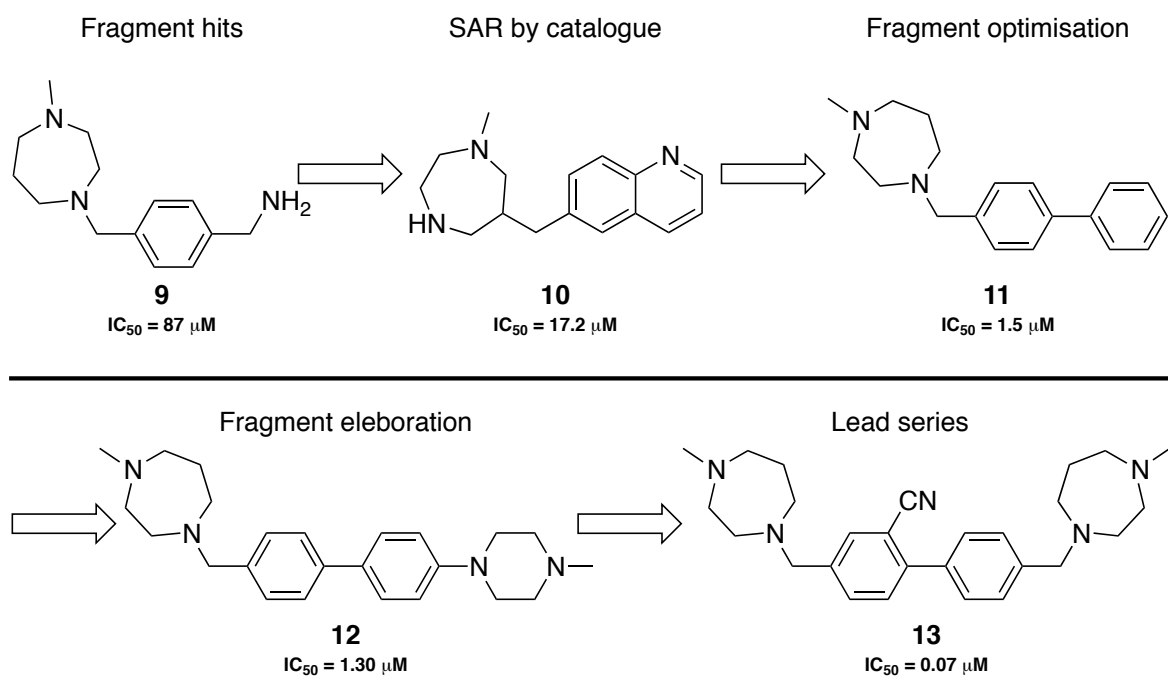


Figure 1.7: Summary of the FBDD process of the discovery of a ChoKa inhibitor.

1.4. Three Dimensionality in Drug and Fragments

1.4.1 Importance of Three-dimensional Character in Drugs

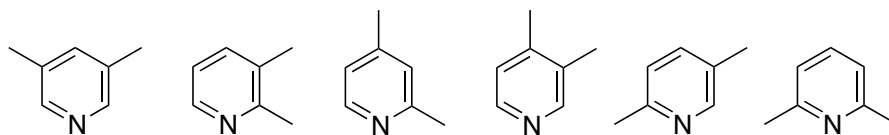
There is growing interest in three-dimensionality in drug molecules and studies have investigated the shapes and functionality of different drugs. Lovering *et al.*²⁶ introduced the concept of measuring molecular complexity by carbon saturation and chiral centres. Their rationale was that as the level of saturation increased, more three-dimensional shapes followed. In addition, the higher the number of chiral centres, the greater the number of potential isomers for a particular compound.

Lovering introduced a molecular descriptor called fraction sp^3 (F_{sp^3}) for the calculation of a molecule's saturation. F_{sp^3} is defined as the number of sp^3 hybridised carbons divided by the total number of carbon atoms in the molecule:

$$F_{sp^3} = \left(\frac{\text{Number of } sp^3 \text{ hybridised carbons}}{\text{total carbon count}} \right)$$

As shown in Figure 1.8, there are only six isomers of dimethylpyridine. In contrast, for the more saturated analogue, dimethylpiperidine, there are 32 isomers even though there is little increase in molecular weight.[†] There are more dimethylpiperidine isomers because there are more positions to attach the methyl groups and *cis/trans* isomers are possible.

[†] Lovering incorrectly calculated the total number of isomers for both dimethylpyridine (5) and dimethylpiperidine (34).

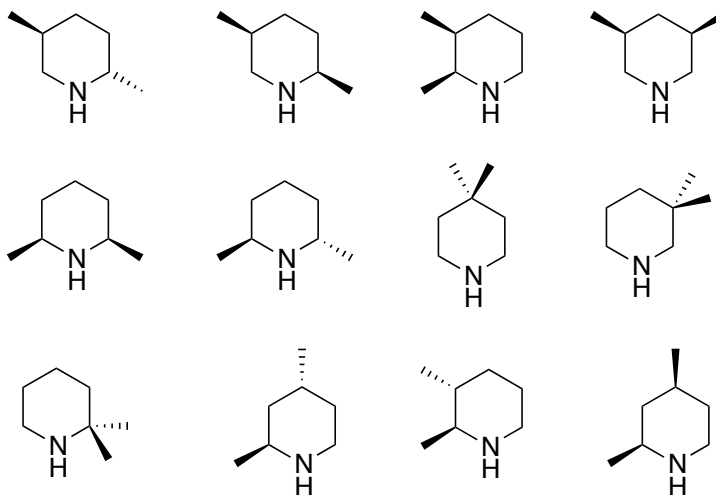


Dimethylpyridine

6 isomers

MW = 107

$F_{sp^3} = 0.29$



Dimethylpiperidine

32 isomers

(only showing 12 examples)

mw = 113

$F_{sp^3} = 1.0$

Figure 1.8: Comparison of the number of isomers of dimethylpyridine and dimethylpiperidine (a representative set of isomers).

Lovering's study compared the F_{sp^3} values and number of chiral centres in compounds at different stages of the drug development process. For example, F_{sp^3} values increased by 31% from the lead compounds to the final drugs. The number of chiral centres followed the same trend, increasing by 21%. Moreover, compounds with higher F_{sp^3} at the beginning of the drug discovery process are more likely to survive during the process and become drugs. Saturated compounds are more likely to have higher aqueous solubility with lower melting points, which are desirable properties in

a drug. High values of Fsp^3 mean that the compound has higher complexity, but it can not necessarily be concluded that the compound has higher three-dimensionality. Therefore, a correlation can only be drawn between complexity with Fsp^3 and chiral centre count.²⁶

In a separate study, researchers at GlaxoSmithKline studied the influence of aromatic ring count on the drug development process. In order to carry out the study, they defined the developability parameters as follows: aqueous solubility, lipophilicity (ClogP), and bioassays with serum albumin binding, CyP450 inhibition and hERG inhibition. These parameters are useful guidelines to indicate how likely a candidate is to become a drug. In their analysis, they selected 280 compounds from the GlaxoSmithKline pipeline which came from preclinical candidate selection, first time in human, phase 1, phase 2 and proof-of-concept trials. The number of compounds in each category and their mean aromatic ring count are shown in Table 1.2.

Table 1.2: Mean aromatic ring count in compounds in the GlaxoSmithKline pipeline.

	CS ^a	FTIH ^a	P1 ^a	P2 ^a	POC ^a
Count ^b	50	68	35	53	96
Mean aromatic ring count	3.3	2.9	2.5	2.7	2.3

(a) CS=Preclinical candidate selection; FTIH=first time in human; P1=phase 1; P2=phase 2; POC= proof-of-concept trials. (b) Count=total number of compounds in each category.

This analysis of mean aromatic ring count showed a decreasing trend in each stage of drug development, from 3.3 for the preclinical candidate selection to 2.3 for the proof-of-concept compounds. Furthermore, the average aromatic ring number in oral drugs

is 1.6, as there is a downward trend in number of aromatic ring during the drug development process. Therefore, the results support the idea that the lower the aromatic ring count of a compound, the better the chance of it progressing over the developmental process. This result might be correlated to the aqueous solubility and lipophilicity.

Based on this observation, they investigated whether there is any correlation of the aromatic ring count with the developability parameters. ~26 000 compounds from their collection were analysed for their number of aromatic rings and *ClogP*. The results showed a perfect correlation between these two indexes (Figure 1.9). As the aromatic ring count rose, the lipophilicity also increased and the aqueous solubility decreased.

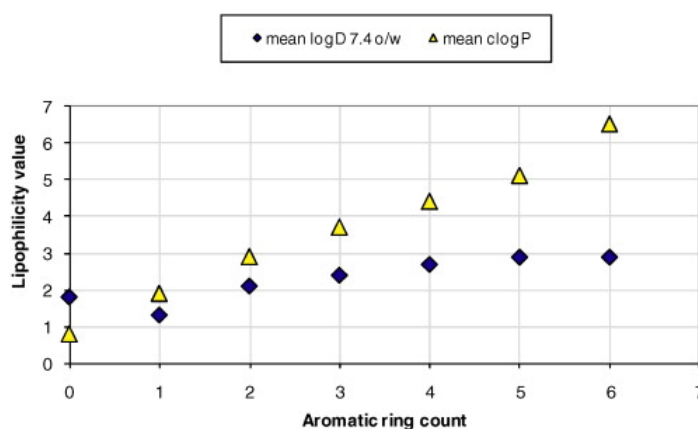


Figure 1.9: Mean lipophilicity against aromatic ring count. (Figure adapted from reference 27)

The results from bioassays also show a tendency of increased activity within all bioassays as the aromatic ring count increases (Table 1.3). Serum albumin binding assay is a bioassay which tests the ‘mobility’ of a drug in plasma. There is a low availability of the drug for the target if the serum albumin binding activity is high. For

CyP450 inhibition and hERG inhibition, bioassays are used to test the toxicity level *in vivo*. If the activities are high in these bioassays, the *in vivo* toxicity levels are high, which is an undesirable property of a drug.

Table 1.3: Number of aromatic ring in a molecule and its activity with different bioassays.

No. of aromatic rings	1	2	3	4	5
Serum albumin binding (%)	78	88	93	96	96
P450 3A4 inhibition (pIC ₅₀)	4.7	4.9	5.2	5.4	5.6
hERG inhibition (pIC ₅₀)	5.2	5.6	5.7	5.7	5.5

Overall, the GlaxoSmithKline results clearly pointed out that the higher the number of aromatic rings, the lower the potential for drug developability into an oral drug, which is reflected by the developability parameters. Moreover, they suggested that fewer than three aromatic rings in a molecule is more favourable for its development into a drug.²⁷

In another study, Aldeghi *et al.* looked further into ring structures in different drugs by analysing the architectures of marketed drugs and their biological targets. For their study, ring structures were defined in the following way. All ring systems should have at least one shared atom. The three-dimensional parts in a given drug should have a ring with at least one sp³ hybridised atom in them. If there are only sp² hybridised atoms, the rings are defined as two-dimensional. This is shown using the example of the drug Indinavir (Figure 1.10). Ring structures highlighted in red are two-

dimensional, in dark blue is three-dimensional and in light blue is three-dimension hybrid/fused (3D-h) ring system.

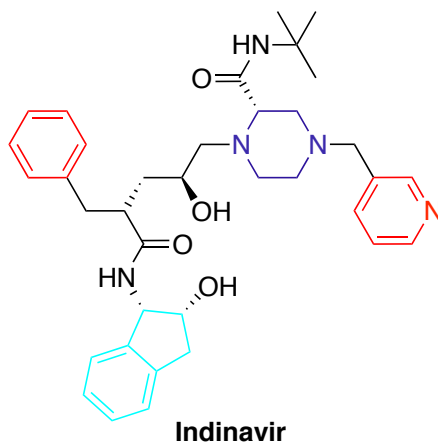


Figure 1.10: Two- and three-dimensional features in Indinavir.

Aldeghi evaluated and categorised the drug biological targets information which were extracted from the DrugBank database and EBI DrugPort into 15 target classes. Each drug was assigned to a single target class. GPCRs, ion channels and nuclear receptors were the most common drug target classes. The results are shown as percentages in Figure 1.11. The two- and three-dimensional ring systems of each drug were formulated in every target class. The analysis showed that three-dimensional systems appeared in all target classes. Moreover, most of the target classes were targeted more with three- than two- dimensional systems. For instance, nuclear receptors had the highest amount of three-dimensional systems (91.7%), whereas ligases had the lowest (50%). The findings showed that three-dimensional systems in drugs had the highest proportion across the whole range of classes, which could indicate that three-dimensional structures are more selective than two-dimensional structures.

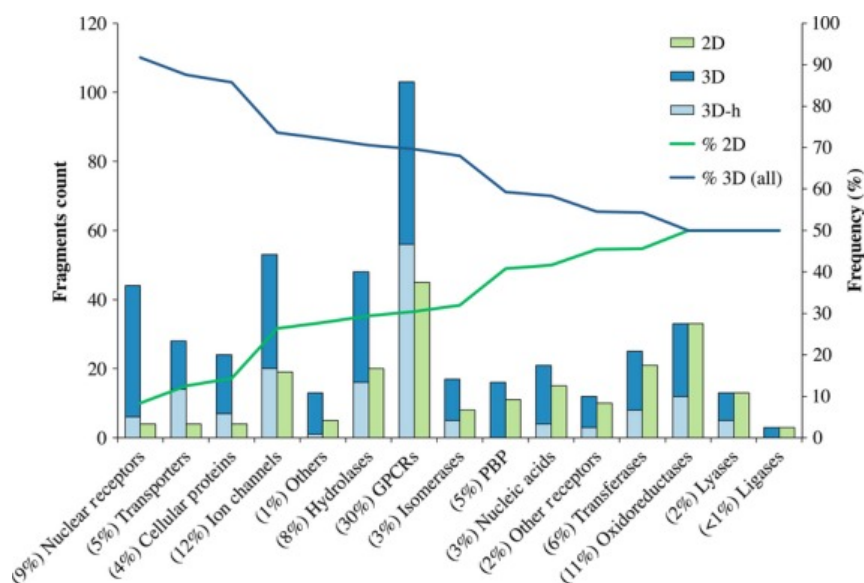


Figure 1.11: Ring systems in different biological targets. (Figure adapted from reference 28)

In their study, they also explored which rings are associated in each type of systems and they identified the top five most commonly found ring types in marketed drugs (Figure 1.12). There were two two-dimensional ring structures and phenyl was the most frequently found ring in marketed drugs. There were three three-dimensional rings in the top five. Based on this result, they also examined the ‘privileged’ structure for each target class. These results suggested that three-dimensional rings occur more frequently than two-dimensional ring structures in marketed drugs.²⁸

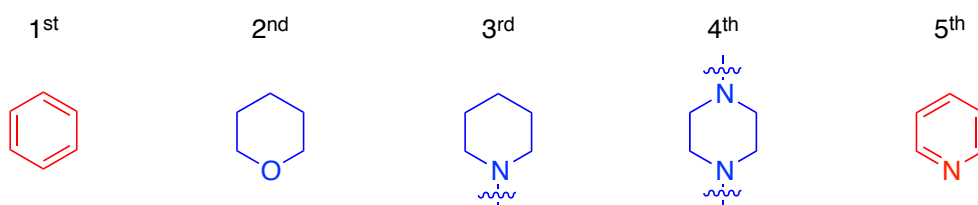


Figure 1.12: Top five ring systems commonly found in marketed drugs.

In conclusion, the results from different studies suggest the benefit of increasing F_{sp^3} and reducing aromatic ring count in developing drugs. Therefore, in drug design by including more three-dimensional saturated heterocyclic ring structures, hit rates could potentially be improved.

1.4.2 Topographical Descriptors for Quantifying the Three-dimensionality of Molecules.

There are different methods that have been developed to define shape and provide three-dimensional information on molecules. In all cases, a computational approach is used.

Molecular globularity was introduced by Meyer in 1985 for the evaluation of molecular shape by determining how spherical it is. This globularity descriptor is a calculation of the radii of three spheres, R_1 , R_2 and R_3 , in a compound to give a ratio R_m which is called the globularity. The radii are the Van der Waals volume (R_1), the molecular volume (R_2) and the outer circle of the circumscribing sphere (R_3). Globularity, R_m , is defined by the following equation:

$$R_m = \left(\frac{R_3 - R_2}{R_2 - R_1} \right)$$

For instance, in a perfectly-spherical shaped compound, each of the cross-sections through the centre of the compound should have the same area. Therefore, the smaller the value of R_m , the higher the molecular globularity. This method can be used to rationalise the shape of molecules by their globularity and is a preliminary method for determining molecular shape.²⁹

Since there was growing interest in molecular shapes, more robust and better representation methods to define molecule shapes of compounds in libraries were desired. Therefore, a number of topographical descriptors have been reported for this application. Principal moments of inertia (PMI) by Sauer *et al.* (2003)³⁰ and plane-of-best-fit (PBF) by Firth *et al.* (2012)³¹ are the most common descriptors for the comparison and presentation of molecular shape of a compounds.

Principal moments of inertia (PMI) is a method to describe molecular shape. The three-dimensional structural information of a compound is translated into a two-dimensional plot using three principal moments of inertia, I_3 , I_2 and I_1 , where I_3 is the largest. The values I_3 , I_2 and I_1 are generated by a molecular mechanics computer algorithm. For each conformation of a compound, two sets of normalised principal moments ratios, NPR1 and NPR2, are calculated as shown below:

$$\text{NPR1} = I_1/I_3 ; \text{NPR2} = I_2/I_3$$

A triangular diagram is used for plotting these two sets of values where NPR1 is on the x-axis with a range of 0.5 to 1 and NPR2 is on the y-axis with a range of 0 to 1 (Figure 1.13). The coordinates represent the molecular shape. For instance, a completely rod-shaped molecule, such as a di-alkyne compound, has coordinates (0,1) at the top left corner. A perfect disc-shaped molecule, benzene, has coordinates (0.5,0.5) at the bottom, whereas a perfect sphere-shaped molecule, such as adamantane, has coordinates (1,0) at the top right corner. A PMI plot is a useful diagram to visualise the distribution of molecular shapes of compounds. The relative position of the coordinates on the plot indicate the shape of a given compound and show whether it is flat or three-dimensional.

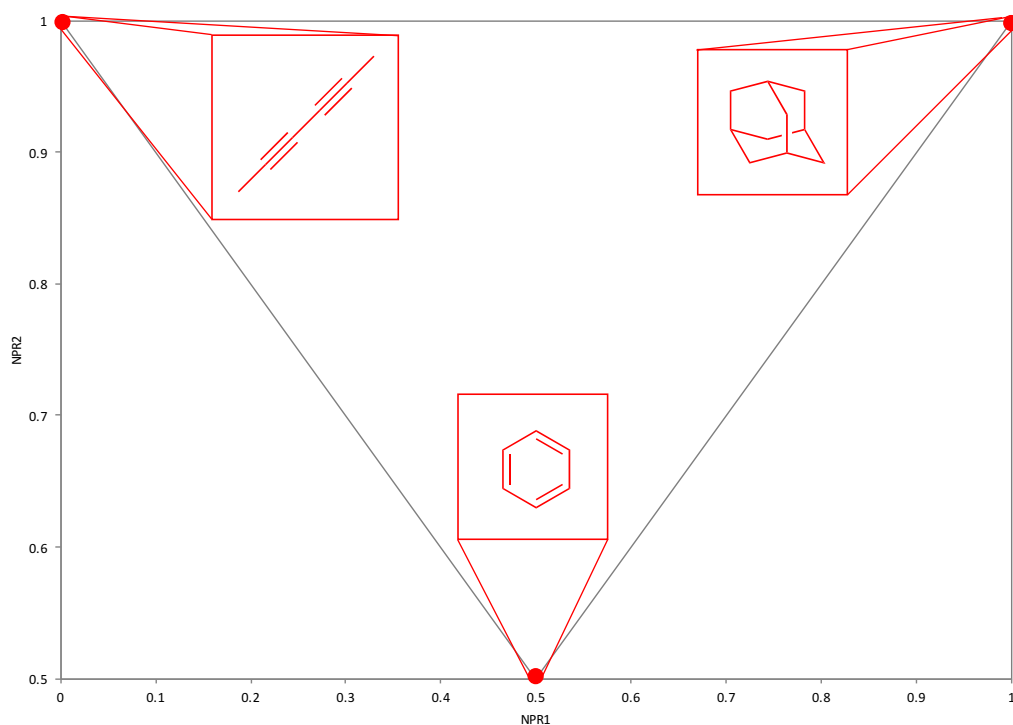


Figure 1.13: Triangular plot of PMI.

Different groups have used PMI plots to describe and evaluate the shapes of compounds in their libraries. For example, Spring *et al.* carried out a diversity oriented synthesis (DOS) of 73 macrocyclic compounds and compared their three-dimensional shapes with other compounds using PMI. DOS is an approach that has been widely used in HTS for building large collections of compounds systematically. The PMI plot of their macrocyclic DOS library is shown in Figure 1.14 together with the 40 top-selling brand-name drugs, 24 macrocyclic natural products and 60 structurally diverse natural products. The drug reference set used in their PMI plot had predominantly rod-like shapes with disc-like features (green squares), whereas the natural product sets had more shape diversity with more sphere-like character (blue triangles). The

macrocycles (red circles) were more similar to the spread and shape of the natural products than the drugs.³²

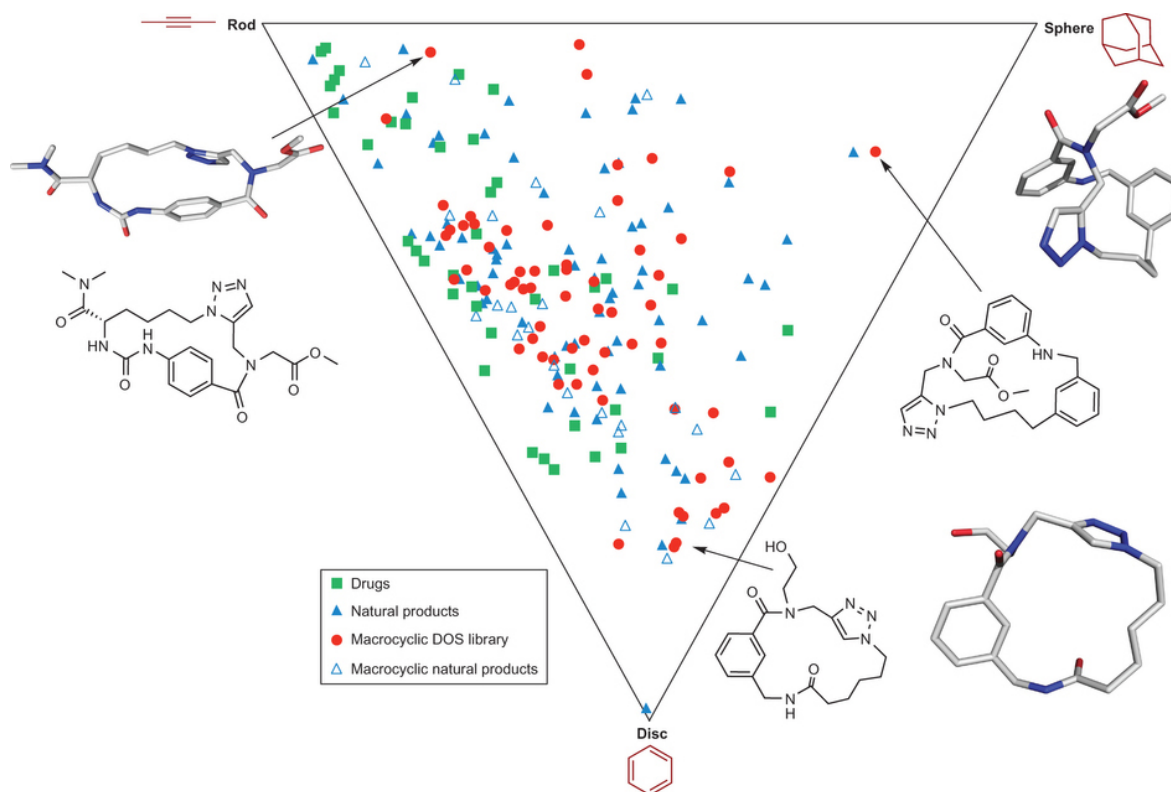


Figure 1.14: An example of a PMI plot of Spring's macrocyclic DOS library with the 40 top-selling brand-name drugs, 24 macrocyclic natural products and 60 structurally diverse natural products. (Figure adapted from reference 32)

Although a PMI plot is a good graphical method to translate the three-dimensional shape information of molecules into a two-dimensional triangular graph, it only uses the normalised size of each compound, without any correlation to the size of the molecule (i.e. molecular weight, HAC). This is one of the disadvantages of PMI plots.

Plane-of-best fit (PBF) is a newer molecular shape graphical descriptor which takes size (HAC) into account in the calculation process. In a similar way to PMI, PBF also

involves generation of the low energy conformers before calculation of the PBF score. In Firth's paper,³¹ the low energy conformation was generated by a programme called CORINA. Using the conformation, a PBF can be determined from all of the heavy atoms in a molecule. To describe how far a molecule is from two-dimensional shape, the average distance of all the heavy atoms from the PBF is calculated. Figure 1.15 illustrates the PBF for cyclohexane in a chair conformation.

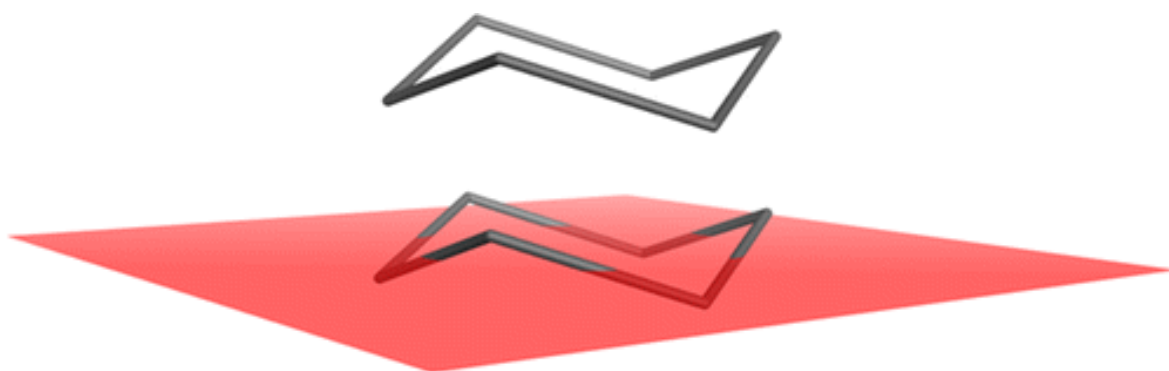


Figure 1.15: Illustration of the PBF for a chair conformation of cyclohexane. (Figure adapted from reference 31)

The PBF score is from 0 to infinity. For small drug-like molecules, the PBF is usually below 2, whereas for proteins PBF is usually below 10. A planar molecule which has a lower PBF score, whereas a molecule with more three-dimensional shape has a higher PBF score. An example of the PBF score of several different compounds is shown in Figure 1.16. A compound which has a flat conformation, such as **14**, has a PBF value of 0 Å, whereas compound **20** with a more three-dimensional conformation has PBF value of 1.06 Å.

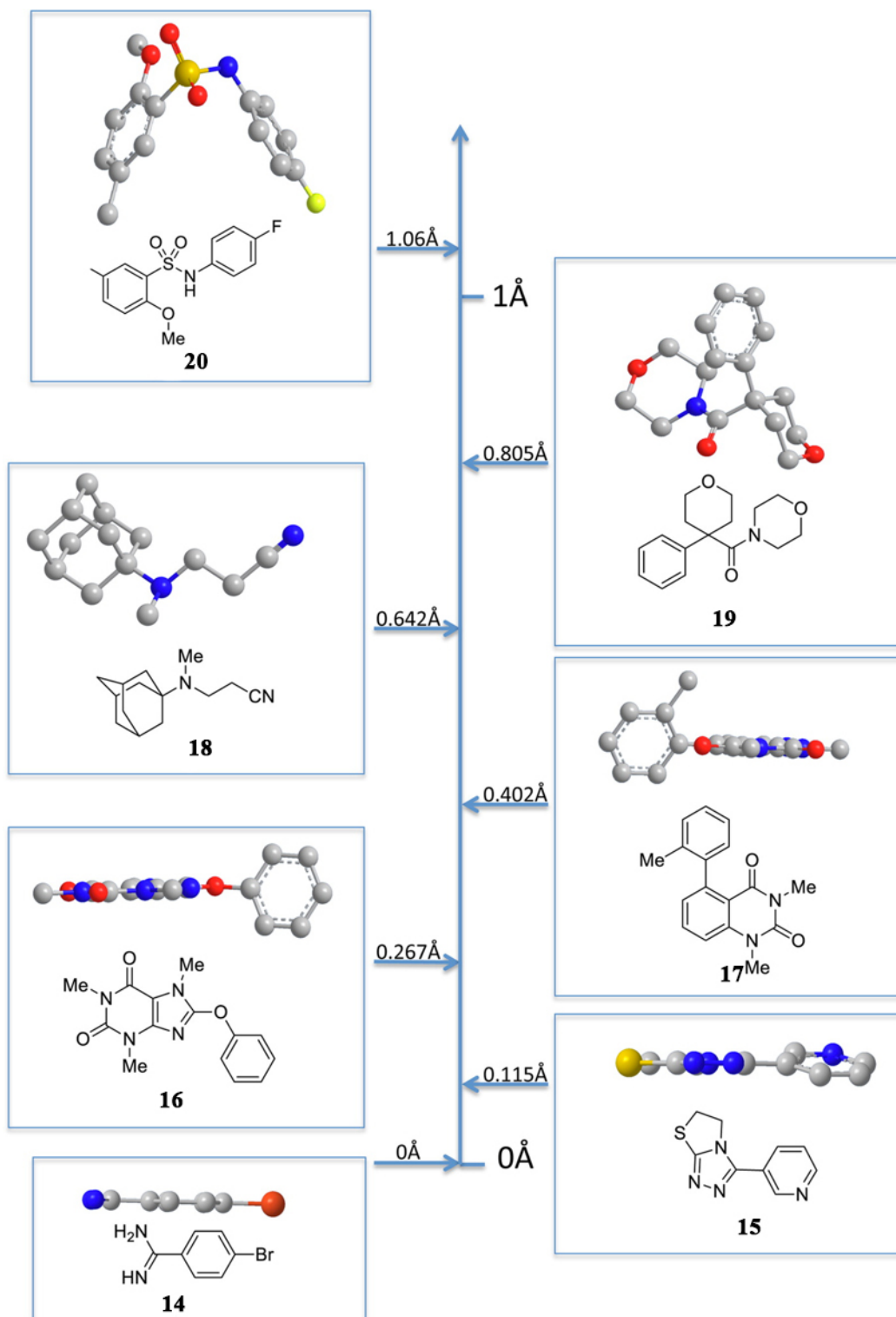


Figure 1.16: Example of the PBF score of molecules from a library in Å. (Figure adapted from reference 31)

In their study, PBF values were compared with PMI plots for analysing three-dimensional shape. Figure 1.17 is an example of a density plot of PBF score *versus* NPR1 + NPR2 from an eMolecules data set. They defined the cut-off for ‘flat’ molecules as when the NPR1 + NPR2 is the horizontal black line ($\text{NPR1} + \text{NPR2} \leq 1.07$). For the PBF score, flat molecules were defined by the vertical black line ($\text{PBF} \leq 0.6$). The top right corner (three-dimensional molecules) and bottom left (flat molecules) contains the shape of molecules that both descriptors agreed with. Hence, PMI contains more three-dimensional molecules (top left) than PBF contains (bottom right). Therefore, there is only a weak correlation between PMI and PBF and there are differences in three-dimensionality between the two methods.³¹

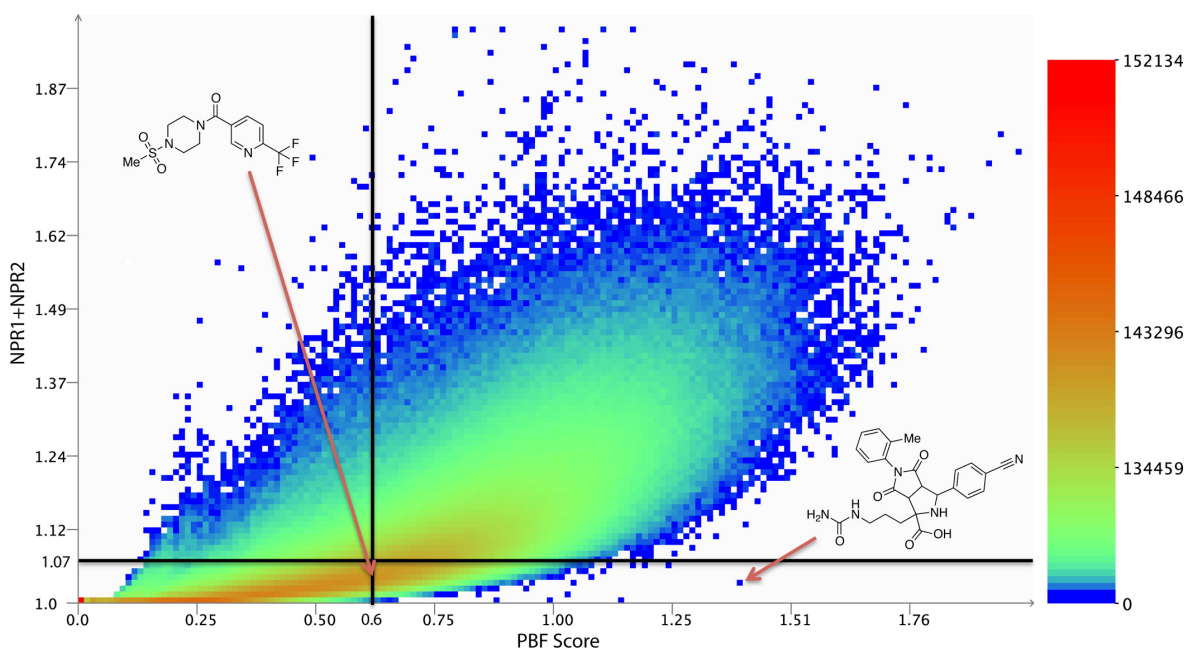


Figure 1.17: An example of plot NPR1 + NPR2 versus PBF scores of an eMolecules data set. (Figure adapted from reference 31)

1.5 Three-Dimensionality in Fragment Libraries

One way to increase chemical space coverage and diversity of fragment library collections is to increase the three-dimensional character of the fragments. Traditionally, the majority of fragment libraries contain ‘flat’ compounds and are rich in aromatic and sp^2 hybridised compounds which could reduce the scope of chemical and pharmacological space.³³ This is perhaps the reason why fragment hits are more common for the flat ATP-binding pockets in kinases than for the fundamentally different pockets in protein-protein interactions (PPIs). In order to address this issue, three-dimensional fragments could be the solution and there has been growing interest in three-dimensional fragments. Another reason for increasing the three-dimensionality of fragments is that such three-dimensional molecules could be better recognised by proteins. It was suggested that three-dimensional fragments would have a broader range of biological activities and could achieve greater interaction with proteins.^{34,35}

Hung *et al.* used diversity-oriented synthesis (DOS) strategies to produce a library collection with a large quantity of sp^3 -rich fragments, in order to cover wider chemical space. In this study, DOS is a three-step system of build, couple and pair, aimed to produce compounds with diversity of shape and stereochemistry. Hung began with the synthesis of three proline derivatives **21**, **22** and **23** as building blocks to access different spirocyclic fragments (Figure 1.18). These building blocks are useful as their *R* and *S* enantiomers are easily obtained and they can be used to generate a large amount of stereochemically diverse fragments from a pyrrolidine-based scaffold.

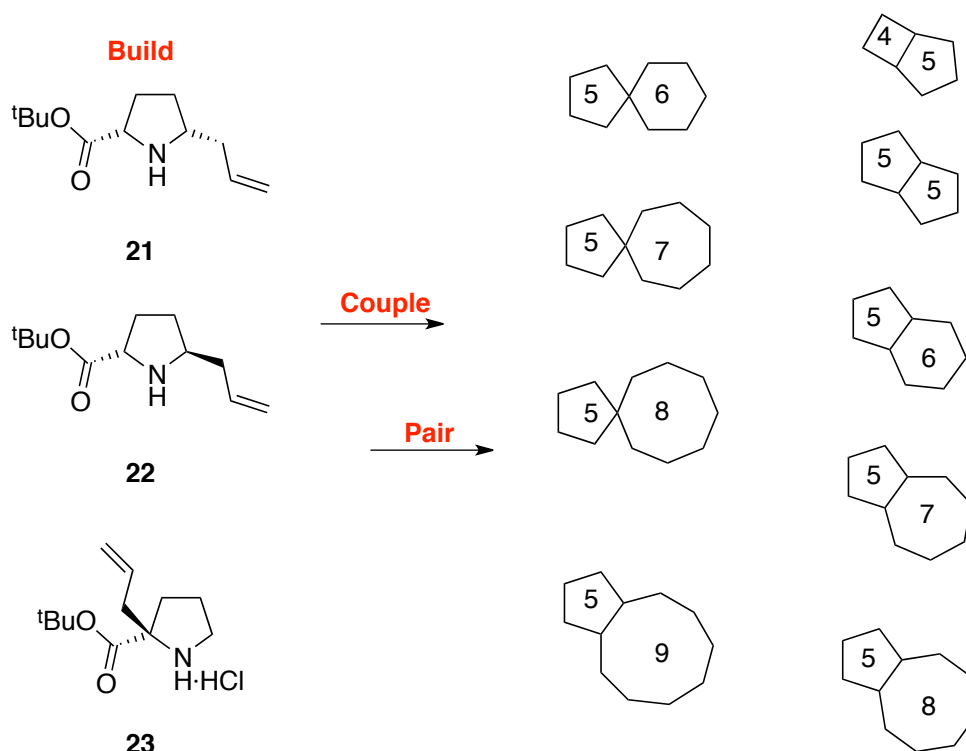


Figure 1.18: **21**, **22** and **23** were building blocks for their DOS system to generate large number of *sp*³-rich fragments (*MW* < 300).

Building blocks **21**, **22** and **23** underwent the couple-pair phase to generate different ring sizes with diverse stereochemistry. For the coupling phase, different alkenes were coupled with the corresponding building blocks. Subsequently, a pairing phase composed of a ruthenium-catalysed ring-closing metathesis reaction yielded 35 structurally and stereochemically diverse spirocyclic and bicyclic fragments. Figure 1.19 shows the structures of five of their fragments **24**, **25**, **26**, **27** and **28**, together with a PMI plot of all 35 fragments (red circles) and 18 534 fragments from the ZINC database (blue circles). The fragments in the ZINC database are more rod-disc in shape, whereas the shapes of the new fragments are much more spread out and three-dimensional.³⁵

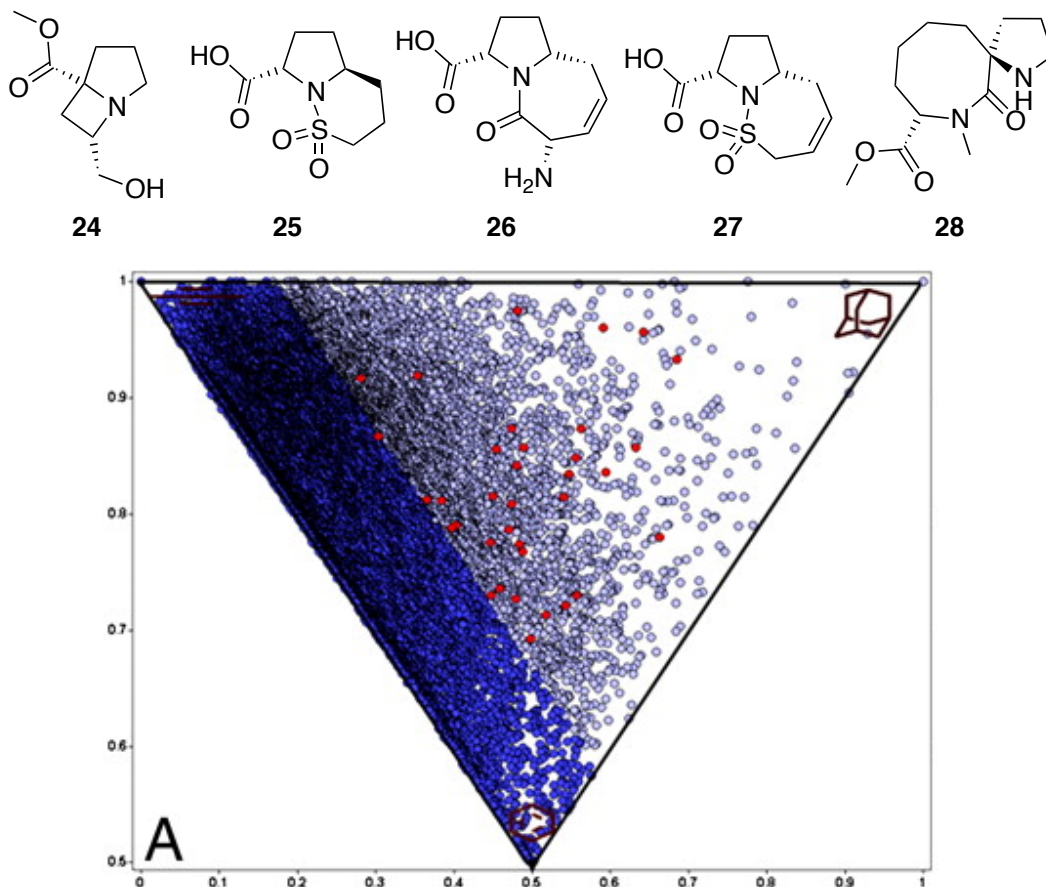


Figure 1.19: Five of their fragments 24, 25, 26, 27 and 28 and a PMI plot of all 35 fragments (red circles) and 18 534 fragments from ZINC data base (blue circles). (Figure adapted from reference 35)

In 2013, the 3D Fragment Consortium, which is constituted of several UK not-for-profit drug discovery institutes and academic groups published their first paper. The aim of their project is ultimately to construct a fragment screening library that contains 500–3000 fragments, which has shape diversity and three-dimensional fragments. Compounds in the library also need to satisfy the ‘rule of three’ criteria.

To start, they constructed their foundation set of fragments from eMolecules and the ZINC database which have around 13.4 million compounds. They applied a filter on HAC, and typical fragment criteria, and they also removed unwanted functional groups.

This left 180 000 compounds. Subsequently, they selected 5000 shape diverse compounds using their NPR1/2 values. Then, they further removed compounds based on their availability, cost and internal controls to end up with 200 compounds in their 3D Fragment Consortium foundation set. Figure 1.20 is the PMI plot of their library and three fragments are identified. The PMI plot shows a good shape diversity, with a high proportion towards three-dimensional chemical space.³⁶

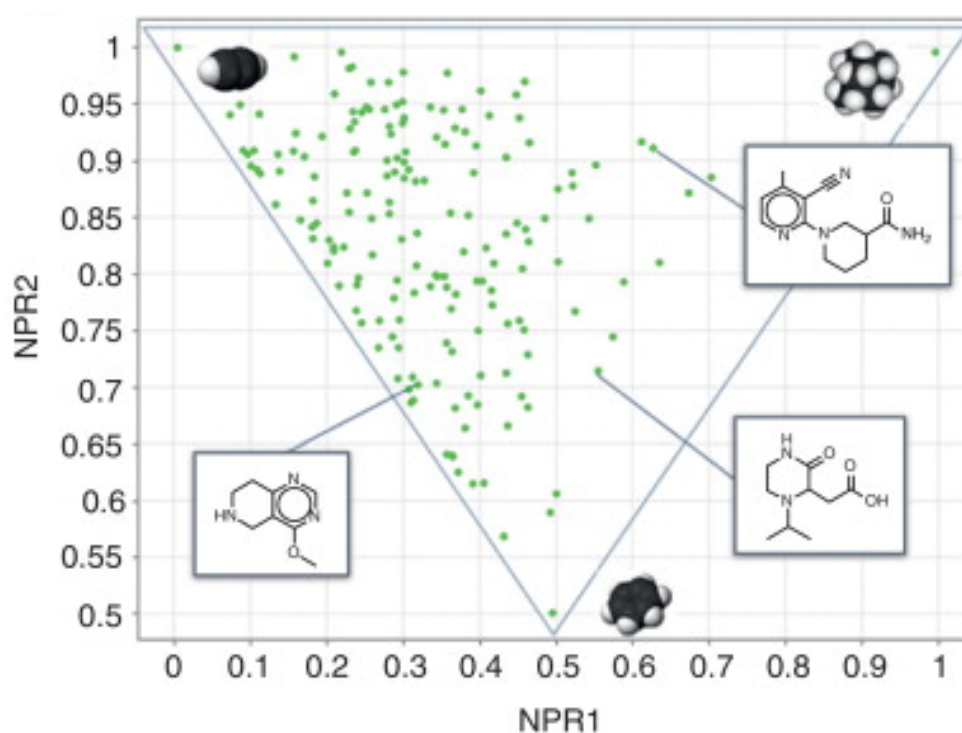


Figure 1.20: The PMI plot of the 3D Fragment Consortium foundation set. (Figure adapted from reference 36)

The consortium also introduced an online tool for evaluation of fragments, called 3DFIT (three-dimensional fragment idea tool). This software allowed calculation of the predicted physicochemical properties of a molecule that is submitted by the user. The software was also equipped with Pipeline Pilot which could to generate the PMI plot of a given molecule for the different energy conformations. Figure 1.21 shows the

predicted properties and PMI plots of compound **29** and **30**. In each compound, there are up to nine lowest energy conformations generated and plotted on the triangular PMI plots. This software is useful for generating new ideas in fragment design. Moreover, they suggest that synthesis of new three-dimensional fragments from non-commercial scaffolds would increase the chance of making novel compounds.³⁶

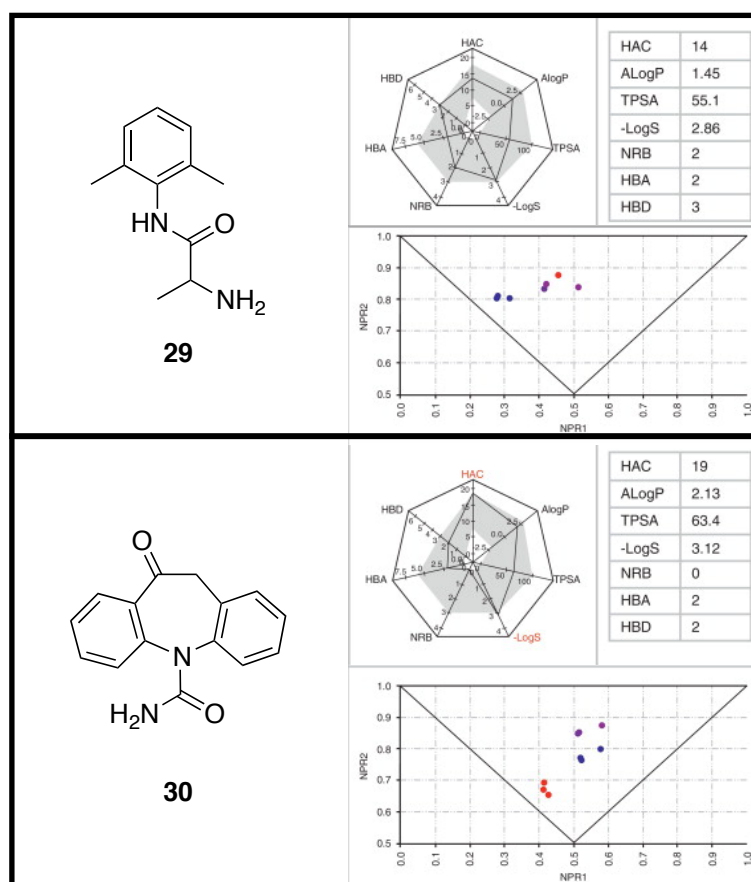
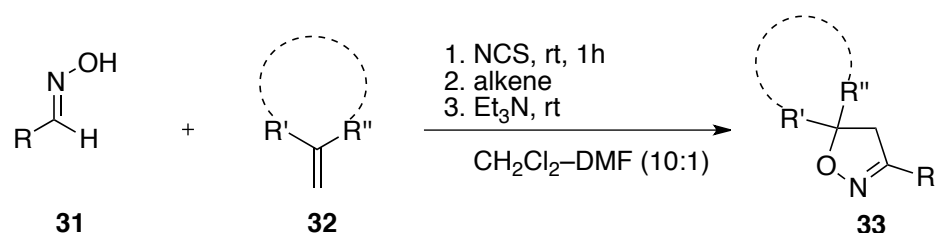


Figure 1.21: Predicted physicochemical properties of **29** and **30** and PMI plots of their nine lowest energy conformation generated by 3DFIT. (Figure adapted from reference 36)

In 2015, Tran *et al.* repeated the design and synthesis of novel sp^3 -rich, spirocyclic fragments based on a 2-isoxazoline scaffold. Their aim was to produce compounds in the underrepresented area of three-dimensional chemical space. Isoxazolines

derivatives are commonly found in natural products and bioactive compounds. Tran's were selected as they approach involved a one-pot, 1,3-dipolar cycloaddition strategy as shown in Scheme 1.1. Treatment of oximes **31** with *N*-chlorosuccinimide and subsequent reaction with alkenes **32** in the presence of base gave the spirocyclic isoxazolines **33** in 16-88% yield.



Scheme 1.1: The one-pot 1,3-dipolar cycloaddition.

Using this synthetic approach, Tran *et al.* prepared 21 spirocyclic isoxazoline fragments and some examples are shown in Figure 1.22. Analysis of the molecular shape of their fragments using PMI showed that they have a good shape and structural diversity. However, some the compounds had some rod-like character. Figure 1.22 shows the six most three-dimensional fragments from their collection.³⁷

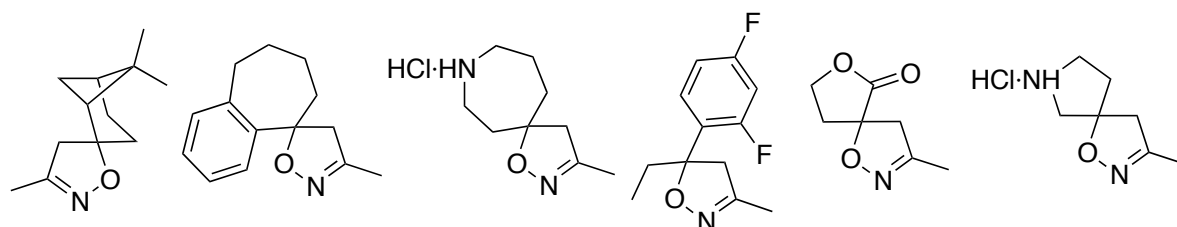
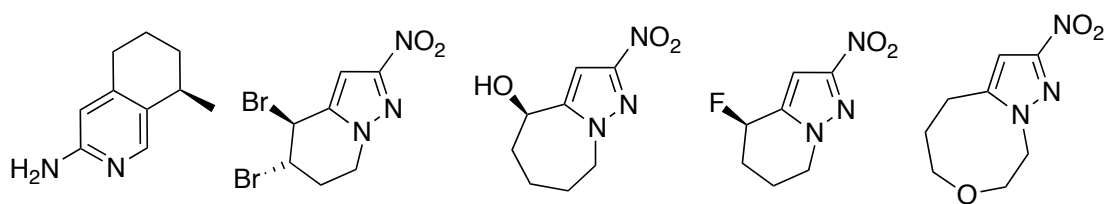


Figure 1.22: The six most three-dimensional fragments Tran's isoxazoline compounds.

In another study, Spring *et al.* used the partially saturated bicyclic heteroaromatics (PSBH) approach to synthesise a collection of sp^3 -enriched fragments. In general, PSBH-containing compounds have shown bioactivity with different protein targets. Spring's strategy used simple cross-coupling and alkylation reactions, followed by ring-closing metathesis to introduce precise ring sizes and to allow further functionalisation of the ring to give shape diversity. Their resulting compounds mostly fulfil the 'rule of three' ideal fragment criteria. Table 1.4 shows some of their fragments and a table of the mean physicochemical properties of their fragment collection together with two other commercial library collections.

Table 1.4: Example of fragments from this study and the mean of physicochemical properties of their fragments with Chembridge and Maybridge commercial libraries.



Property	Spring's library	Chembridge	Maybridge
SlogP	1.45	1.31	2.55
MW	190	222	265
PSA	58.0	53.9	57.5
HBA and HBD	1.35 & 0.55	1.81 & 1.04	2.12 & 0.81
HAC	12.8	15.5	18.0
NROT	0.6	3.2	2.8
No. of chiral centres	0.88	0.27	0.18
Fraction aromatic	0.43	0.42	0.52

As shown in Table 1.4, Spring's fragments have lower molecular weight, SlogP and fraction aromatic with a higher number of chiral centres than the Maybridge library. Spring did not provide an analysis of the shapes of their fragment collection using a quantitative method such as PMI or PBF. They only demonstrated the increased shape diversity using Fsp^3 and the number of chiral centres.

In a more recent study, researchers at AstraZeneca evaluated and compared the results of their two generations of fragment libraries, FL1 and FL2, in screening campaigns. Fragment screening projects started at AstraZeneca in 2002 and the number of successes improved over time, including an increase in the three-dimensionality of the fragments. AstraZeneca analysed their fragment-based lead generation (FBLG) programmes for 2002-2014 and the results are shown in Figure 1.23. The results show that there was an increase in the proportion of successes in this time period despite the number of FBLG projects decreasing. From 2012 onwards, the success rate increased to over 60%, which is a significant improvement on the success rate during 2002-2010 (around 30%). This improvement was due to a more robust crystallography method and an associated structure-based approach. Also from 2012 onwards, a chemistry team was assigned to support FBLG in order to improve their collection and this is when their second generation library, FL2, was constructed.

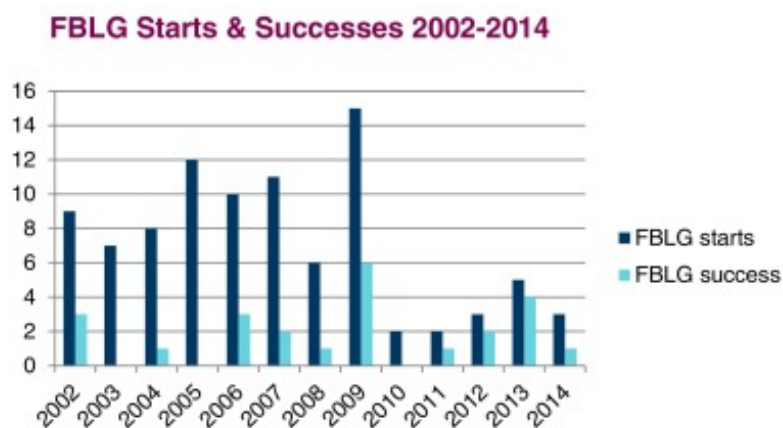


Figure 1.23: A plot of the number of AstraZeneca's FBLG programmes and success during 2002-2014. (Figure adapted reference 38)

AstraZeneca's FL2 collection contained around 15000 compounds and around 25% of their fragments obey the 'rule of three' criteria. The shape of the compounds in the

library was analysed using PBF and PMI plots and showed a good shape diversity with a good proportion of fragments having three-dimensional character. Figure 1.24 shows the shape analysis by PBF and PMI plots of the FL2 collection and all FL2 hits. The shape of compounds in FL2 has high three-dimensionality. Around 60% of fragments have PBF > 0.25, which is their definition of three-dimensional fragment. However, less than half of their hits are for fragments above this score and, as a result, they suggest that their library is slightly too rich in three-dimensional character.

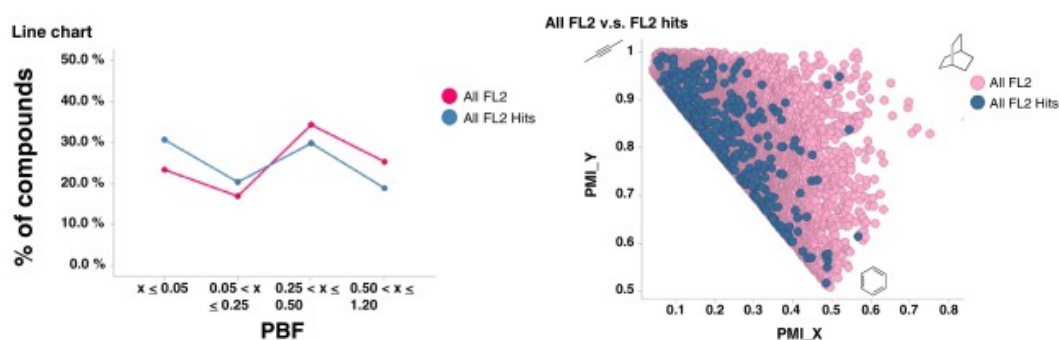


Figure 1.24: The PBF scores and PMI plot of FL2 and FL2 hits fragments. (Figure adapted reference 38)

In order to better study the three-dimensional fragments, they carried out an analysis of pocket volume filling for two- and three-dimensional fragment hits and their protein targets. The results showed that three-dimensional fragments better filled the pocket space in protein-protein interaction (PPI), nuclear hormone receptors and oxidoreductase/dehydrogenases, whereas two-dimensional fragments were better for kinases (Figure 1.25). Therefore, a library with balanced compound shapes could lead to higher success rates for different classes of protein targets.

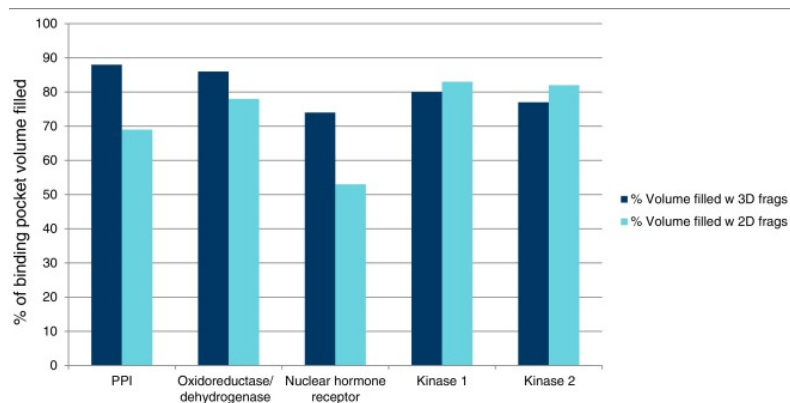


Figure 1.25: The percentage of pocket volume filled in different target by two- and three-dimensional fragment. (Figure adapted reference 38)

The AstraZeneca study pointed out that shape diversity does have an influence on hit rate. In addition, their results show that three-dimensional fragments can improve the hit rate and could have better binding with some target classes, especially with protein-protein interaction.³⁸

1.6 Project Outline

The aim of this project is to design and synthesise novel three-dimensional fragments for use in drug discovery programmes. This project is a sub-set of a larger project at York which aims to construct a fragment library with ~300-500 compounds. This will address the under-represented areas of three-dimensional chemical space.

In this project, we planned to carry out PMI plots of a range of three-dimensional pyrrolidine fragments with different regio- and stereochemistry to select compounds for synthesis. Some of the fragments that have been designed and synthesised are shown in Figure 1.26. The long term aim of the project is to screen the new three-dimensional fragments against proteins of medicinal interest.

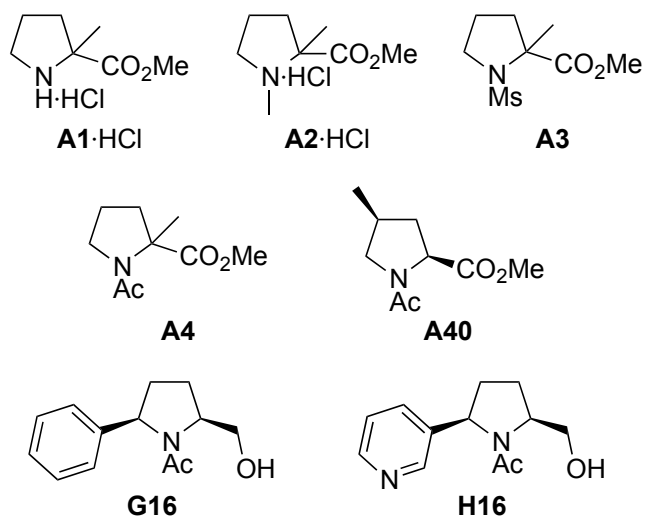


Figure 1.26: Examples of fragments in this project.

Chapter 2: Computational Analysis and Selection of Three-Dimensional Pyrrolidine Fragments

In this chapter, we present the protocol that we use to evaluate the three-dimensional shapes of compounds. In general terms, a PMI analysis of all possible regio- and stereoisomers of different pyrrolidines was carried out. Then, the PMI plots were analysed in order to select the most three-dimensional compounds for synthesis.

In Section 2.1, the computational protocol is introduced. In addition, the protocol is used to analyse the three-dimensional shape of ~1000-member fragment library from Maybridge. Section 2.2 discusses our fragment design based on a pyrrolidine with two substituents, methyl and methyl ester, and four different nitrogen groups, allowing some compounds for synthesis to be identified. Finally, in Section 2.3, a PMI analysis of a range of substituents on the pyrrolidine scaffold are described.

2.1 Introduction to Computational Protocol and Analysis of a Maybridge Fragment Library

The generation of conformations and PMI data was carried out using the protocol that was developed by Mary Wheldon, a former PhD student in the group, together with Paul Bond and Rod Hubbard from the York Structural Biology Laboratory. Prior to the generation of conformations, a SMILES file of each fragment is entered into the Pipeline Pilot 8.5 software. The SMILES file for a compound can be imported from a database of compounds or generated using ChemDraw 12.0.

The BEST tool in the Pipeline Pilot 8.5 was used for the generation of conformers as we believe that this provides the best coverage of conformational space. In principle, there is an infinite number of conformers for each molecule that could be generated and therefore constraints of conformational energy difference and root-mean-square deviation (RMSD) were used in this protocol. Conformational energy difference provides the energy difference between an individual conformer and the lowest energy conformer for the selected compound. Variation of this value could affect the total number of conformers. The RMSD indicates the difference in Å between atoms, or points of the conformer and the standard. If the RMSD is 0 Å, a conformer that only changes slightly from the standard will be kept, whereas if the RMSD is 1 Å, only very different conformers will be kept. Hence, the larger the RMSD, the fewer conformers that will be selected. In this study, the conformational energy difference was calculated up to 20.0 kcal mol⁻¹ and the RMSD was set to 0.1.

As discussed in Sections 1.4.2 and 1.4.3, most of the examples in the literature that use PMI plots normally consider only the lowest energy conformation of a compound. In contrast, with this protocol, a number of conformations for each compound are generated within the constraints. By including other energy conformations of a given compound a better representation of the shape of the compound is provided. This could be useful as the conformation which binds in the protein binding pocket is not necessarily the lowest energy conformation.

To start with, we decided to evaluate a Maybridge fragment library that contained 1000 fragments using our computational protocol. Maybridge is a commercial vendor that provides screening and fragment libraries. The results of a PMI analysis using our protocol are shown in Figure 2.1. There are almost 16000 conformers generated from 1000 fragments with a conformational energy difference less than 20 kcal mol⁻¹. In the PMI plot, it is difficult to identify the position of an individual conformation as there are far too many data points on the PMI plot. Therefore, we concluded that a better method is required and, in particular, we needed to reduce the number of conformations.

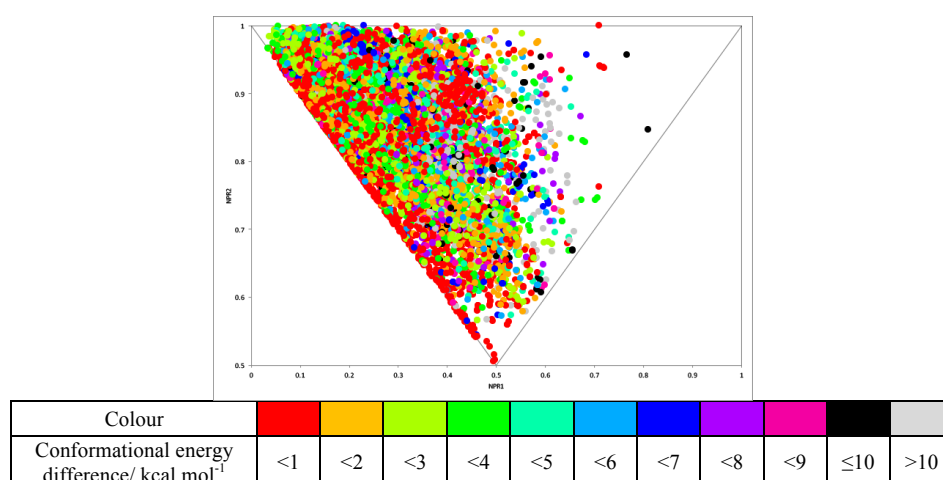


Figure 2.1: PMI plot of the all conformations of a Maybridge fragment library with of conformational energy difference of less than 20.0 kcal mol⁻¹.

In order to analyse the PMI plot for more three-dimensional shapes i.e. away from the rod-disc axis, we decided to divide the PMI plot into 10 sections with diagonal lines that are parallel to the rod-disc axis (Figure 2.2). Each data point on the PMI plot is defined by the (x,y) coordinates and they have NPR1 (x-axis) and NPR2 (y-axis) values. The sum of the NPRs, Σ NPRs, can be useful for defining the shape distribution. Each of the diagonal lines is effectively the Σ NPRs, and ranges from 1 to 2 where 1 is on the rod-disc axis. As Σ NPRs gradually increases, the conformations become more three-dimensional in shape. The number of conformers in the Σ NPRs categories is a useful way of analysing the PMI plot.

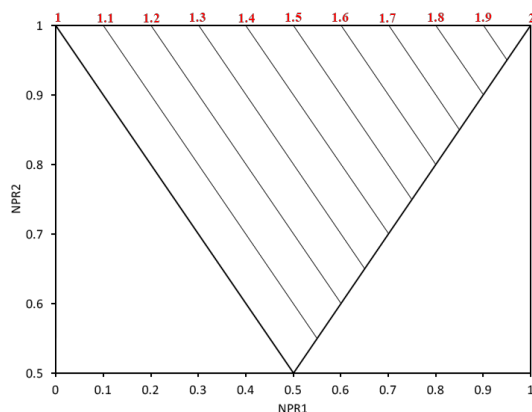


Figure 2.2: PMI plot with the Σ NPRs of each category.

With the purpose of trimming down the large number of conformations but retaining the conformational diversity of the compounds, the conformational energy difference of the selected fragments could be reduced. Using the Maybridge dataset, there are 6498 conformers generated if the conformational energy difference is set at ≤ 1.5 kcal mol⁻¹. The conformational energy difference is the energy above the lowest energy ground state conformer. Even with this conformational energy difference cut-off, the PMI plot still retains a good diversity of conformations (Figure 2.3). Figure 2.3 shows two PMI plots of the Maybridge library that contain conformational energy difference

$\leq 1.5 \text{ kcal mol}^{-1}$ and the lowest energy conformers with the corresponding pie chart that contains the percentage distribution of conformers in each energy category. With the higher energy cut-off, there are 15% fewer conformers in the PMI category 1–1.1 and 13% more in the next PMI category (1.1–1.2) than the lowest energy cut-off.

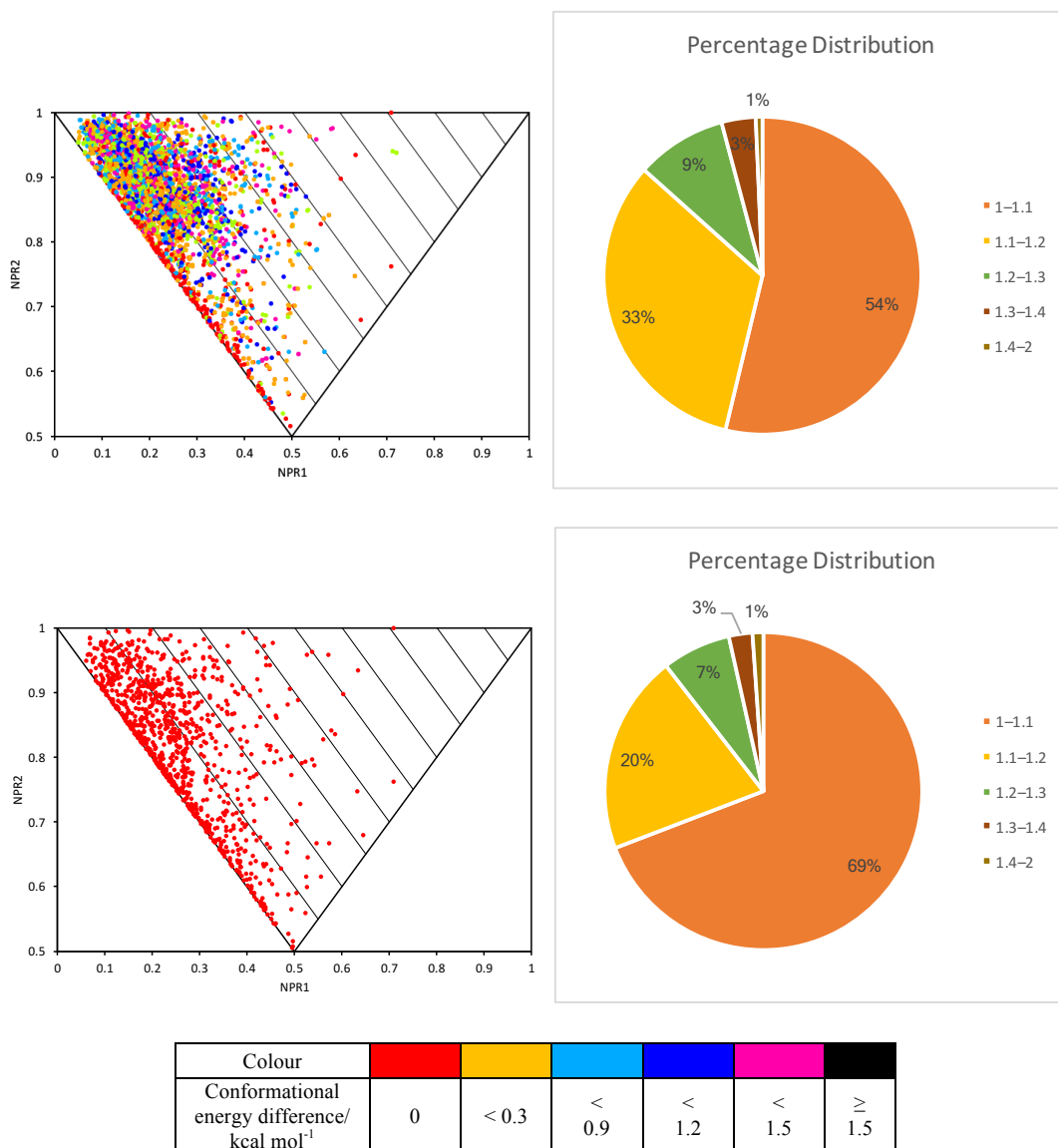


Figure 2.3: PMI plot of the conformations with energy difference energy $\leq 1.5 \text{ kcal mol}^{-1}$ and the lowest energy conformers of Maybridge fragments and the corresponding PMI category distributions.

The same PMI data for the energy difference ≤ 1.5 kcal mol⁻¹ in Figure 2.3 is also presented in Table 2.1. From Table 2.1, it is clear that more than 85% of the conformers are in the PMI category between 1–1.2. This is the category closest to the rod-disc axis, and so the Maybridge library contains mostly flat compounds and has a lack of shape diversity. However, there are still some of the fragments that have three-dimensional shapes. The ten most three-dimensional structures in the Maybridge library are shown in Figure 2.4. They have Σ NPRs values ≥ 1.4 and contain different heterocyclic ring systems.

Table 2.1: Number of conformations and percentage in each PMI category with conformational energy difference ≤ 1.5 kcal mol⁻¹.

PMI category	Number of conformations	Percentage (%)
1–1.1	3493	53.76
1.1–1.2	2135	32.86
1.2–1.3	600	9.23
1.3–1.4	226	3.48
1.4–1.5	31	0.48
1.5–1.6	8	0.12
1.6–1.7	4	0.06
1.7–1.8	1	0.02
1.9–2	0	/
Total	6570	/

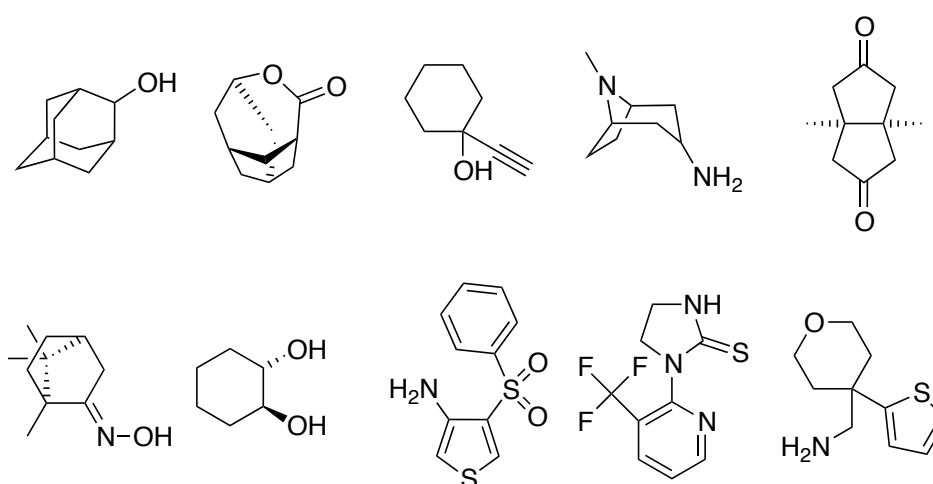


Figure 2.4: 10 Maybridge fragments Σ NPRs values ≥ 1.4 .

The ‘Rule of three’ is a general guideline of physicochemical properties for fragments. In Pipeline Pilot 8.5, physicochemical properties of compounds can also be predicted, including the number of hydrogen bond donors and acceptors, HAC and ALogP. This information could be useful for evaluation of library properties and fragment selection. Table 2.2 summarises the predicted mean of physicochemical properties of the Maybridge fragment library that was generated by Pipeline Pilot 8.5. They clearly fit within the ‘rule of three’.

Table 2.2: Predicted average physicochemical properties of a Maybridge fragment library using Pipeline Pilot 8.5.

Physicochemical Properties	Mean
Molecular Weight	180.13
AlogP	1.3
PSA	45.92
HBA & HBD	1.94 & 0.79
HAC	12.51
NROT	1.78
No. of ring (aromatic)	1.6 (1.17)

In summary, the PMI analysis shows that the shapes of the conformations in the Maybridge fragment library are mostly flat. Furthermore, by considering a conformational energy difference $\leq 1.5 \text{ kcal mol}^{-1}$, conformational diversity is achieved, compared to the lowest energy conformation.

2.2 Fragment Design and Overview of Our Enumeration and Selection Approach

For our three-dimensional fragment library design, a systematic approach for fragment selection was required. To start with, we devised a systematic way of drawing all of the possible isomers of a particular scaffold. This format would also be helpful for comparing different systems. In our drawing approach, the order of nitrogen substituents was always NH, NMe, NMs and NAc. With the two substituents on the scaffold, any geminal disubstituted fragments were drawn first, followed by the lowest priority group (R^1) in the 2-position and R^2 opposite. For the diastereomer order, *trans* was drawn before *cis*. R^2 was drawn around the ring to the position of R^1 . Afterwards, R^1 was moved to the 3-position and repeated. Then, all isomers could be drawn.

Using the above guidelines, the first pyrrolidine fragments with methyl and methyl ester substituents were drawn and their 14 isomers are shown in Figure 2.5. With four different nitrogen groups, there are 56 fragments in total, excluding enantiomers.

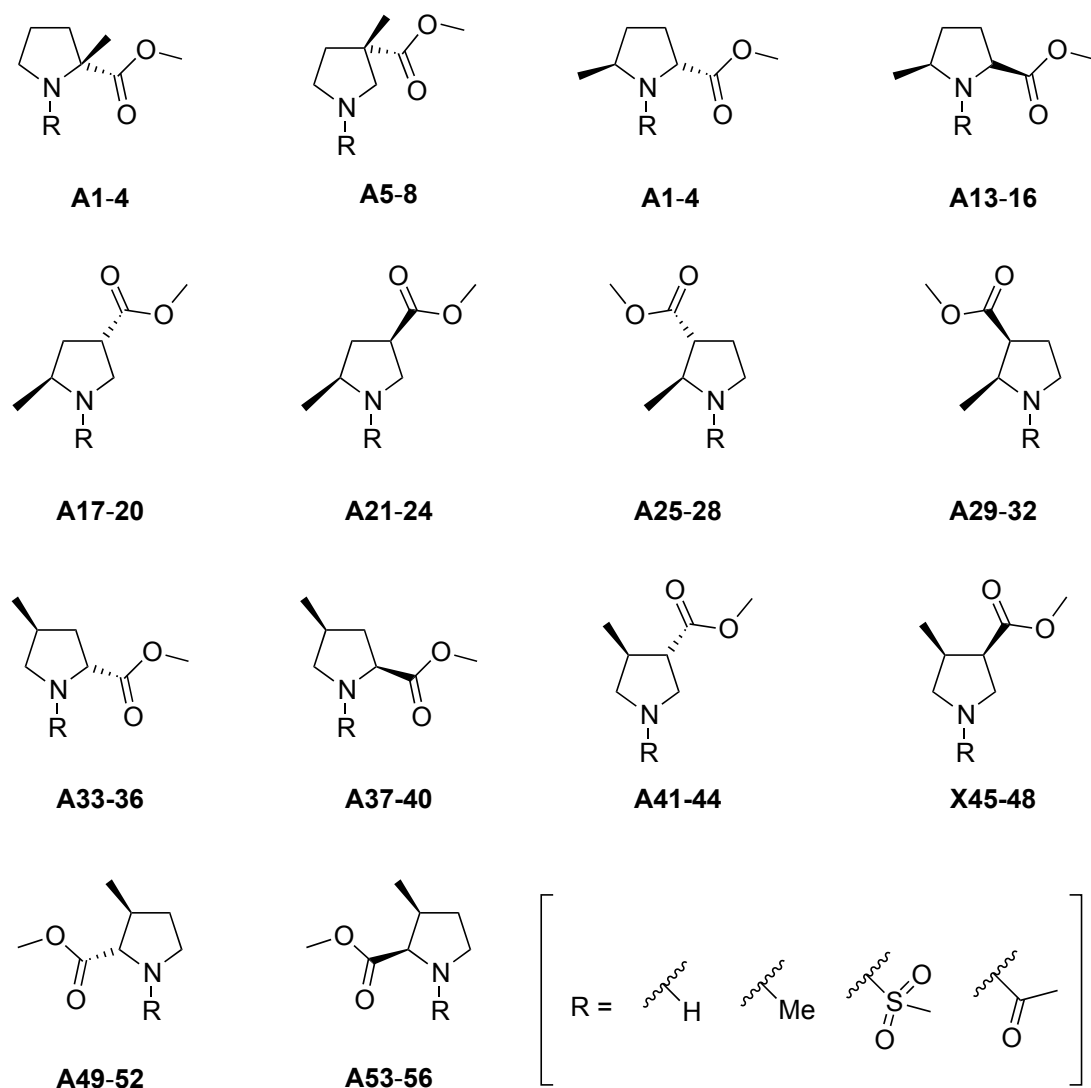


Figure 2.5: The 14 different isomers of methyl, methyl ester disubstituted pyrrolidine. The four different nitrogen substituents are also shown.

These 56 compounds were then submitted to the standard PMI analysis in Pipeline Pilot 8.5. The PMI plot of the lowest energy conformations and conformations with an energy difference $\leq 1.5 \text{ kcal mol}^{-1}$ for these 56 fragments are shown in Figure 2.6. Table 2.3 shows the number and percentage of conformers up to $1.5 \text{ kcal mol}^{-1}$ conformational energy difference in each PMI category. From the PMI plot, it can be seen that the majority of fragments are away from the rod-disc axis and they have some three-dimensional character in their shapes. Moreover, in the PMI category 1–1.2,

there are fewer lowest energy conformers (32%) than the conformers with a conformational energy difference ≤ 1.5 kcal mol⁻¹ (62%). However, the higher energy conformers had a wider spread and a higher PMI category coverage on the PMI plot than the lowest energy conformers.



Figure 2.6: PMI plot of the conformations with energy difference energy ≤ 1.5 kcal mol⁻¹ and the lowest energy conformers of pyrrolidine ester derivatives and the corresponding PMI category distributions.

Table 2.3: Number of conformations and percentage in each PMI category with conformational energy difference $\leq 1.5 \text{ kcal mol}^{-1}$.

PMI category	Number of conformations	Percentage (%)
1–1.1	117	20.17
1.1–1.2	244	42.07
1.2–1.3	144	24.83
1.3–1.4	57	9.83
1.4–1.5	13	2.24
1.5–1.6	5	0.86
1.6–1.7	0	/
1.7–1.8	0	/
1.9–2	0	/
Total	580	/

Further analysis considered how the fragments are distributed in each PMI category. The number of fragments and their percentage contribution in each PMI category is shown in Table 2.4. There are around 75% of the fragments distributed in the more three-dimensional areas between PMI categories 1.2–1.6. The PMI category 1.3–1.4 has the most fragments. The PMI categories 1.3–2 contained over 45% of the fragments and these are the most three-dimensional fragments.

Table 2.4: Number of fragments and percentage in each PMI category with conformational energy difference $\leq 1.5 \text{ kcal mol}^{-1}$.

PMI category	Number of fragments	Percentage (%)
1–1.1	2	3.57
1.1–1.2	11	19.64
1.2–1.3	17	30.36
1.3–1.4	18	32.14
1.4–1.5	5	8.93
1.5–1.6	3	5.36
1.6–1.7	0	/
1.7–1.8	0	/
1.8–1.9	0	/
1.9–2	0	/
Total	56	/

The next stage involved using the PMI plot of the conformers with energy difference $\leq 1.5 \text{ kcal mol}^{-1}$ in Figure 2.6 to select the most three-dimensional compounds for

synthesis. We planned to synthesise a selection of fragments that would represent all 56 compounds. In the area $\Sigma\text{NPRs} \geq 1.40$, eight fragments would be selected for synthesis, whereas it would increase to 17 fragments with $\Sigma\text{NPRs} \geq 1.34$ (Table 2.5). Further inspection of the region between PMI categories 1.40–1.34 was carried out to identify a suitable number of compounds for the synthetic work. In the end, 14 fragments were selected for synthesis i.e. ΣNPRs value ≥ 1.36 (Table 2.5).

Table 2.5: Analysis of ΣNPRs values to select a suitable number of fragments for synthesis.

ΣNPRs	Number of fragments
≥ 1.40	8
≥ 1.39	9
≥ 1.38	9
≥ 1.37	10
≥ 1.36	14
≥ 1.35	15
≥ 1.34	17

The selected 14 fragments have a total of 117 conformations with a relative energy $\leq 1.5 \text{ kcal mol}^{-1}$. Figure 2.7 shows the structures of the selected fragments together with their corresponding PMI plot. These 14 fragments have a diversity of disubstituted pyrrolidines. There are geminal disubstituted fragments such as fragments **A1–5** and there are 2,3-disubstituted pyrrolidines **A28** and **A29** which have *cis* and *trans* stereochemistry. For the nitrogen substituents, **A1**, **A5**, and **A45** contain a NH group, **A2**, **A18** and **A56** have a NMe, **A3** having a NMs, whereas **A4**, **A16**, **A28** and **A50** contain a NAc. Therefore, with the 14 selected fragments shown positional, stereochemical and functional group diversity.

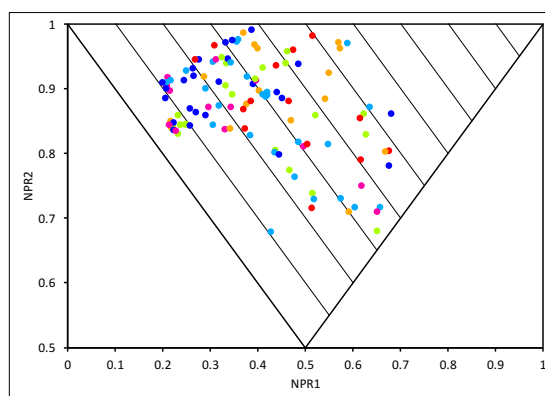
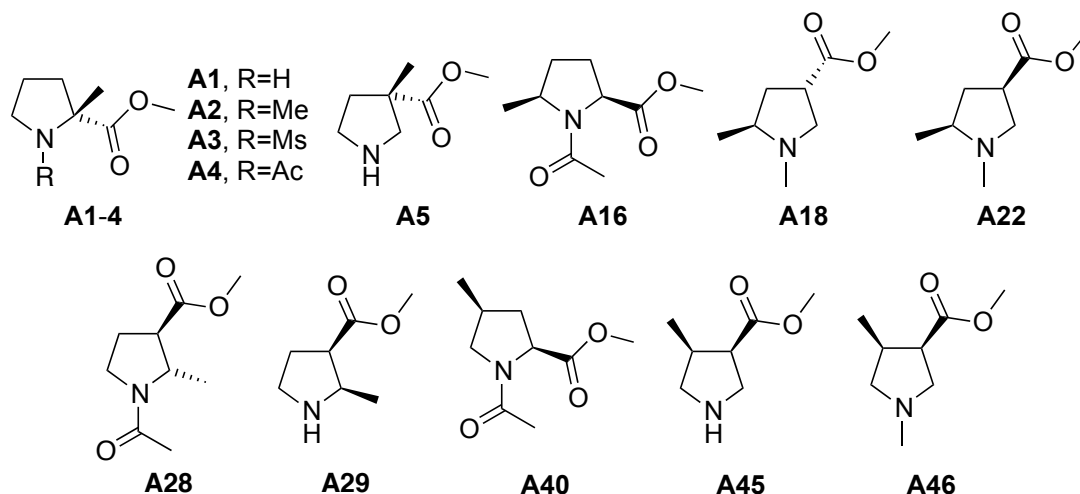


Figure 2.7: The selected 14 pyrrolidine fragments, and the PMI plot containing their 117 conformations with a relative energy ≤ 1.5 kcal mol⁻¹.

The physicochemical properties of the selected fragments were also evaluated to see how well they fitted with the ‘rule of three’ criteria. The mean of the predicted physicochemical properties of the selected compounds is shown in Table 2.6. All 14 selected fragments had physicochemical properties that fulfilled the ‘rule of three’ criteria, although the average AlogP values are relatively low.

Table 2.6: Predicted average physicochemical properties of 14 selected fragment from Pipeline Pilot 8.5.

Physicochemical Properties	Mean
Molecular Weight	166.43
AlogP	-0.54
PSA	56.06
HBA & HBD	2.43 (0.64)
HAC	11.5
NROT	2.07
No. of ring (aromatic)	1 (0)

The results of the PMI analysis have shown that the selected designed pyrrolidine fragments have good three-dimensional shape as well as positional, stereochemical and functional group diversity. They also have good physicochemical properties. The strategy of using a basic pyrrolidine scaffold with decoration of two substituents can achieve the aim of three-dimensional shape and desirable physicochemical properties. Therefore, further investigations of variations of the substituents was carried out.

2.3 Comparison of the Three-dimensionality of Pyrrolidine Fragments with Different Substituents

In this section, we present the application of the PMI analysis of different three-dimensional pyrrolidine fragments. This includes the selection of some additional fragments for synthesis. Different substituents on the pyrrolidine scaffold were explored. Methyl, methyl ester, hydroxymethyl, phenyl, 3-pyridyl, 5-pyrazolyl and tetrazolyl group were chosen as substituents and they were paired with each other (Figure 2.8). Each disubstituted pyrrolidine gives 14 different isomers and functionalising the nitrogen with H, Me, Ms and Ac gives a 56 members in each library.

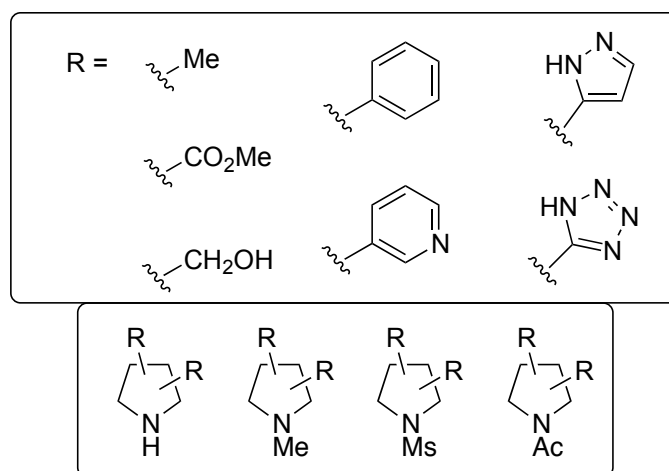


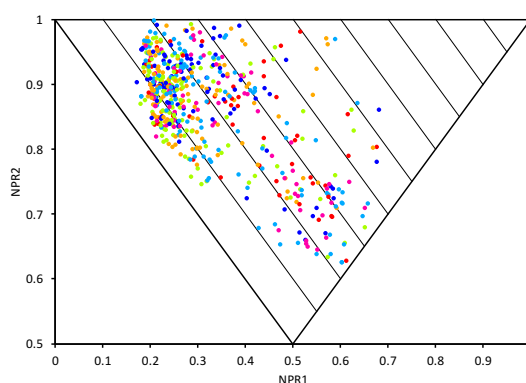
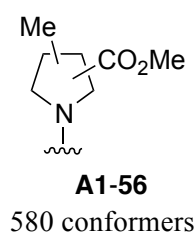
Figure 2.8: Different substituents on the pyrrolidine scaffold.

The substituents shown in Figure 2.8 provide a range of protein-binding interactions. The hydroxymethyl group provides both hydrogen bond donor and acceptor properties. Moreover, it can easily be obtained from the methyl ester series by reduction of the ester. The phenyl group is hydrophobic and can provide π stacking interactions with the proteins. Also, it is the most commonly found ring system in marketed drugs.²⁸

Similarly, a 3-pyridyl group can provide a π stacking interaction with proteins as well as a hydrogen bonding interaction, and also it is a top five commonly found ring system in marketed drugs.²⁸ 5-pyrazolyl and tetrazolyl are also listed as frequently found ring systems in marketed drugs and a tetrazoles provides an acidic protein as it is an isostere of a carboxylic acid.²⁸ Thus, we chose these substituents to evaluate their three-dimensionality.

To start with, the methyl ester group was paired with five other substituents (methyl, phenyl, 3-pyridyl, 5-pyrazolyl and tetrazolyl) and their PMI plots of conformational energy difference ≤ 1.5 kcal mol⁻¹ are shown in Figure 2.9. The tetrazolyl group gave the most conformers (1258 conformers) (Figure 2.9e) whereas the methyl group had the least conformers (580 conformers) (Figure 2.9a). In terms of the shape of their conformers, the four aromatic groups had similar spread over the PMI plot as most the conformers were populated between PMI category 1.1–1.2 (Figure 2.9b-e).

(a)



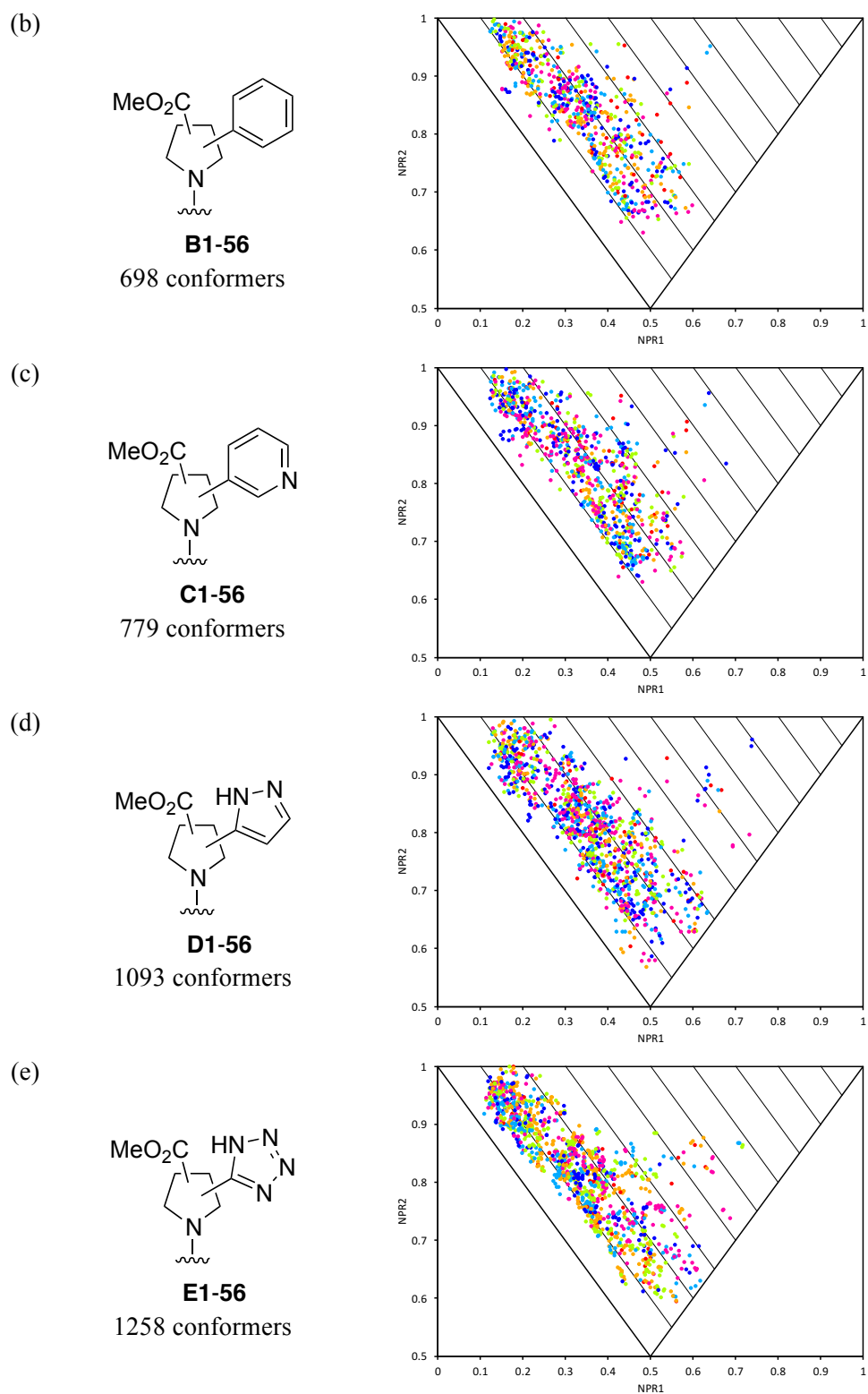


Figure 2.9: PMI plots of the conformations with energy difference $\leq 1.5 \text{ kcal mol}^{-1}$ for methyl ester and five different substituents.

Further analysis was considered in order to determine how many fragments and their conformers had $\Sigma\text{NPRs} \geq 1.4$. These compounds would have the most three-dimensional conformations and therefore would be selected for synthesis. Each disubstituted system with their number of conformers and fragments are listed in Table 2.7. The tetrazolyl and methyl ester disubstituted system (**E1-56**) had the highest number of conformers (22), but they came from only 3 fragments. The methyl and methyl ester disubstituted system (**A1-56**) had the highest number of fragments (8) which gave 18 conformers.

Table 2.7: $\Sigma\text{NPRs} \geq 1.4$ with conformational energy difference $\leq 1.5 \text{ kcal mol}^{-1}$.

Substituent 1	Substituent 2	No. of conformers	No. of fragments
Methyl	Methyl ester	18	8
Phenyl	Methyl ester	8	2
3-Pyridyl	Methyl ester	10	2
5-pyrazolyl	Methyl ester	16	4
Tetrazolyl	Methyl ester	22	3

Using $\Sigma\text{NPRs} \geq 1.4$ as our cut-off, the selected fragments from the new systems are shown as in Figure 2.10. The geminal disubstituted NMs compounds were selected with all systems and the geminal disubstituted NAc appeared in phenyl, 3-pyridyl and 5-pyrazolyl. The 5-pyrazolyl and tetrazolyl systems also included the examples with 2,5-disubstitution. Overall, the geminal disubstituted *N*-substituted sulfonamide fragments in these series had the highest three-dimensional shapes.

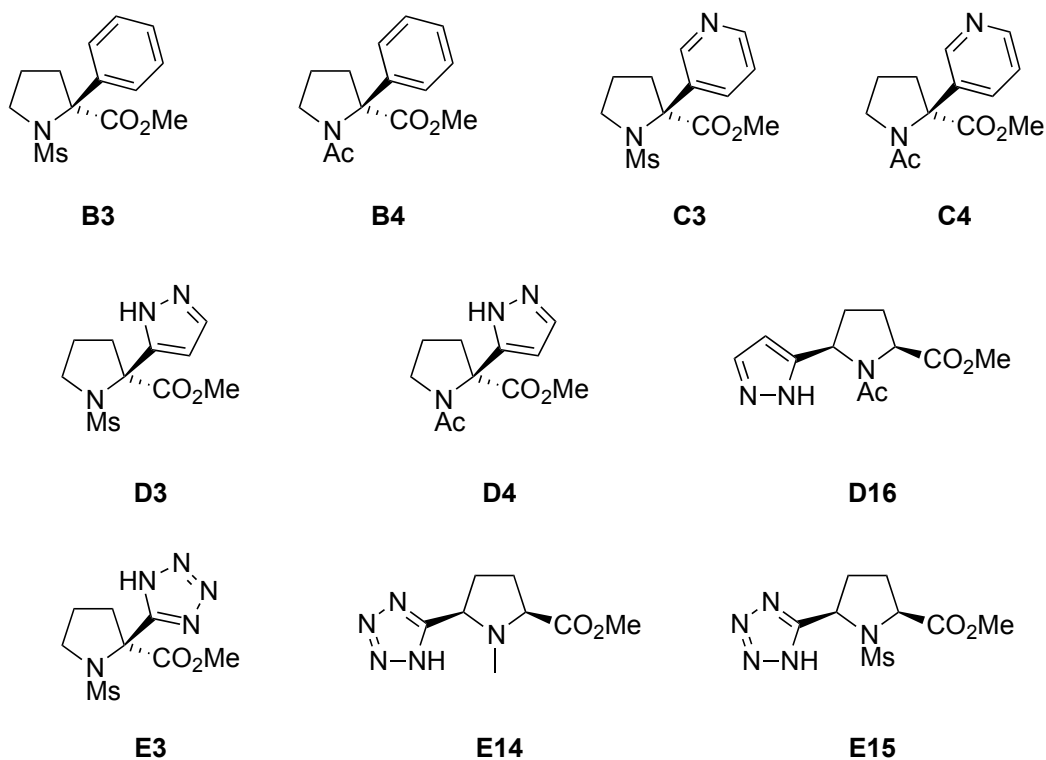
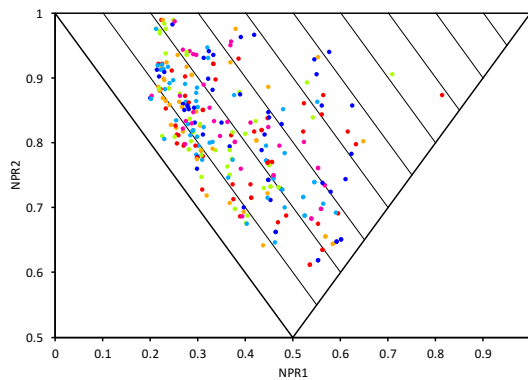
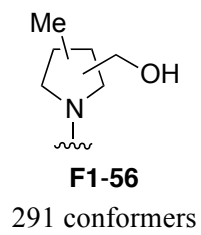


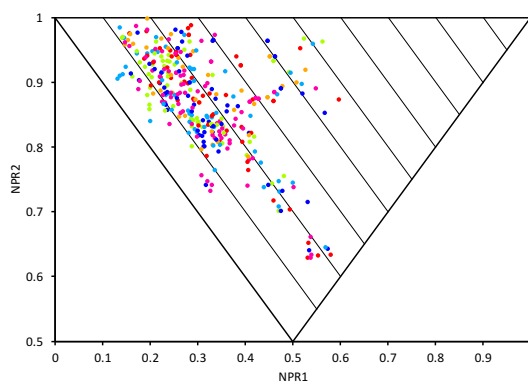
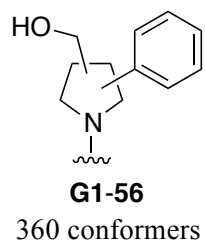
Figure 2.10: Structure of selected fragments from phenyl, 3-pyridyl, 5-pyrazolyl and tetrazolyl.

Next, the hydroxymethyl group was paired with five other substituents (methyl, phenyl, 3-pyridyl, 5-pyrazolyl and tetrazolyl) and their PMI plots for a conformational energy difference $\leq 1.5 \text{ kcal mol}^{-1}$ are shown in Figure 2.11. In these case, the 5-pyrazolyl group had the most conformers (670 conformers) (Figure 2.11d) whereas the methyl group had the least conformers (291 conformers) (Figure 2.11a). In terms of the shape of their conformers, the four aromatic groups had similar spread over the PMI plot as most the conformers were populated between PMI category 1.1–1.2 (Figure 2.11b-e)

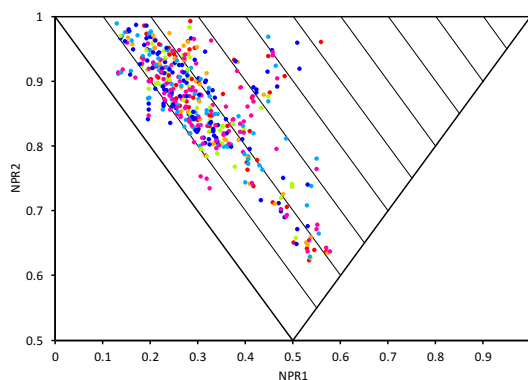
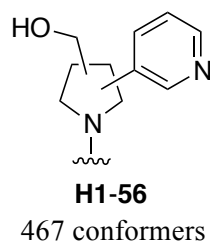
(a)



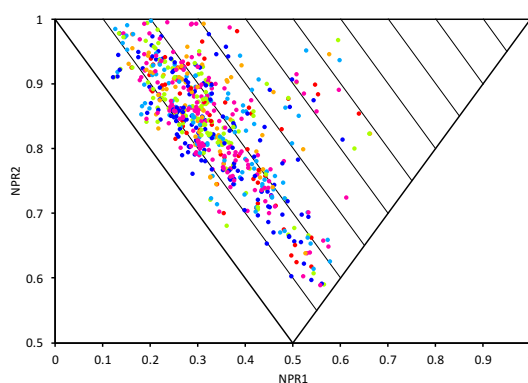
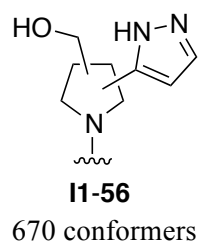
(b)



(c)



(d)



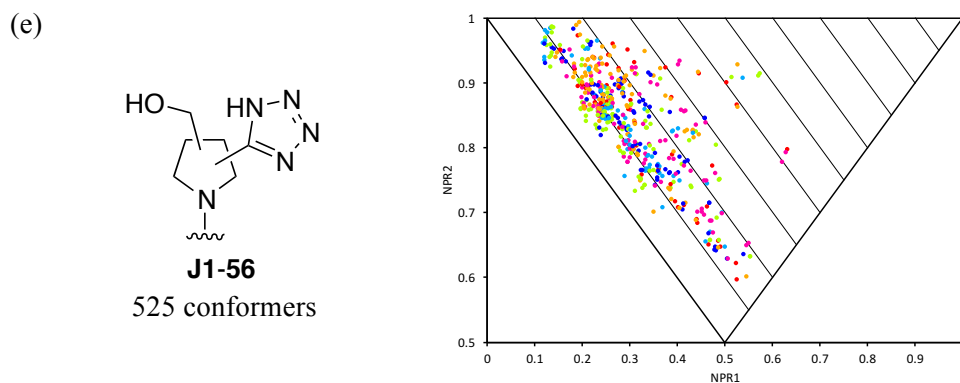


Figure 2.11: PMI plots of conformations with energy difference $\leq 1.5 \text{ kcal mol}^{-1}$ for hydroxymethyl group and five different substituents.

Further analysis was considered to explore how many fragments and their conformers had $\Sigma\text{NPRs} \geq 1.4$. Each disubstituted system with their number of conformers and fragments are summarised in Table 2.8. The phenyl group (**G1-56**) had the highest number of conformers (17) and these were came from only four fragments. The methyl group (**A1-56**) had the highest number of fragments (6) which gave 16 conformers.

Table 2.8: $\Sigma\text{NPRs} \geq 1.4$ with conformational energy $\leq 1.5 \text{ kcal mol}^{-1}$.

Substituent 1	Substituent 2	No. of conformers	No. of fragments
Methyl	Hydroxymethyl	16	6
Phenyl	Hydroxymethyl	17	4
3-Pyridyl	Hydroxymethyl	6	3
5-pyrazolyl	Hydroxymethyl	6	3
Tetrazolyl	Hydroxymethyl	8	3

Using a cut-off of $\Sigma\text{NPRs} \geq 1.4$, the selected methyl and hydroxymethyl disubstituted fragments are shown in Figure 2.12. All 2,2-disubstituted fragments **F1-5**, and 3,3-disubstituted NH fragment **F5** and 2,3-disubstituted NMe fragment **F30** had the highest three-dimensional shapes in this series.

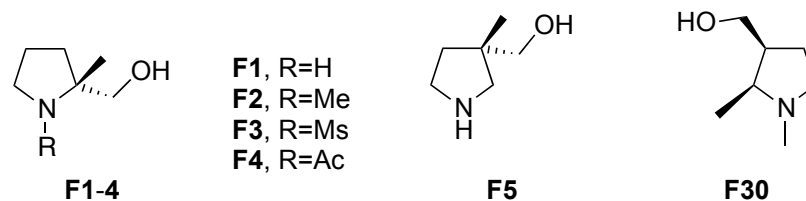


Figure 2.12: Structure of selected methyl and hydroxymethyl disubstituted fragments.

For the aromatic substituents, the selected fragments had similar isomers. Therefore, only the phenyl and 3-pyridyl groups (as representative examples) are shown in Figure 2.13. For both phenyl and 3-pyridyl groups, their 2,2-disubstituted NMs (**G3/H3**) and NAc (**G4/H4**) and 2,5-disubstituted NAc (**G16/H16**) were selected. With a phenyl group, 2,4-disubstituted NAc fragment (**G20**) was also included.

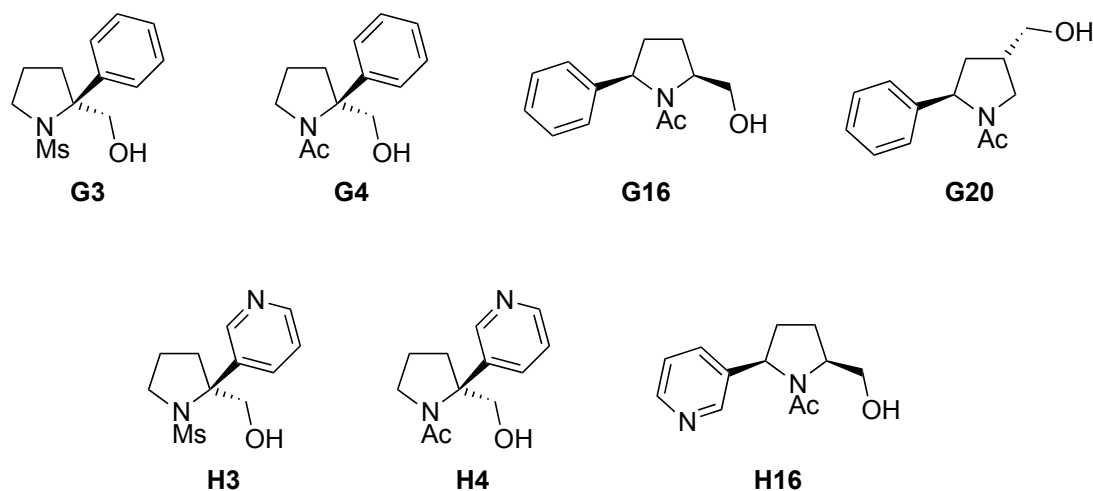
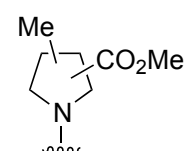


Figure 2.13: Structure of selected phenyl and 3-pyridyl fragments.

Overall, with a hydroxymethyl substituent, the 2,2-disubstituted isomers appeared to give the most three-dimensional shapes. In addition, the non-aromatic substituent gave a better three-dimensional shape of fragments.

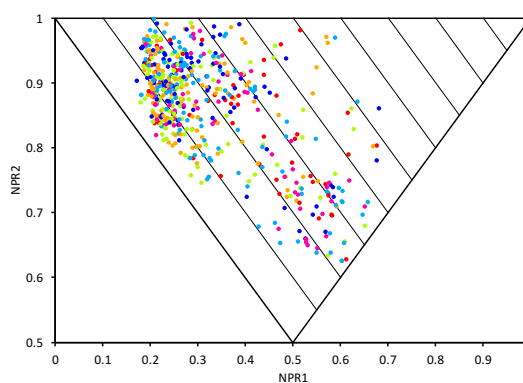
Finally, a methyl group was paired with six other substituents (methyl ester, phenyl, hydroxymethyl, 3-pyridyl, 5-pyrazolyl and tetrazolyl) and their PMI plots for a conformational energy difference ≤ 1.5 kcal mol⁻¹ are shown in Figure 2.14. This time, the 5-pyrazolyl group had the most conformers (670 conformers) (Figure 2.14e) whereas the hydroxymethyl group had the least conformers (291 conformers) (Figure 2.14b). In terms of the shape of their conformers, they aromatic groups had similar spread over the PMI plot as most the conformers were populated between PMI category 1.1–1.2 (Figure 2.14c-f).

(a)

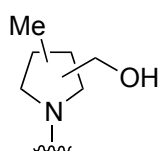


A1-56

580 conformers

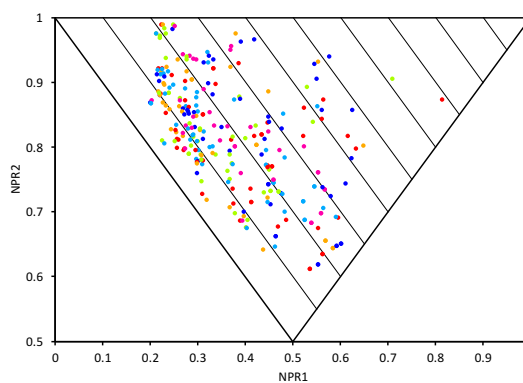


(b)

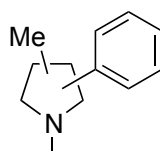


G1-56

291 conformers

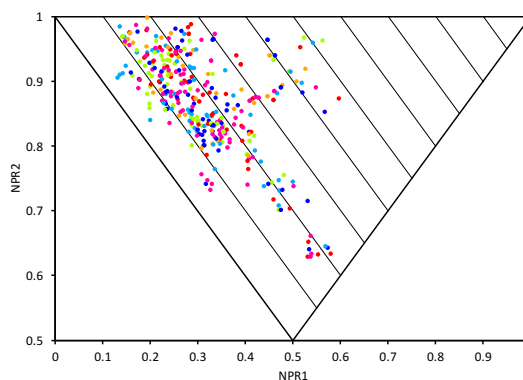


(c)



K1-56

360 conformers



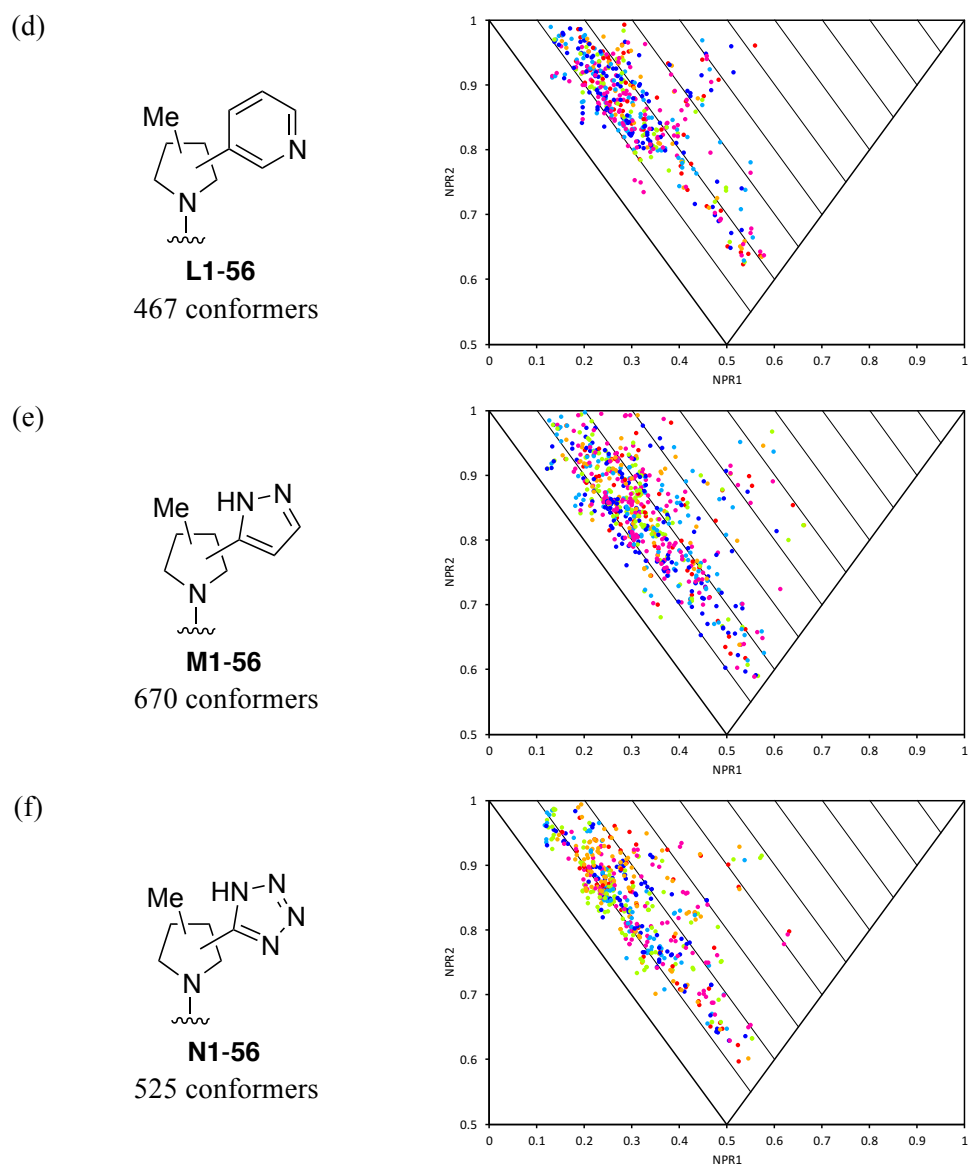


Figure 2.14: PMI plots of conformations energy difference $\leq 1.5 \text{ kcal mol}^{-1}$ for methyl and six different substituents systems.

Analysis of how many fragments and their conformers had $\Sigma\text{NPRs} \geq 1.4$ was investigated next. Each disubstituted system with their number of conformers and fragments are listed in Table 2.9. For the aromatic substituents, the 5-pyrazolyl group (**M1-56**) had the highest number of fragments (3), which gave the most conformers (6).

Table 2.9: $\Sigma\text{NPRs} \geq 1.4$ with conformational energy difference energy conformations ≤ 1.5 kcal mol⁻¹.

Substituent 1	Substituent 2	No. of conformers	No. of fragments
Methyl ester	Methyl	18	8
Phenyl	Methyl	2	1
3-Pyridyl	Methyl	2	1
5-pyrazolyl	Methyl	6	3
Tetrazolyl	Methyl	1	1

For the aromatic substituents, their selected fragments from a cut-off of $\Sigma\text{NPRs} \geq 1.4$ were similar isomers. Their structures are shown in Figure 2.15 and all selected fragments were 2,2-disubstituted isomers.

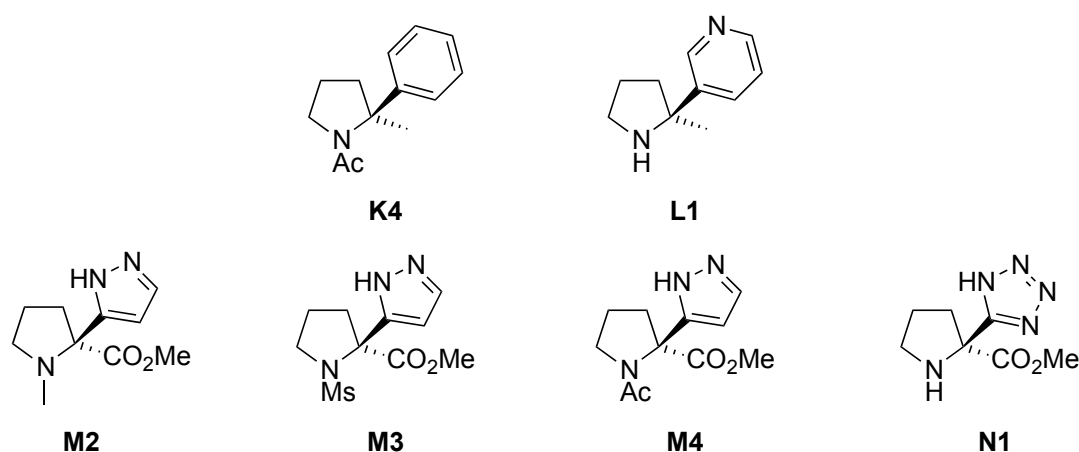


Figure 2.15: Structure of selected aromatic fragments.

Based on all of the analyses of these new systems, we decided to identify a set of fragments for synthetic studies. We chose phenyl and 3-pyridyl fragments due to the expected easier synthesis. The 11 selected fragments and the corresponding PMI plots of their 58 conformations are shown in Figure 2.16. All these fragments were selected based on a PMI cut-off of $\Sigma\text{NPRs} \geq 1.4$.

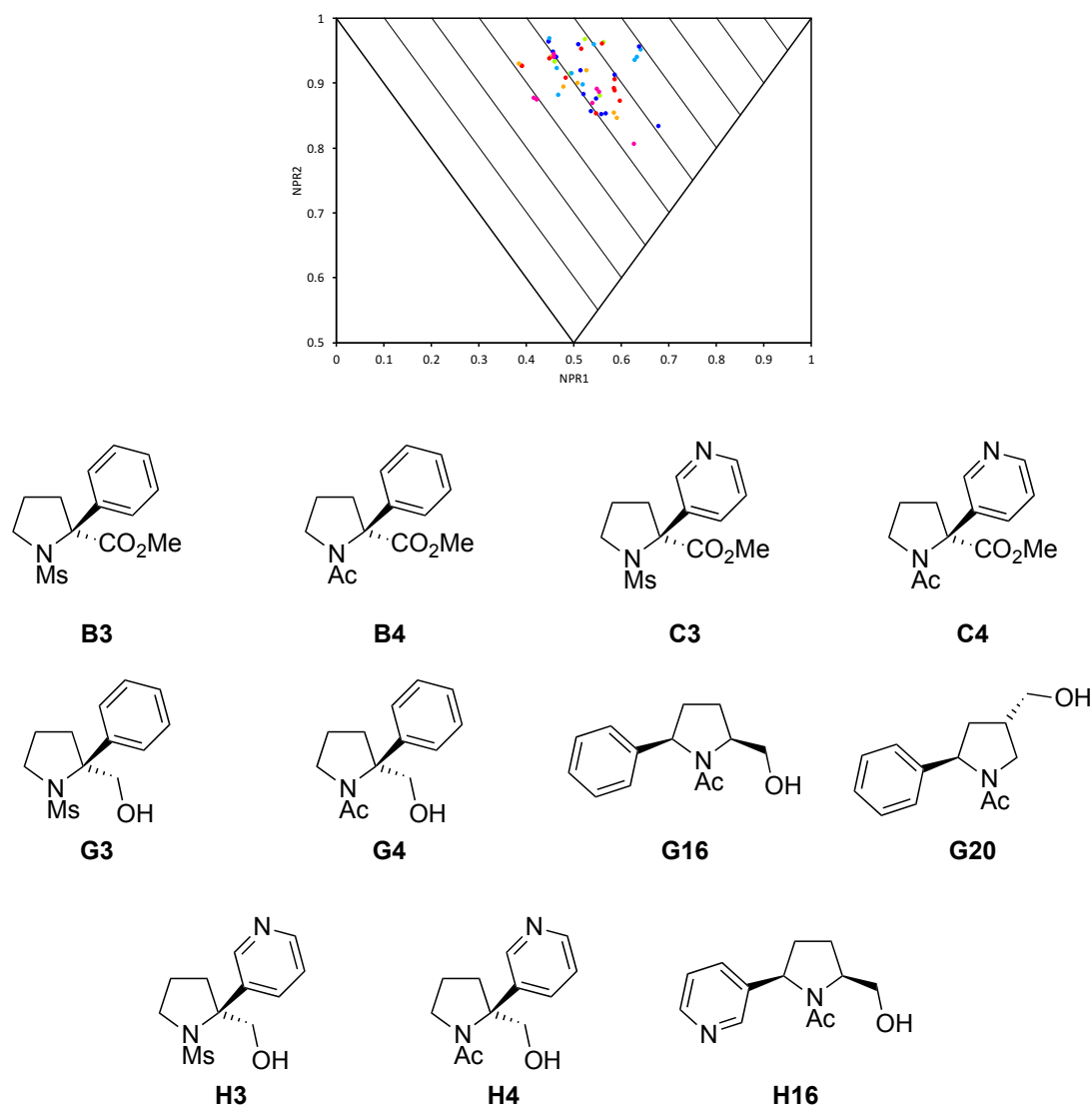


Figure 2.16: The selected 11 pyrrolidine fragments and PMI plot containing their 58 conformations with a relative energy ≤ 1.5 kcal mol⁻¹.

The predicted physicochemical properties of these 11 selected fragments were also evaluated by Pipeline Pilot 8.5 as shown in Table 2.10. Most of the physicochemical properties of the 11 selected fragments fulfilled the ‘rule of three’ criteria and only their HBA and PSA were higher than the criteria.

Table 2.10: The predicated average physicochemical properties of the 11 selected fragment from Pipeline Pilot 8.5.

Physicochemical Properties	Mean
Molecular Weight	243.02
AlogP	0.58
PSA	93.97
HBA & HBD	3.18 (0.63)
HAC	17.1
NROT	2.73
No. of ring (aromatic)	2(1)

2.4 Conclusions

The main conclusions from the chapter are as follows. First, the PMI analysis of the Maybridge fragment library showed that 85% of their compounds were in the PMI category 1–1.2. This means that nearly all of the Maybridge fragments are two-dimensional in shape.

Second, we show that a simply designed pyrrolidine set of fragments with methyl and methyl ester substituents is much more three-dimensional in shape (by PMI analysis) than the Maybridge library. Furthermore, using a PMI cut-off of ≥ 1.36 , 14 fragments were selected for synthesis. Their structures and PMI plot are summarised in Figure 2.7.

Third, the PMI analysis of 13 other pyrrolidine systems showed that addition of aromatic groups generally led to less three-dimensional shapes. However, with a PMI cut-off of ≥ 1.4 , 11 other pyrrolidine fragments were identified for synthetic studies. Their structures and PMI plot are shown in Figure 2.16.

Thus, using a new PMI analysis approach, 25 three-dimensional fragments have been identified. These fragments were designed to not only be three-dimensional, but also to fit the ‘rule of three’ fragment criteria. Overall, the approach of selecting compounds for synthesis based on their three-dimensional shape could be applied and extended to any new fragment scaffold.

Chapter 3: Synthesis of Three-Dimensional Pyrrolidine Fragments

In this chapter, we present our synthetic efforts towards seven of the 25 designed three-dimensional fragments (Figure 3.1). Other members of the O'Brien group have worked on the synthesis of some of the other fragments.

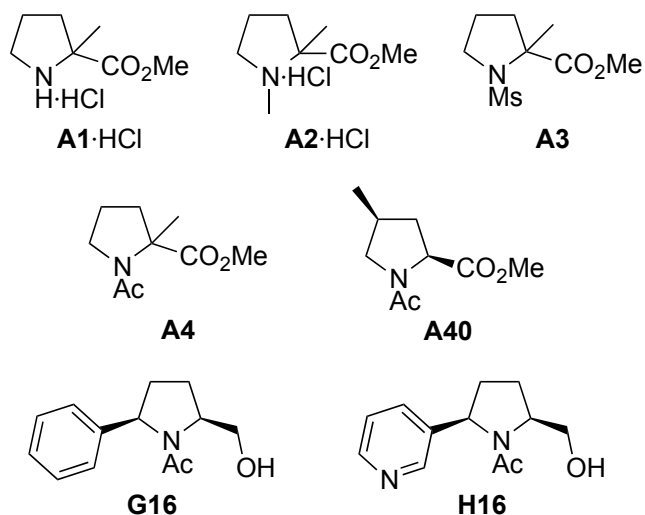


Figure 3.1: The seven of the 25 designed three-dimensional fragments to synthesise.

In Section 3.1, we report our efforts on methods for the *N*-functionalisation of the fragments on a model proline-derived system. The development of a synthetic approach to 2,2-disubstituted fragments **A1·HCl**, **A2·HCl**, **A3** and **A4** is presented in Section 3.2. All four fragments were successfully synthesised. In Section 3.3, the synthesis of 2,4-*cis*-disubstituted pyrrolidine **A40** is described. Finally in Section 3.4, our efforts towards fragments are **G16** and **H16** presented.

3.1 Model Studies on *N*-functionalisation of Pyrrolidine Fragments

For the purpose of increasing the diversity of the compounds in the library, we planned that there would be four different nitrogen substituents: NH, NMe, NMs and NAc (Figure 3.2). The synthetic approaches for installing these *N*-substituents would require the development of a short synthetic route with good yield and without giving any by-products. In this section, *N*-functionalisation methods for adding NH, NMs and NAc groups on a model system will be discussed.

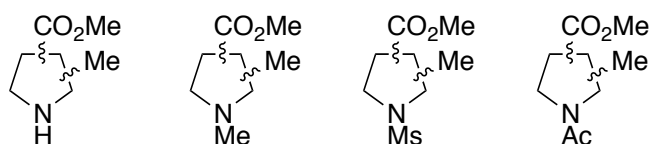
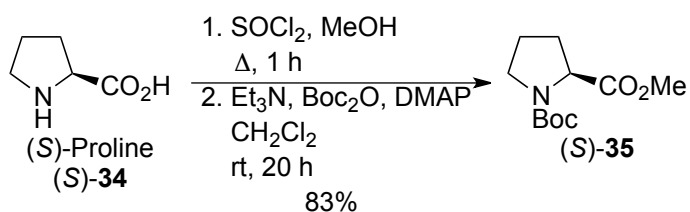


Figure 3.2: The four different nitrogen substituents in the final fragments.

In order to identify suitable methods and conditions for *N*-functionalisation, the *N*-protected, methyl ester pyrrolidine (*S*)-**35** was selected. Using a literature route,³⁹ treatment of (*S*)-proline (*S*)-**34** with thionyl chloride in methanol at reflux formed the methyl ester. The methyl ester intermediate was then treated with triethylamine and Boc_2O to form the *N*-Boc methyl ester (*S*)-**35**. After work-up, purification of the crude product by flash column chromatography gave (*S*)-**35** in 83% yield (Scheme 3.2).

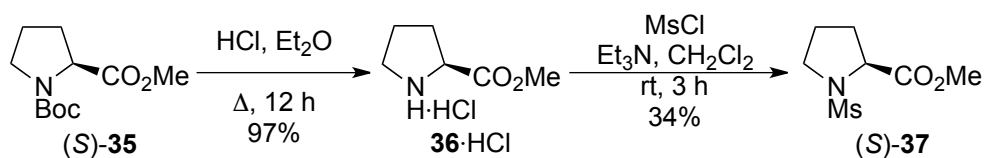


Scheme 3.2: Synthesis of *N*-Boc methyl ester (*S*)-**35**.

The synthesis of *N*-Boc methyl ester (*S*)-**35** was proven by characterisation by ^1H NMR spectroscopy. In the ^1H NMR spectrum, there were two signals at δ 1.42 and

1.37 (9H integration in total) which were assigned to the Boc group. There were two *t*-butyl signals for the Boc group due to rotamers. The methyl ester gave a 3H singlet at δ 3.68. All of the ^1H NMR spectroscopic data matched the literature.⁴⁰

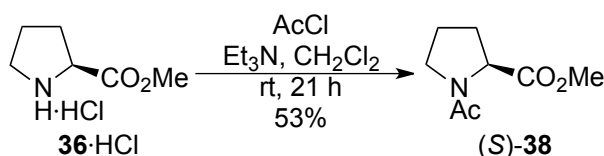
Next, we planned to study the Boc deprotection and subsequent sulfonylation and acylation to from the NMs and NAc groups respectively. The Boc deprotection was achieved by a literature procedure.⁴¹ *N*-Boc methyl ester (*S*)-**35** was treated with hydrochloric acid in Et₂O at reflux for 12 h to give the crude pyrrolidine salt **36**·HCl in 97% yield, which was not fully characterised. The crude pyrrolidine salt **36**·HCl was then reacted with methanesulfonyl chloride and triethylamine. After an aqueous work-up, the crude product was purified by flash column chromatography to give sulfonamide (*S*)-**37** in 34% yield (Scheme 3.3).



Scheme 3.3: Synthesis of sulfonamide (S)-37.

In the ^1H NMR spectrum of sulfonamide (*S*)-**37**, the disappearance of the two rotameric singlets at δ 1.42 and 1.37 were the first piece of information showing that a new product had formed. There was also a 3H multiplet at δ 4.47-4.4 which was assigned to the proton α to the ester. The ^{13}C NMR spectrum of (*S*)-**37** showed a CH₃ signal at δ 39.1 due to the newly installed methanesulfonyl group. These spectroscopic data matched with those reported in the literature.⁴²

Similarly, the synthesis of acetamide (*S*)-**38** was carried out using acetyl chloride and triethylamine. Following an aqueous work-up and purification of the crude product by flash column chromatography, (*S*)-**38** was isolated in 53% yield from hydrochloride salt **36**·HCl (Scheme 3.4).



Scheme 3.4: Synthesis of acetamide (S)-38.

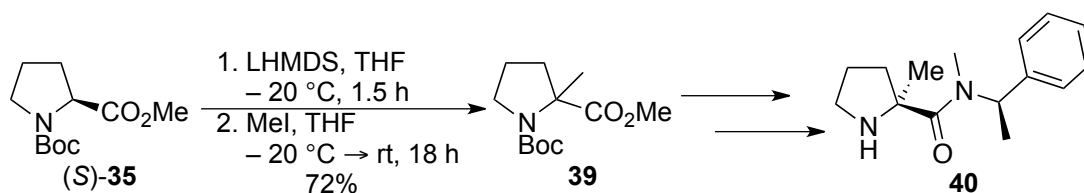
The synthesis of acetamide (*S*)-**38** was confirmed by ^1H NMR spectroscopy. In the ^1H NMR spectrum, there were two singlets at δ 2.06 and 1.94 (3H integration in total) which were assigned to the methyl protons in the acetamide. There were two acetyl groups due to rotamers. The proton α to the ester gave two rotameric sets of double doublets at δ 3.45 and 3.35. The ^{13}C NMR spectrum of (*S*)-**38** showed a CH_3 signal at δ 22.3 due to the acetyl moiety. These spectroscopic data matched with those reported in the literature data.⁴³

Thus, suitable conditions for Boc deprotection, sulfonylation and acetamide formation have been identified. However, the yields of sulfonamide (*S*)-**37** (34%) and acetamide (*S*)-**38** (53%) were unfortunately not very high. It was decided not to optimise these conditions further on the model system, but to move on to the real fragment system.

3.2 Synthesis of 2,2-Disubstituted Pyrrolidine Fragments

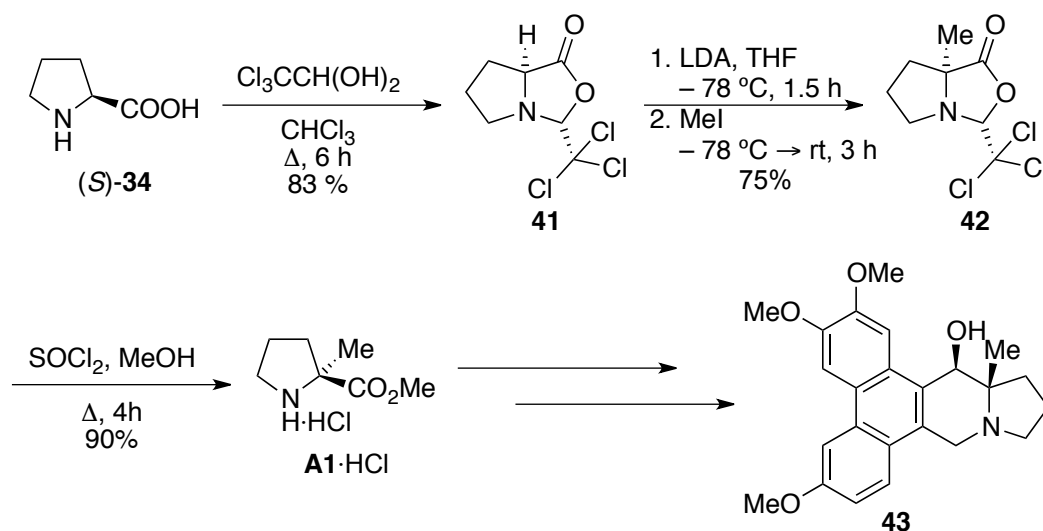
3.2.1 Previous Routes to 2,2-Disubstituted Pyrrolidines with Methyl and Methyl Ester Groups

In 2010, Kelleher *et al.* described a method for the direct alkylation of *N*-Boc proline methyl ester (*S*)-**35** as a synthetic strategy to form spirocyclic lactams and α -methyl prolinamides **40**. These 2,2-disubstituted pyrrolidines, such as **40**, were used as organocatalysts in asymmetric Michael addition reactions. Methyl ester (*S*)-**35** was treated with LHMDS at $-20\text{ }^{\circ}\text{C}$ to give the enolate. Subsequently, trapping with methyl iodide gave the 2,2-disubstituted pyrrolidine **39** in 72% yield (Scheme 3.5). The racemic product was formed because the reaction went *via* a planar enolate, and the electrophile could attack from either side of the molecule with equal chance.



Scheme 3.5: Synthesis of 2,2-disubstituted pyrrolidine rac-40 via enolate formation and electrophile trapping.

An asymmetric synthesis of 2,2-disubstituted pyrrolidines was developed by Seebach *via* the stereoselective alkylation of amino acid derivatives.⁴⁴ This method was adapted by Su *et al.* for one of the key steps in the synthesis of hypoestestatin **43**.⁴⁵ In this synthesis programme, (*S*)-proline (*S*)-**34** was reacted with chloral hydrate to give the oxazolidinone **41** in 83% yield. This was followed by the addition of LDA at $-78\text{ }^{\circ}\text{C}$ to form the enolate, which allowed the trapping with methyl iodide to give oxazolidinone **42** in 75% yield. Then, the oxazolidinone ring was cleaved by treatment with thionyl chloride to form the 2,2-disubstituted pyrrolidine salt **A1**·HCl as a single enantiomer in 98% yield (Scheme 3.6).

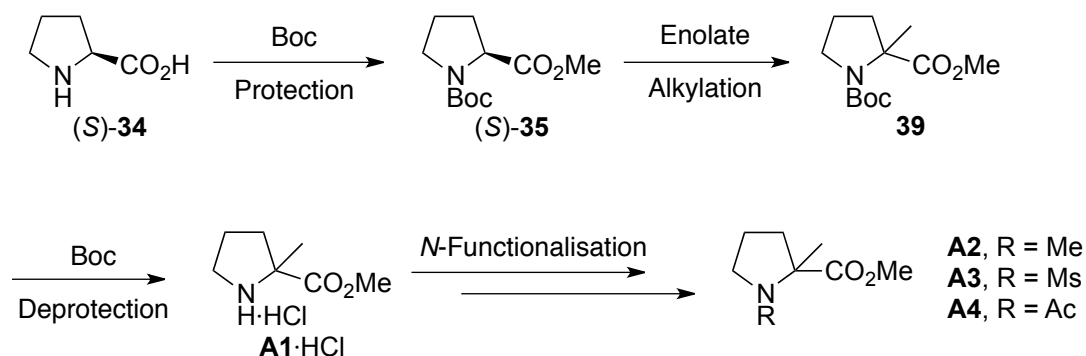


Scheme 3.6: Synthetic steps in the attempted synthesis of hypoestestatin **43**.

With Seebach's relay of chirality approach, chloral hydrate was used to retain the chirality of (*S*)-proline. After the enolate has formed, only one face of the molecule is available for trapping with the electrophile. Subsequently, cleavage of the ring system allowed the formation of the enantiopure pyrrolidine salt **A1·HCl**.

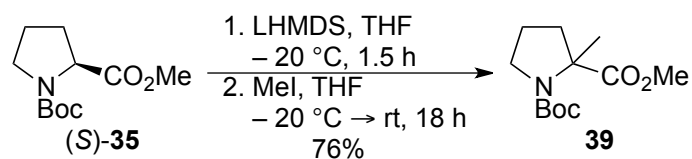
3.2.2 Synthesis of 2,2-Disubstituted Pyrrolidines with Methyl and Methyl Ester Groups

As described in the previous section, the 2,2-disubstituted pyrrolidines could be synthesised by enolate formation from (*S*)-proline (**S**)-**34** and then trapping with an appropriate electrophile. Therefore, the synthetic plan for the first fragments of the series would begin with the Boc-protected methyl ester (**S**)-**35** formed from (*S*)-proline (**S**)-**34**. Then, enolate formation and trapping with methyl iodide would give the geminal alkyl substitution to form **39**. Subsequent Boc deprotection would give the first fragment pyrrolidine salt **A1·HCl** and further *N*-functionalisation with three substituents (NMe, NMs, and NAc) would give fragments **A2**, **A3** and **A4** accordingly (Scheme 3.7).



Scheme 3.7: Proposed synthesis of A1-4.

The enolate alkylation step was investigated first. Deprotonation of methyl ester (S)-**35** to form the lithium enolate was carried out with LHMDS in THF at $-20\text{ }^{\circ}\text{C}$ based in the procedure reported by Kelleher *et al.*³⁹ (see Scheme 3.3). Then, methyl iodide was added at $-20\text{ }^{\circ}\text{C}$ to allow the enolate to trap the electrophile and to attach the methyl substituent. The crude product was purified by flash column chromatography and a 76% yield of **39** was obtained (Scheme 3.8).



Scheme 3.8: Enolate alkylation to give methylated Boc protected methyl ester **39**.

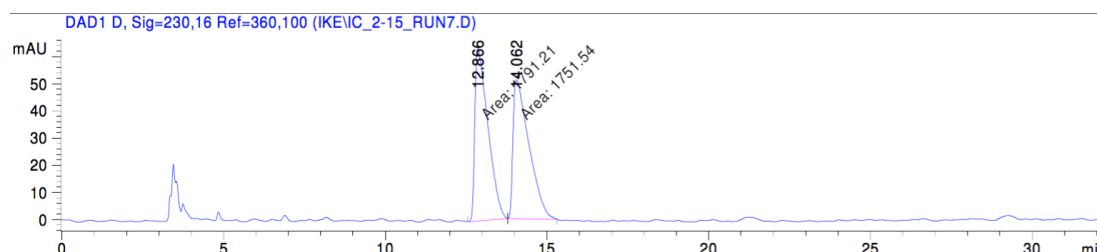
The yield for the enolate alkylation with LHMDS varied depending on the scale of the reaction (Table 3.11). With smaller scale reactions (1.5–2.5 mmol scale), the yield was less than 40% (entries 1-3). On larger scales (4.8–21.5 mmol), the yield improved to around 70% (entries 4–6). This may be due to the presence of small amounts of water in the set-up having a larger effect on the yield of the smaller scale reactions.

Table 3.11: Effect of scale on the yield of the enolate alkylation.

Entry	Scale (mmol)	Yield (%)
1	1.53	32
2	2.18	32
3	2.50	37
4	4.79	68
5	8.71	76
6	21.5	68

The synthesis of **39** was proven by characterisation by ^1H NMR spectroscopy. In the ^1H NMR spectrum, there were two singlets at δ 1.47 and 1.40 (3H in total, rotamers) which were assigned to the newly introduced methyl group. The ^{13}C NMR spectrum of **39** showed two CH_3 signals at δ 22.9 and 22.3 which were due to rotamers.

Since this reaction proceeded *via* an enolate, the alkylated product **39** should be racemic. To confirm that **39** was racemic, the optical rotation was measured. This did not confirm that the sample was racemic because *N*-Boc ester **39** had an optical rotation value, $[\alpha]_{\text{D}}$, of -0.97 (c 1.0 in CHCl_3). Therefore, chiral HPLC was carried out to determine the enantiomeric ratio of the sample. The chiral-HPLC was recorded with a Chiralpak® ID column, eluting with 95:5 hexane-*i*-PrOH (1 mL min^{-1}) and the result showed that **39** was formed as a 51:49 mixture of enantiomers (Figure 3.3).

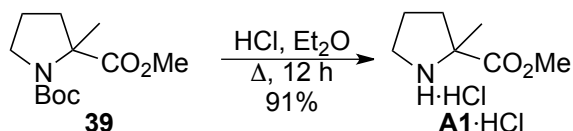


Signal 4: DAD1 D, Sig=230,16 Ref=360,100

Peak #	RetTime [min]	Type	Width [min]	Area [mAU*s]	Height [mAU]	Area %
1	12.866	MM	0.4688	1791.20947	63.67430	50.5599
2	14.062	MM	0.5709	1751.53662	51.13630	49.4401
Totals :				3542.74609	114.81060	

Figure 3.3: CSP-HPLC chromatogram of **39**.

In the final synthetic steps towards **A1-4**, Boc deprotection would be next and then the various *N*-functionalisations would be carried out to give **A2-4**. The Boc deprotection of **39** was achieved by treating **39** with hydrochloric acid in Et₂O at reflux for 12 h. This gave pyrrolidine salt **A1**·HCl in 91% yield (Scheme 3.9). Salt **A1**·HCl was collected as a crude product, as it had good purity.



Scheme 3.9: Boc deprotection of **39** to give crude pyrrolidine salt **A1**·HCl.

The purity and characterisation of pyrrolidine salt **A1**·HCl was proven by ¹NMR spectroscopy (Figure 3.4). In the ¹H NMR spectrum, there were two broad peaks at δ 10.69 and 9.47 which were assigned to the two protons on the nitrogen. These signals appeared far downfield due to the positive charge on the nitrogen which means that these protons experience far less shielding. The diastereotopic pair of protons α to nitrogen appeared as a 2H multiplet at δ 3.68-3.58. Also, there was no signal due to the Boc group. In the ¹³C NMR spectrum, there was a CH₂ signal at 46.5 which was

assigned to the NCH₂ carbon. All results indicated that fragment **A1**·HCl had been successfully synthesised.

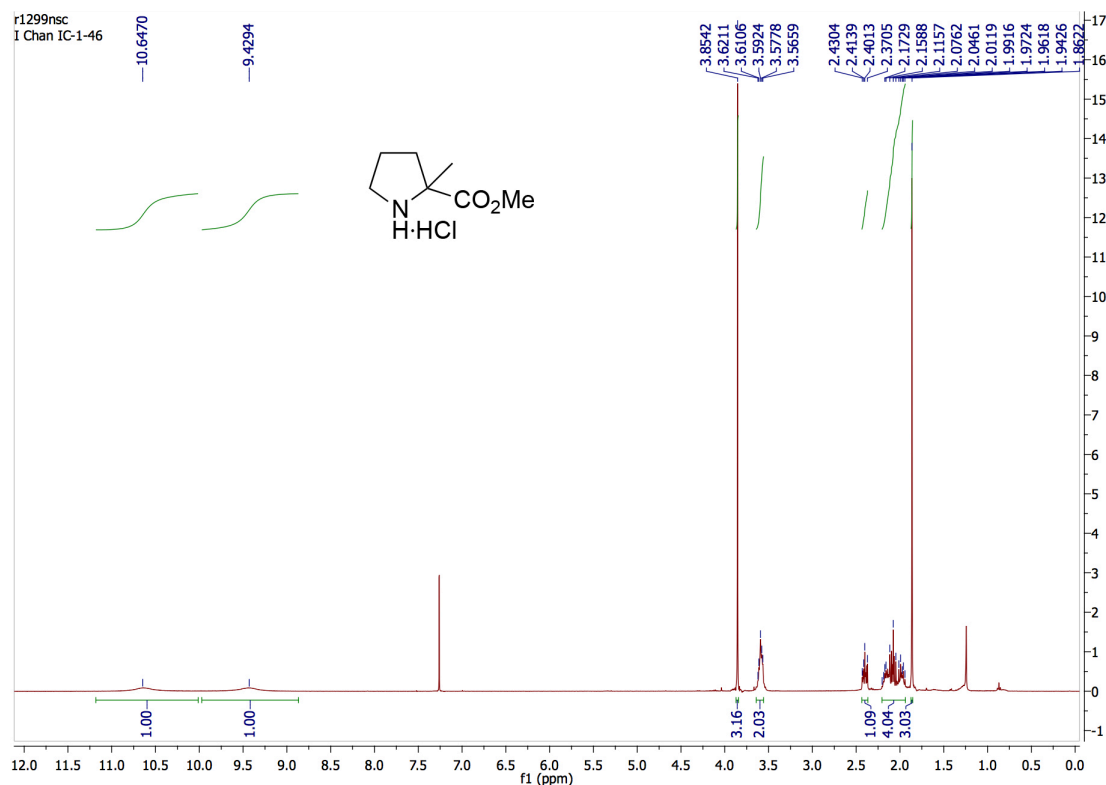
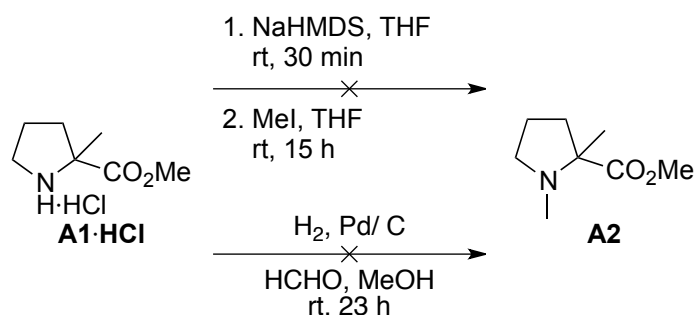


Figure 3.4: ¹H NMR spectrum of **A1**·HCl.

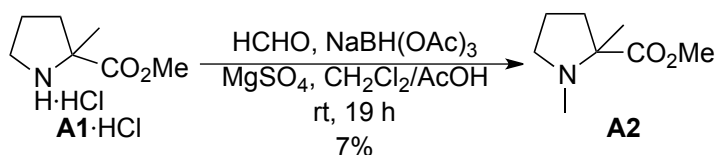
The amine methylation was investigated next. The first attempted synthesis of **A2** followed a related literature reaction⁴⁶ using NaHMDS as the base and methyl iodide to achieve *N*-methylation. Pyrrolidine salt **A1**·HCl was reacted with 2 equivalents of NaHMDS in THF for 30 min. Subsequently, methyl iodide was added and the reaction was left to react for 15 h. After aqueous work-up, the crude product was purified by flash column chromatography. However, no product was isolated (Scheme 3.10). Another attempted synthesis of **A2** used catalytic reductive amination with palladium on carbon.⁴⁷ In this reaction, pyrrolidine salt **A1**·HCl was reacted with catalytic 10 wt.

% Pd/C and 1.1 equivalents of formaldehyde solution in methanol under a hydrogen atmosphere for 23 h. The reaction mixture was filtered through Celite[®] and the filtrate was evaporated and subjected to ¹H NMR spectroscopy. However, there was no product found in the sample.



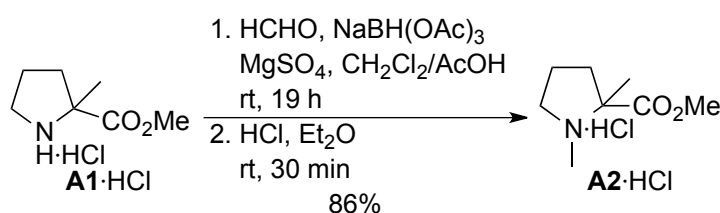
Scheme 3.10: Failed examples of synthesis of methylamine A2.

The synthesis of NMe fragment **A2** was finally achieved by using a different reductive amination procedure from the literature.⁴⁸ In the initial attempt, pyrrolidine salt **A1**·HCl was reacted with sodium triacetoxyborohydride and formaldehyde in a 4:1 mixture of AcOH and CH₂Cl₂ in the presence of MgSO₄ for 19 h. After work-up with ammonia solution, the crude product was purified by flash column chromatography, but it only gave a 7% yield of methylamine **A2** (Scheme 3.11). It was believed that the very low yield was because **A2** was in fact volatile.



Scheme 3.11: Synthesis of methylamine A2·HCl with sodium triacetoxyborohydride and formaldehyde.

To overcome the problem of methylamine **A2** being volatile, it was decided to form the hydrochloride salt from the crude amine product. Thus, in a separate experiment, salt **A1**·HCl was reacted with sodium triacetoxyborohydride and formaldehyde under the usual conditions. Then, the crude product was stirred with hydrochloric acid for 30 min to form methylamine salt **A2**·HCl immediately after the work-up. In this way, methylamine salt **A2**·HCl was isolated in 86% yield (Scheme 3.12).



*Scheme 3.12: Synthesis of methylamine salt **A2**·HCl using sodium triacetoxyborohydride and formaldehyde.*

To confirm the structure of **A2**·HCl, characterisation by ¹H NMR spectroscopy in CDCl₃ was attempted. However, the signals were broad and unclear. Therefore, the NMR solvent was changed to deuterated methanol, which gave a better resolved spectrum. The ¹H NMR spectrum of **A2**·HCl in deuterated methanol is shown in Figure 3.5. In the ¹H NMR spectrum, there was a 3H singlet at δ 3.33 assigned to the newly formed *N*-methyl group. Also, there was a singlet with 3H integration at δ 3.87, which was assigned to the methyl ester group. In the ¹³C NMR spectrum, there was a signal at δ 36.6, which was assigned to the newly formed *N*-methyl group. The signal at δ 54.5 was assigned the methyl ester group (Figure 3.5).

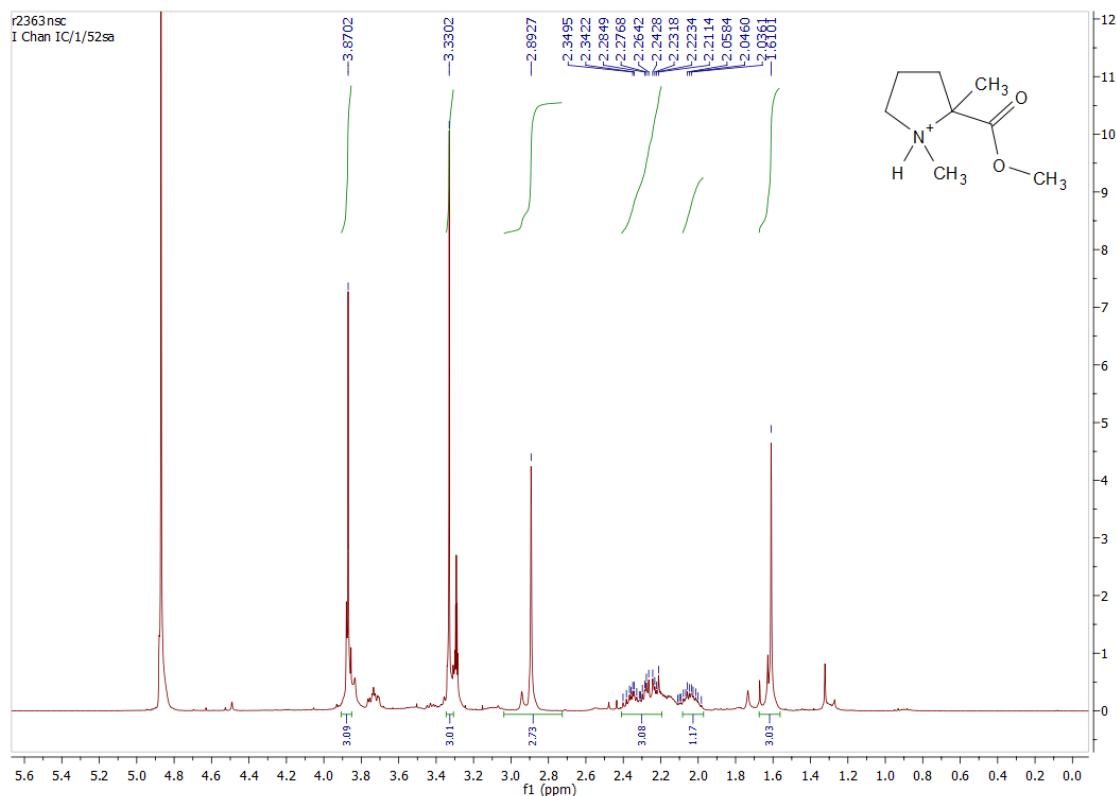
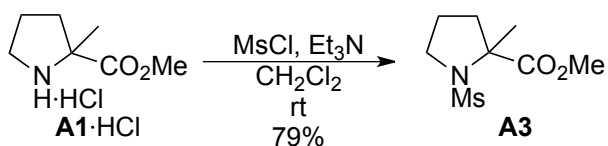


Figure 3.5: ^1H NMR spectrum of $\text{A2}\cdot\text{HCl}$.

The final two fragments in this series were prepared using the conditions from the model study. The synthesis of *N*-sulfonamide **A3** was achieved by the reaction of pyrrolidinium salt **A1** $\cdot\text{HCl}$ with methanesulfonyl chloride and triethylamine in CH_2Cl_2 . Then, aqueous work-up and purification of the crude product by flash column chromatography yielded sulfonamide **A3** with 79% yield (Scheme 3.13).



Scheme 3.13: Synthesis of sulfonamide **A3**.

The synthesis of sulfonamide **A3** was proven by characterisation by ^1H NMR spectroscopy. The ^1H NMR spectrum of **A3** in CDCl_3 is shown in Figure 3.6. In the ^1H NMR spectrum of sulfonamide **A3**, there was a 3H singlet at δ 2.92 due to the methanesulfonyl group. The ^{13}C NMR spectrum showed a CH_3 at δ 39.6, which corresponded to the methanesulfonyl group. In the IR spectrum, there were two $\text{S}=\text{O}$ stretches at 1319 and 1140 cm^{-1} .

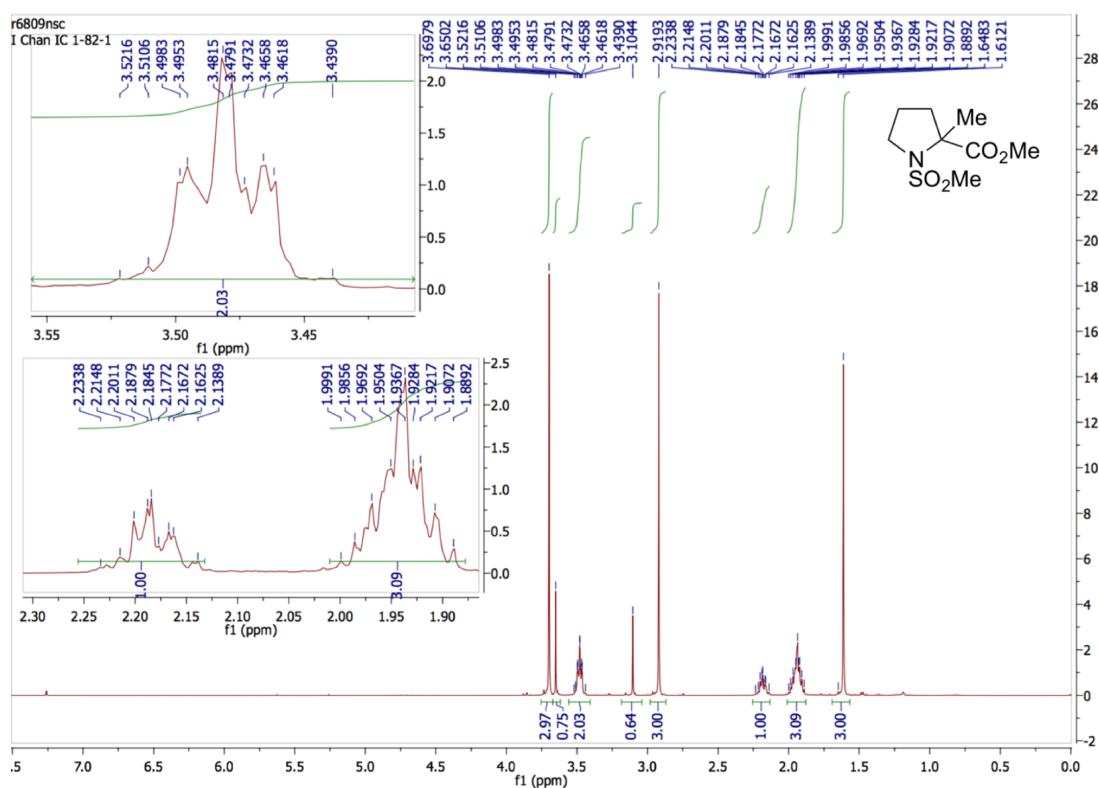
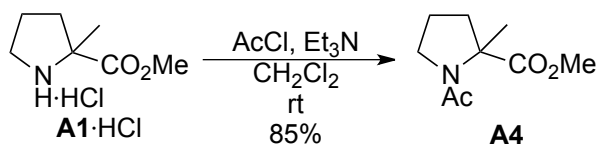


Figure 3.6: ^1H NMR spectrum of sulfonamide **A3**.

The procedure for the formation of acetamide **A4** was similar to the synthesis of sulfonamide **A3**. Pyrrolidine salt **A1**-HCl was reacted with acetyl chloride and triethylamine in CH_2Cl_2 . Following an aqueous work-up and purification of the crude

product by flash column chromatography, acetamide **A4** was obtained in 85% yield (Scheme 3.14).



Scheme 3.14: Synthesis of acetamide **A4**.

The synthesis of acetamide **A4** was proven by characterisation by the ^1H NMR spectroscopy. In the ^1H NMR spectrum (Figure 3.7), there was a singlet at δ 2.00 (3H integration) that was assigned to the acetyl group. In the ^{13}C NMR spectrum, the signal at δ 168.9 was due to the acetyl carbonyl group and the signal at δ 23.1 was assigned to the CH_3 in the acetyl group. In the IR spectrum, there were two carbonyl stretches at 1736 and 1641 cm^{-1} , which were due to the ester and acetyl groups respectively.

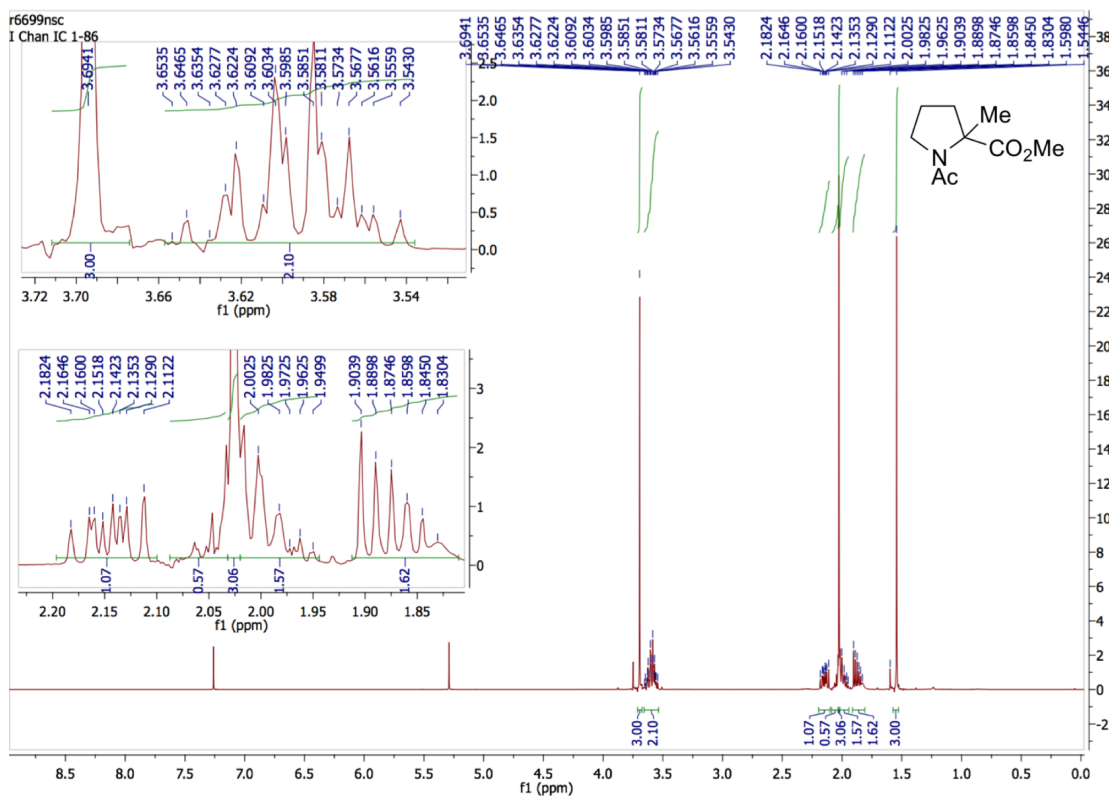
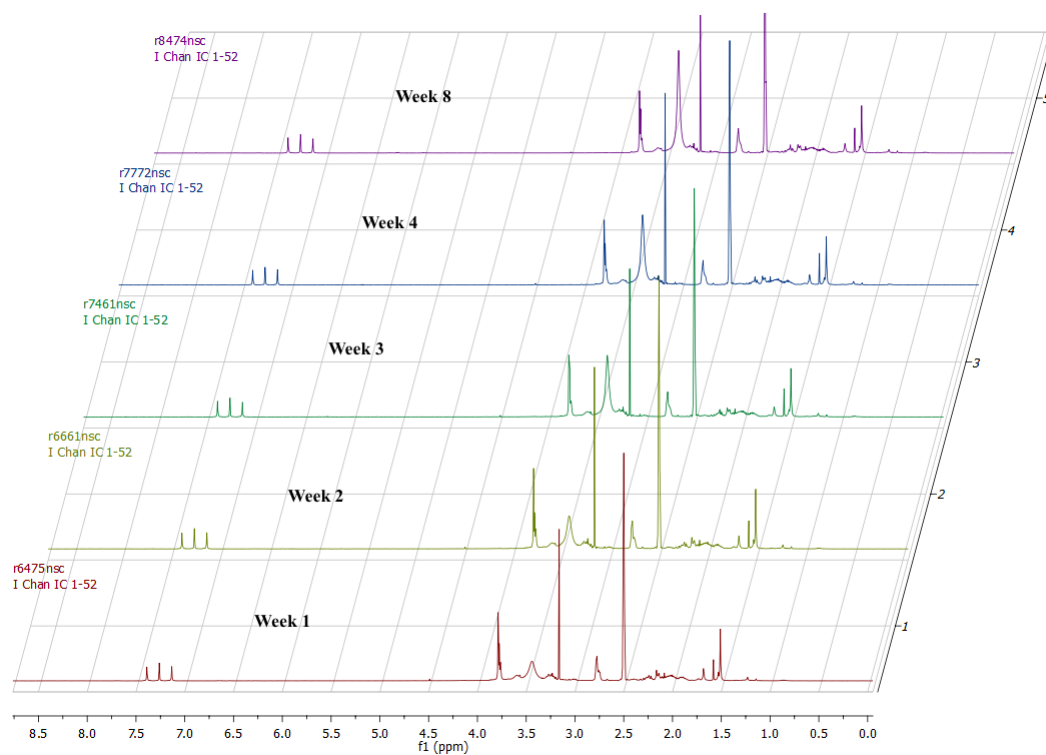


Figure 3.7: ^1H NMR spectrum of acetamide **A4**.

Thus, we have developed synthetic routes to four pyrrolidine fragments, salt **A1**·HCl, methylamine salt **A2**·HCl, *N*-sulfonamide **A3** and *N*-acetyl **A4**. The syntheses proceed in a short number of steps which are high yielding. We were able to prepare 175–1000 mg of the fragments and they had good purity. Therefore, the fragments were stored and are available for fragment screening with proteins.

3.2.2 Evaluation of the Stability of Fragments

It was necessary to store the fragments for a period of time. Thus, it was very important to investigate their stability upon storage. In order to do this, a stability test was carried out on one of the fragments, methylamine salt **A2**·HCl, using ¹H NMR spectroscopy over two months and it was kept at room temperature. For the preparation of the test sample, 5 mg of fragment **A2**·HCl was weight out and dissolved in deuterated DMSO solvent.



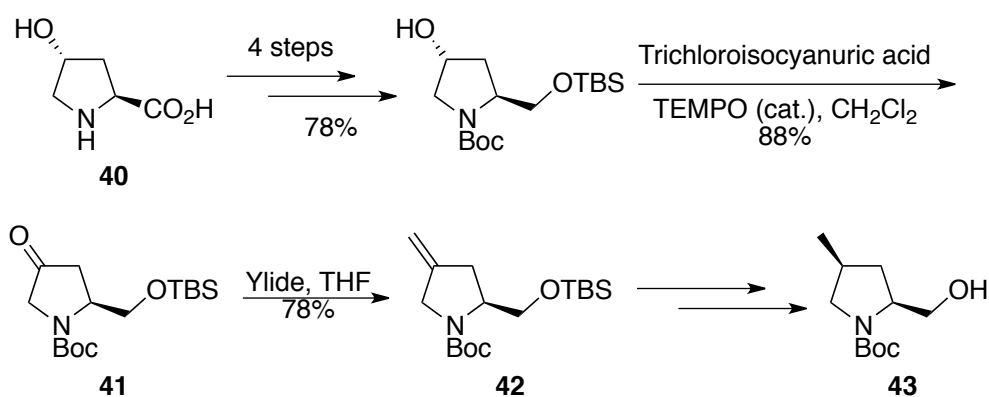
*Figure 3.8: Stability test of the methylamine salt **A2**·HCl.*

This sample was inspected by ¹H NMR spectroscopy after 1, 2, 3, 4 and 8 weeks. The results from these ¹H NMR spectra (Figure 3.8) were that the peaks and the ratio of sample to the solvent remained unchanged over the two-month period. Therefore, we concluded that the methylamine salt **A2**·HCl was stable. This method for testing fragment stability was applied for monitoring the fragment collection in the group.

3.3 Synthesis of a *cis*-2,4-Disubstituted Pyrrolidine Fragment

3.3.1 Previous Routes to 2,4-*cis*-Disubstituted Pyrrolidines and Pyrrolidinones with Methyl and Methyl Ester Groups

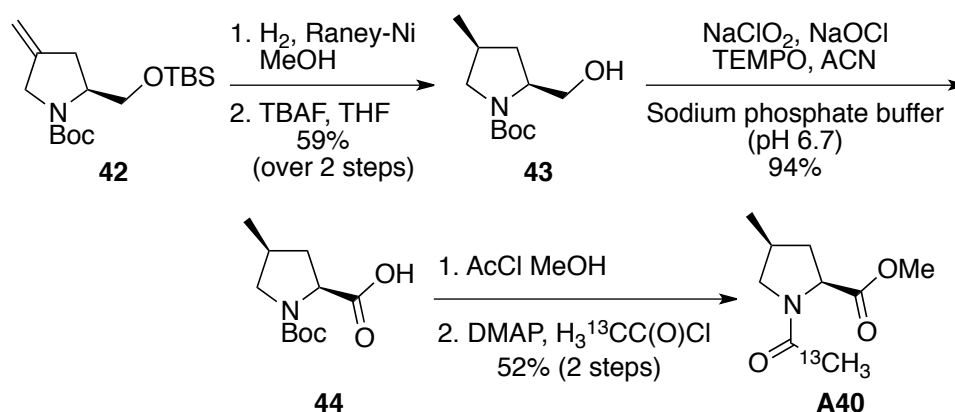
In 2003, Goodman and colleagues⁴⁹ developed a method for the synthesis of Boc protected prolinol **42** via a divergent asymmetric hydrogenation strategy from *trans*-4-hydroxyproline **40** (Scheme 3.15). The synthesis of the key ketone intermediate **41** proceeded via Boc protection of free amino acid **40**, reduction and selective protection of the primary alcohol with TBDMSCl. This was then oxidised using trichloroisocyanuric acid and catalytic TEMPO to form pyrrolidinone **41** in 88% yield. Subsequently, a Wittig reaction of pyrrolidinone **41** with the corresponding triphenylphosphorane afforded TBS protected prolinol **42** in 78% yield.



Scheme 3.15: Synthesis of prolinol **42**.

This method was adapted by Shoulders *et al.*⁵⁰ to prepare the acetamide **A40** (Scheme 3.16). To start, prolinol **42** was hydrogenated and silyl ether deprotection gave free prolinol **43** in 59% over 2 steps. The *cis*-diastereoselectivity results from attack of the hydrogen on the face of the alkene opposite to the sterically bulky silyloxymethyl

group. Subsequent oxidation of the free prolinol **43** by TEMPO formed Boc-protected carboxylic acid **44** in 94% yield, which allowed the acetylation and methyl ester formation to give acetamide **A40** in 52% yield over 2 steps. In this work, the acetylation was carried out using ^{13}C -labelled acetyl chloride to give ^{13}C -labelled acetamide **A40**.

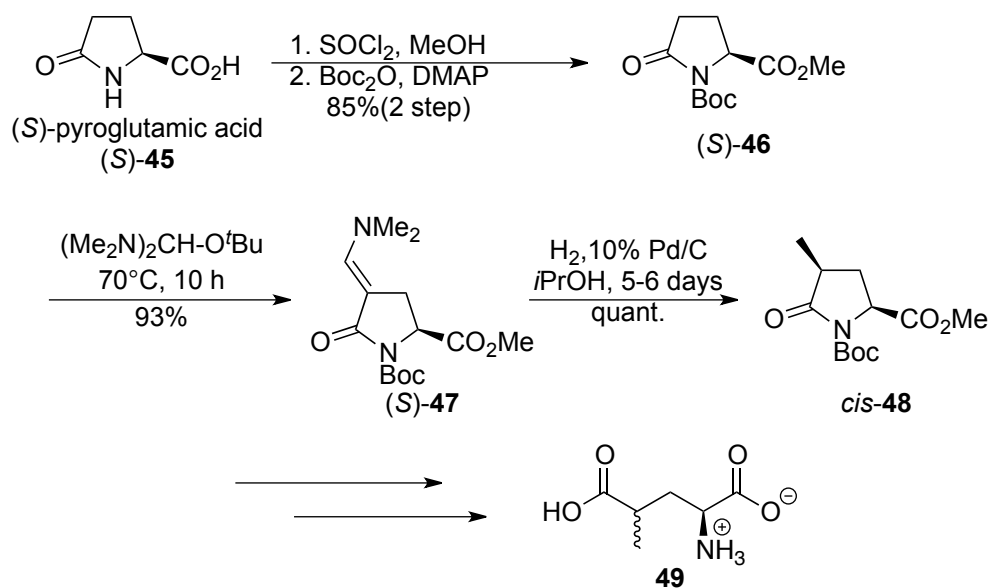


Scheme 3.16: Synthesis of acetamide **A40**.

This approach allows formation of the 2,4-*cis*-disubstituted acetamide **A40** with good yield. However, this required a long synthesis route for obtaining the desired product and other routes have been reported.

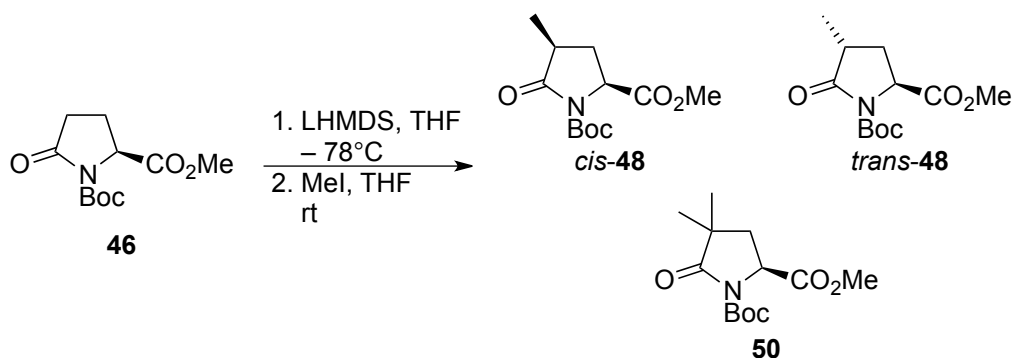
In 1997, Coudert *et al.*⁵¹ investigated the synthesis of methylglutamic acid **49** starting from the pyrrolidinone derivative, pyroglutamic acid (Scheme 3.17). (*S*)-Pyroglutamic acid (*S*)-**45** was protected by esterification with thionyl chloride in methanol and *tert*-butyloxycarbonylation to give (*S*)-**46** in 85% yield over 2 steps. This was followed by reaction of protected pyroglutamate (*S*)-**46** with Bredereck's reagent to afford enaminone (*S*)-**47** with 93% yield. This allowed the catalytic hydrogenation by

palladium on carbon to give a quantitative yield of methylglutamic acid *cis*-**48** after 5-6 days reaction time. As in the previous route, complete *cis*-diastereoselectivity was observed, with hydrogen adding opposite to the ester group. This approach allowed a much shorter scheme to functionalise the C-4 position in pyroglutamic acid although it gave the pyrrolidinones rather than the pyrrolidine.



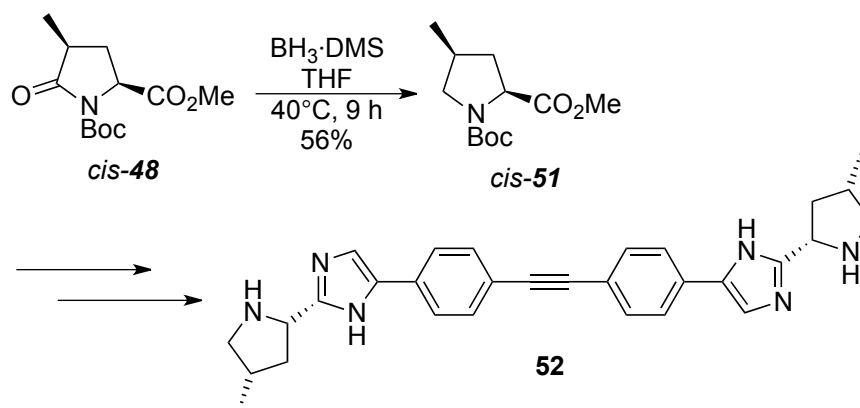
Scheme 3.17: Synthesis of methylglutamic acid **49**.

In 2003, Gu *et al.*⁵² reported a different method to synthesise methylglutamic acid. Boc protected pyroglutamic acid (S)-**46** was prepared as previously, Then, alkylation at the C-4 position in (S)-**46** was carried out by using LHMDS at -78°C to form the enolate. Subsequently, trapping with methyl iodide gave a separable mixture of *cis*-**48**, *trans*-**48**, and disubstituted pyroglutamate **50** with 28%, 37% and 11% yields respectively (Scheme 3.18). The poor diastereoselectivity and the formation of the doubly alkylated product make this approach less suitable than the hydrogenation routes described previously.



Scheme 3.18: Unselective enolate alkylation reaction.

In 2012, Belema and colleagues reported a patent on the synthesis of Hepatitis C virus inhibitor **52** and one of the intermediates was methylglutamic acid derivative *cis*-**48** from Gu *et al.*'s approach. Lactam reduction of pyrrolidinone *cis*-**48** using $\text{BH}_3\cdot\text{DMS}$ in THF gave methyl ester *cis*-**51** in 56% yield (Scheme 3.19). Thus, using the approaches described in this section and this lactam reduction, a route to 2,4-*cis*-disubstituted pyrrolidines *cis*-**51** is possible.⁵³

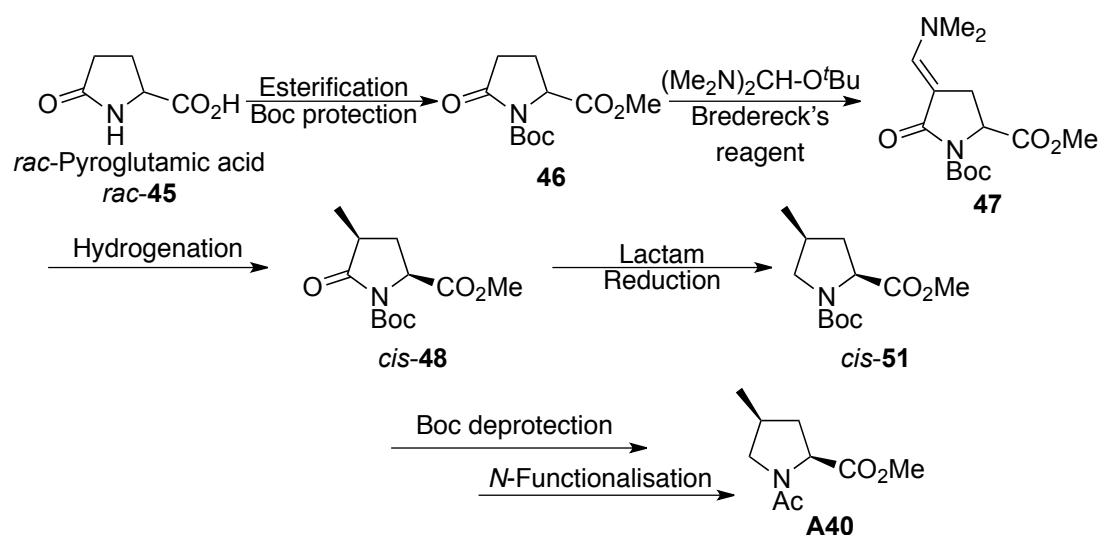


Scheme 3.19: Synthesis of Hepatitis C virus inhibitor **52**.

In summary, a few different approaches to 2,4-*cis*-disubstituted pyrrolidines and pyrrolidinones with methyl and methyl ester groups are known in the literature.

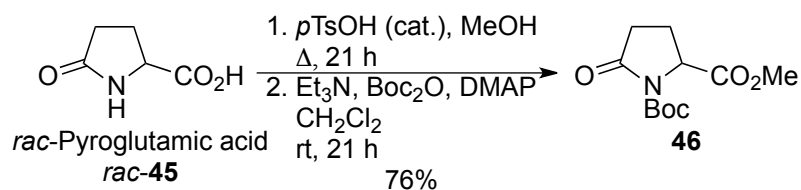
3.3.2 Synthesis of a 2,4-cis-Disubstituted Pyrrolidine with Methyl and Methyl Ester Groups

In this section, a method for introducing a substituent at the 2 and 4 positions on the pyrrolidine was investigated. As shown in the previous section, the synthetic approaches to 2,4-disubstituted pyrrolidines mostly began with pyroglutamic acid **45**. In *N*-Boc pyroglutamate ester **46**, deprotection α to the amide carbonyl is more favoured than α to the ester, so enolate formation occurs more readily at that position. This is driven by the electron withdrawing Boc group and hence led us to propose the synthesis plan as set out in Scheme 3.20. Esterification and Boc protection of racemic pyroglutamic acid *rac*-**45** would give **46**, which allows reaction with Brederick's reagent to form an enaminone at the C-4 position to give enaminone **47**. Then, diastereoselective hydrogenation of enaminone **47** would give the methyl group in *cis*-**48**. Subsequent lactam reduction would give methylpyroglutamic acid *cis*-**51**. This would be followed by Boc deprotection and acetylation to give the desired fragment, acetamide **A40**.



Scheme 3.20: Proposed synthesis of acetamide **A40**.

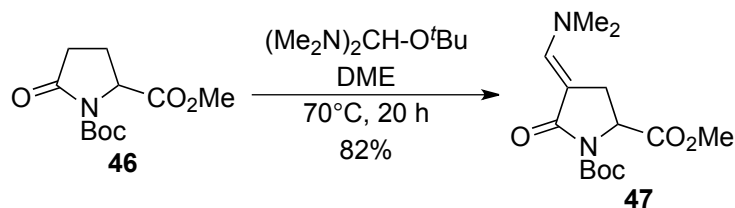
To start with, protected pyroglutamic acid **46** was synthesised. *rac*-Pyroglutamic acid *rac*-**45** was reacted with catalytic *p*-toluenesulfonic acid in methanol at reflux to form the methyl ester. The methyl ester intermediate was then treated with triethylamine and Boc₂O to form the *N*-Boc methyl ester **46**. After work-up, purification of the crude product by flash column chromatography gave **46** in 76% yield (Scheme 3.21).



Scheme 3.21: Synthesis of methyl ester 46.

The synthesis of **46** was verified by ¹H NMR spectroscopy. In the ¹H NMR spectrum, there was a 9H integration signal at δ 1.47, which was assigned to the Boc group. Also, there was a 3H singlet at δ 3.77 due to the methyl ester. In the ¹³C NMR spectrum, there were two carbonyl signals at δ 173.2 and 171.8 due to the lactam carbon and methyl ester group. There was a carbonyl signal at δ 149.2, which was assigned to the Boc group. The alkyl signal at δ 52.5 was due to the methyl ester group. All of the NMR spectroscopic data matched the literature values.⁵¹

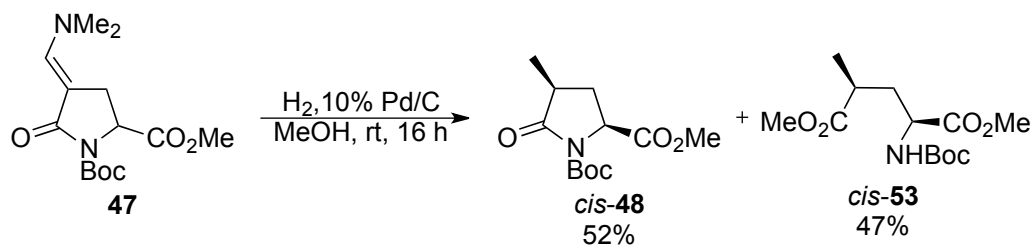
Then, methyl ester **46** was reacted with Bredereck's reagent by using a literature route.⁵¹ Methyl ester **46** was reacted with Bredereck's reagent in DME at reflux to give enaminone **47**. After filtration and eluting with hexane, pure enaminone **47** was obtained in 82% yield (Scheme 3.22).



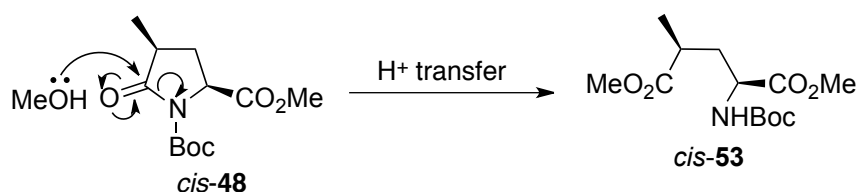
Scheme 3.22: Synthesis of enaminone **47**.

The synthesis of enaminone **47** was proven by ^1H NMR spectroscopy. In the ^1H NMR spectrum, there was a singlet at δ 7.11 (1H integration) which was assigned to the alkene proton. There was a 6H singlet at δ 3.00, which was due to the enaminone methyl groups. The ^{13}C NMR spectrum showed a CH signal at δ 146.6 due to the CH in the alkene group. There was a signal at δ 91.0 due to the tertiary carbon in the alkene group. There was also a CH_3 signal at δ 26.4, which was assigned to the enaminone methyl groups. All of the spectroscopic data matched the literature data.⁵¹

This was followed by an investigation of the catalytic hydrogenation of enaminone **47**. This was carried out by using a literature method.⁵¹ The catalytic hydrogenation of enaminone **47** with palladium on carbon in methanol was carried out first. After the solids were removed by filtration through Celite[®], the crude product was purified by flash column chromatography. This gave a 52% yield of the desired product, methyl pyroglutamate *cis*-**48**, and a 47% yield of the ring-opened dimethyl ester by-product *cis*-**53** (Scheme 3.23). By-product **53** was formed by the methanol attacking the lactam carbonyl in methyl pyroglutamate *cis*-**48** (Scheme 3.24).



Scheme 3.23: Catalytic hydrogenation enaminone 47.



Scheme 3.24: Mechanism for the formation of by-product cis-53.

The synthesis of methyl pyroglutamate *cis-48* was confirmed by characterisation with ^1H NMR spectroscopy. In the ^1H NMR spectrum, there was a 3H doublet signal at δ 1.25 ($J = 7.0$ Hz) due to the protons in the newly formed methyl group. In the ^{13}C NMR spectrum, there was a methyl signal at δ 18.3, which was assigned to the newly formed methyl group. The spectroscopic data matched with those values in the literature.⁵¹

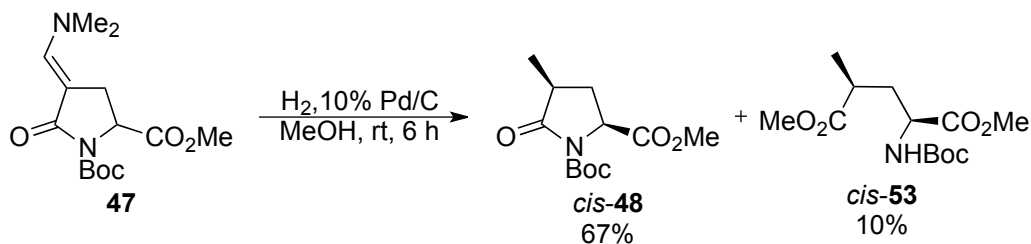
To confirm the structure of the ring-opened by-product dimethyl ester *cis-53* characterisation by ^1H NMR spectroscopy was carried out. In the ^1H NMR spectrum, there was a doublet at δ 4.98 (1H integration), which was assigned to the NH proton. There were two 3H singlets at δ 3.70 and 3.64, which were assigned to the methyl protons in the methyl ester. In the ^{13}C NMR spectrum, there were three carbonyl signals at δ 176.7, 173.1 and 155.6 due to the carbonyl groups in the two methyl esters and in the Boc group respectively. There were two CH_3 signals at δ 52.5 and 51.9,

assigned to the methyl in the two methyl ester groups. The CH₃ signal at δ 17.3 was due to the newly formed methyl group. The molecular formula of the dimethyl ester *cis*-**53** was confirmed by electrospray ionisation (ESI) mass spectrometry. In the ESI spectrum, there was a peak at 312.1423 which fitted well with the calculated C₁₃H₂₃NO₆ (M + Na)⁺ 312.1418. All spectroscopic data matched with those reported in the literature.⁵⁴

In order to optimise the catalytic hydrogenation of enaminone **47**, a solvent screen for this reaction was carried out (Table 3.12). To begin with, two non-protic solvents, EtOAc and THF, were chosen. With EtOAc, enaminone **47** did not dissolve well (Table 3.12, entry 1). With THF, enaminone **47** dissolved, but after reaction for 21 h, the desired product did not form (entry 2). This finding suggested that a protic solvent is required for the reaction. Then, the protic solvent, *i*-PrOH, was investigated (Entry 3). The reaction was carried out for 71 h due to the low solubility of enaminone **47** in *i*-PrOH and the large amount of solvent that was required. Due to the dilute condition, this reaction required a long reaction time (entry 3). However, under these conditions, pyroglutamate *cis*-**48** was isolated in 74% yield without any dimethyl ester *cis*-**53** being formed. Reaction in 2:1 *i*-PrOH–MeOH as solvent was faster and gave a 74% yield of *cis*-**48** after 22 h (entry 4). Finally, the reaction was carried out in methanol and the reaction time was closely monitored (entry 5). The result showed that after 6 h, a good yield of desired product *cis*-**48** was obtained (67%) with some by-product *cis*-**53** (10%). Thus, we concluded that the entry 5 conditions were the best for catalytic hydrogenation of enaminone **47**, as they have the shortest reaction time (Scheme 3.25).

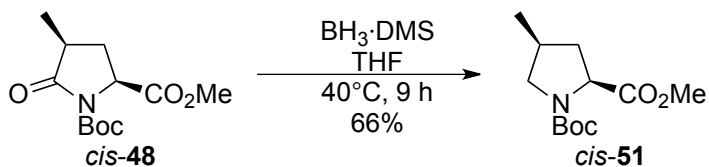
Table 3.12: Conditions trialled to optimise the hydrogenation.

Entry	Solvent	Reaction time	Result
1	EtOAc	/	SM did not dissolve well in the solvent
2	THF	21 h	No product was found
3	<i>i</i> -PrOH	71 h	74% of <i>cis</i> - 48
4	2:1 <i>i</i> -PrOH – MeOH	22 h	74% of <i>cis</i> - 48
5	MeOH	6 h	67% of <i>cis</i> - 48 & 10% of <i>cis</i> - 53



Scheme 3.25: Catalytic hydrogenation of enaminone **48**.

Lactam reduction was investigated next using an approach based on the method described by Belema and colleagues.⁵³ Methylglutamic acid *cis*-**48** was reacted with BH₃·DMS in THF refluxing for 9 h. After aqueous work-up, the crude product was purified by flash column chromatography and methyl ester *cis*-**51** was isolated in 66% yield (Scheme 3.26).

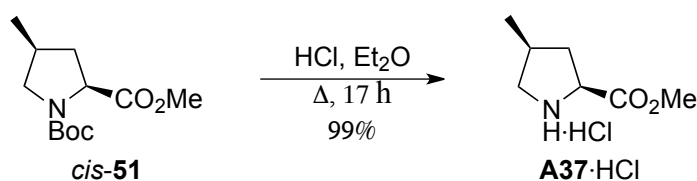


Scheme 3.26: Synthesis of methyl ester *cis*-**49**.

To confirm the successful synthesis of methyl ester *cis*-**51**, characterisation by ¹H NMR spectroscopy was carried out. In the ¹H NMR spectrum, there were two doublets at δ 4.25 and 4.19 (1H integration in total, rotamers), which were assigned to

the α proton next to the ester in the pyrrolidine ring. In addition, there were two new NCH protons at δ 3.75-3.64 (multiplet) and δ 2.98 (double doublet). In the ^{13}C NMR spectrum, there were two signals at δ 173.9 and 173.7, which were assigned to the carbonyls in the methyl ester (rotamers). There were two rotameric NCH₂ signals at δ 53.8 and 53.3 due to the α carbon at the C-5 position in the pyrrolidine ring. The spectroscopic data matched with those in the literature.⁵³

Before synthesising acetamide **A40**, the Boc deprotection of methyl ester *cis*-**51** was investigated. Our standard Boc deprotection conditions were used. Methyl ester *cis*-**51** was treated with hydrochloric acid in Et₂O at reflux for 17 h to give pyrrolidine salt **A37**·HCl in 99% yield. Salt **A37**·HCl was collected as a crude product and did not require any purification (Scheme 3.27).

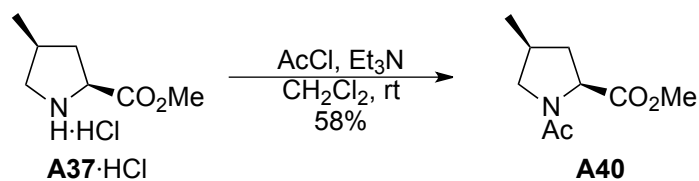


Scheme 3.27: Boc deprotection of 51 to give pyrrolidine salt A37·HCl.

The synthesis of pyrrolidine salt **A37**·HCl was proven by ^1H NMR spectroscopy. In the ^1H NMR spectrum, the Boc signal (normally a 9H integration singlet at around δ 1.40) was not detected. This information suggested that the Boc group was successfully removed. There was a singlet at δ 3.89 (3H integration), which was assigned to the methyl ester group. There was a 3H doublet at δ 1.12 due to the methyl group at the C-4 position. In the ^{13}C NMR spectrum, the Boc carbonyl signal (normally

around δ 155.0) was not detected. There was a signal at δ 170.6, which was assigned to the methyl ester carbonyl group. There was a signal at δ 60.8 due to the NCH. There was a signal at δ 53.9 due to the NCH₂. The CH₃ signal at δ 53.1 was assigned to the methyl in the methyl ester group.

The final fragment in this series was prepared using the conditions from the model study. *N*-acetamide **A40** was synthesised by reaction of pyrrolidine salt **A37**·HCl with acetyl chloride and triethylamine in CH₂Cl₂. Then, aqueous work-up and purification of the crude product by flash column chromatography yielded *N*-acetamide **A40** in 58% yield (Scheme 3.28).



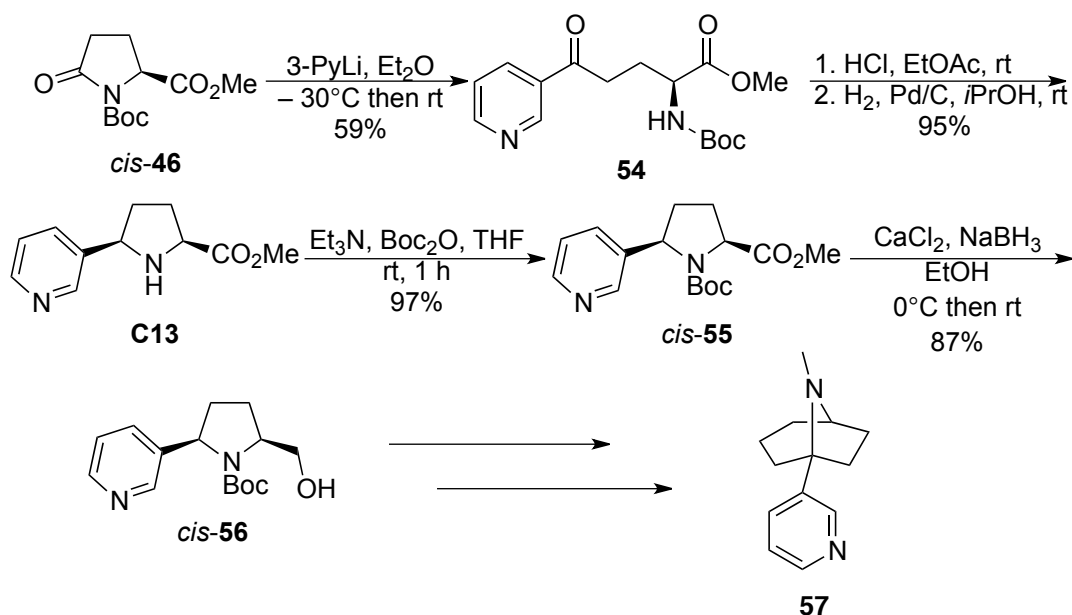
Scheme 3.28: Synthesis of acetamide A40.

Acetamide **A40** was characterised by ¹H and ¹³C NMR spectroscopy. In the ¹H NMR spectrum (Figure 3.9), there were two singlets at δ 2.07 and 1.93 (3H integration in total) that were assigned to the rotameric methyls in the acetyl group. In the ¹³C NMR spectrum, the two rotameric signals at δ 173.2 and 173.1 were due to the acetyl carbonyl group and the two rotameric signals at δ 22.4 and 21.4 was assigned to the acetamide groups. In the IR spectrum, there were two carbonyl stretches at 1740 and 1641 cm⁻¹, which were due to the ester and acetyl group respectively. The spectroscopic data matched with those reported in the literature.⁴³

3.4 Attempted Synthesis of 2,5-*cis*-Disubstituted Pyrrolidine Fragments

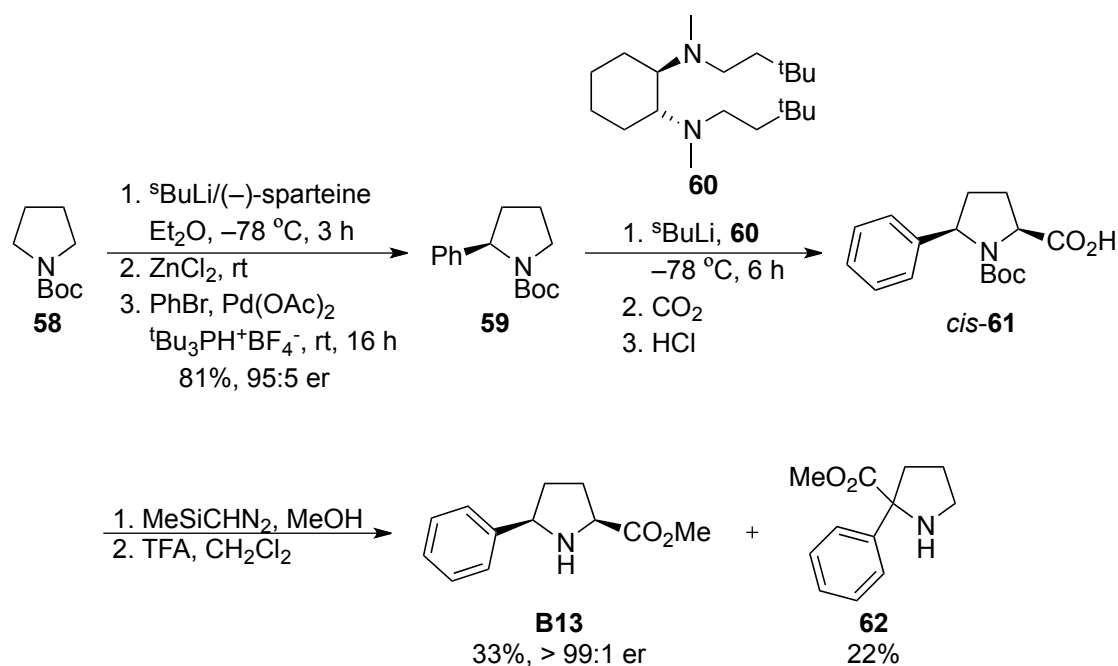
3.4.1 Previous Routes to 2,5-*cis*-Disubstituted Pyrrolidines with Phenyl or Pyridine and Primary Alcohol Groups

In 1999, Xu *et al.*⁵⁵ reported a synthetic strategy toward the nicotine analogue **57**. Their approach began with the synthesis of pyridinyl ketone **54**. The coupling of 3-pyridinyllithium with Boc protected pyroglutamate *cis*-**46** in Et₂O gave ketone *cis*-**54** in 59% yield. This was followed by cyclisation. Boc deprotection of **54** with hydrochloric acid in EtOAc gave an imine intermediate. Subsequently, hydrogenation with palladium on carbon in *i*-PrOH gave amine **C13** in 97% yield. Then, Boc protection of **C13** gave methyl ester *cis*-**55** in 97% yield. This was then followed by the reduction of the methyl ester to a primary alcohol *cis*-**56** in 87% yield using Ca(BH₄)₂ which was formed *in situ* from CaCl₂ and NaBH₄ (Scheme 3.29).



Scheme 3.29: Synthesis of nicotine analogue **57**.

In another study, our group reported a method using a sparteine surrogate to achieve asymmetric deprotonation of *N*-Boc pyrrolidine **58**. In this approach, the lithiation-Negishi coupling of *N*-Boc pyrrolidine was mediated by *s*-BuLi and (–)-sparteine to give the arylated adduct **59** in 81% yield (95:5 er). This was followed by lithiation of **59** with *s*-BuLi and diamine **60**, trapping with CO₂ and acidification to give an acid *cis*-**61** without purification by flash column chromatography. Acid *cis*-**61** was then esterified and Boc deprotected. After flash column chromatography, pyrrolidine **B13** (>99:1 er) was isolated in 33% yield together with the competitive benzylic deprotonation product pyrrolidine **62** in 22% yield (Scheme 3.30).

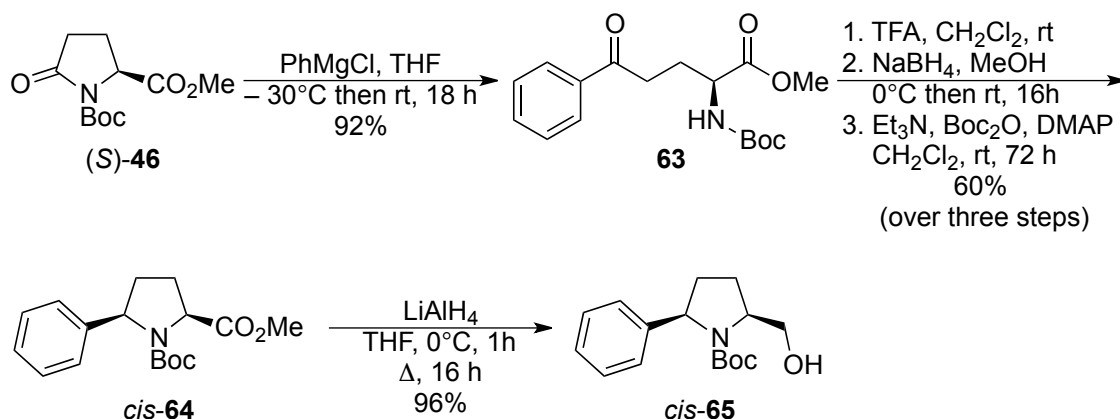


Scheme 3.30: Synthesis of pyrrolidine **B13**.

This approach provided good stereocontrol with overall good yield *via* a short route (only three steps). However, it involved complicated synthetic methods to get to the

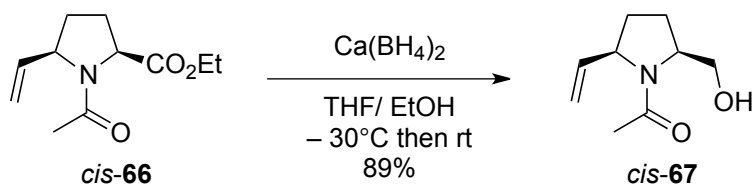
final product and this might not be the most suitable route for synthesising our fragments.

In 2014, Scharnagel *et al.*⁵⁶ described a synthetic approach to *cis*-**64** by using a Grignard reagent to introduce a phenyl group into the C-5 position (Scheme 3.31). In their approach, methyl ester (*S*)-**46** was reacted with phenylmagnesium chloride to give keto ester **63** in 92% yield. This was followed by Boc deprotection by TFA and cyclisation to give an imine. Then, the imine was reduced using NaBH₄ and Boc protection gave pyrrolidine *cis*-**64** in 60% yield over 3 steps. Subsequently, methyl ester reduction of *cis*-**64** was carried out to give primary alcohol *cis*-**65** in 96% yield.



Scheme 3.31: Synthesis of *cis*-**65**.

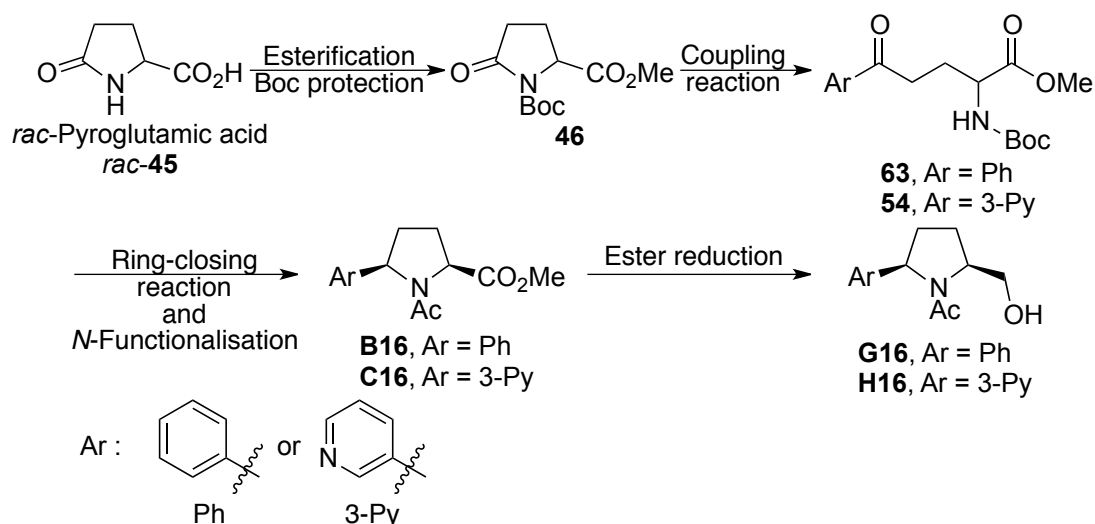
In 2006, Banfi *et al.*⁵⁷ reported the chemoselective reduction of an ester to a primary alcohol in the presence of *N*-acetamide. In this study, the vinyl ester acetamide *cis*-**67** was treated with Ca(BH₄)₂ to give *cis*-**68** in 89% yield (Scheme 3.32). Similar to Xu *et al.*⁵⁵, Ca(BH₄)₂ was formed *in situ* by reacting CaCl₂ with NaBH₄.



Scheme 3.32: Chemoselective reduction of ester **cis-66**.

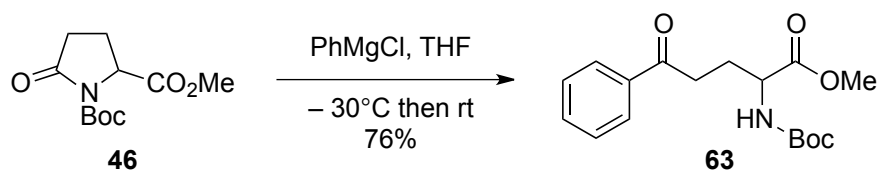
3.4.2 Attempted Synthesis of a 2,5-cis-Disubstituted Pyrrolidine with Phenyl or Pyridine and Primary Alcohol Groups

In this section, methods for introducing substituents at the 2,5 positions on the pyrrolidine was investigated. As shown in the previous section, the synthetic approaches to 2,5-disubstituted pyrrolidines mostly began with pyroglutamic acid, which is similar to the 2,4-disubstituted pyrrolidine series. Thus, the proposed synthesis plan is as set out in Scheme 3.33. Esterification and Boc protection of racemic pyroglutamic acid **rac-45** would give **46**. This allows reaction with the corresponding organometallic reagent to introduce a phenyl or 3-pyridinyl group at the C-5 position to give keto ester **63** or keto ester **54** respectively. Then, ring-closing and *N*-acetylation of **63** and **54** would give the fragment **B16** and **C16**. Subsequent chemoselective ester reduction would give primary alcohol acetamide fragments **G16** and **H16**.



Scheme 3.33: Proposed synthesis of **G16** and **H16**.

The introduction of the phenyl group at the C-5 position was investigated first. Reaction of Boc protected methyl ester **46** was carried out with phenylmagnesium chloride in THF at $-30\text{ }^{\circ}\text{C}$ based on the procedure reported by Scharnagel *et al.*⁵⁶ (see Scheme 3.31). Then, the resulting mixture was stirred at rt for 30 h. The crude product was purified by flash column chromatography and a 76% yield of keto ester **63** was obtained (Scheme 3.34).

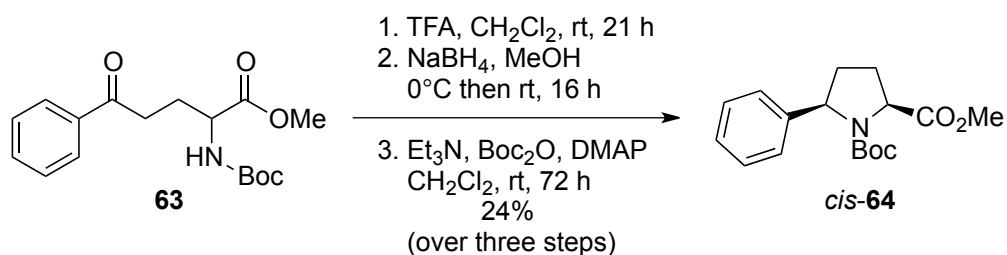


Scheme 3.34: Synthesis of keto ester **63**.

The synthesis of keto ester **63** was confirmed by characterisation by ^1H NMR spectroscopy. In the ^1H NMR spectrum, there were signals at δ 7.96, 7.57 and 7.46 which were assigned to the protons in the phenyl group. There was a doublet (1H

integration) at δ 5.16 due to the NH. There was a 3H integration singlet at δ 3.75 which was assigned to the protons in the ester group. The protons from the *tert*-butyl in the Boc group gave a 9H integration singlet at δ 1.42. The ^{13}C NMR spectrum of **63** showed a carbonyl signal at δ 199.0 due to the carbon at the phenyl ketone. There were other signals at δ 173.1 and 155.6, which were assigned to the carbonyl ester and Boc groups respectively. There was a signal at δ 80.2 due to the tertiary *tert*-butyl carbon in the Boc group. There was a CH_3 signal at δ 28.4 which was assigned to the *tert*-butyl in the Boc group. These spectroscopic data matched with those reported in the literature.⁵⁵

The ring-closing reaction was carried out in the following way (Scheme 3.35). Boc deprotection and cyclisation of keto ester **63** was carried out by reacting with TFA in CH_2Cl_2 to give the crude imine. Without purification, the crude imine was reacted with NaBH_4 in methanol for 16 h. Subsequently, Boc protection for 71 h gave a crude product which was purified by flash column chromatography. In this way, methyl ester *cis*-**64** was isolated in 24% yield over 3 steps.

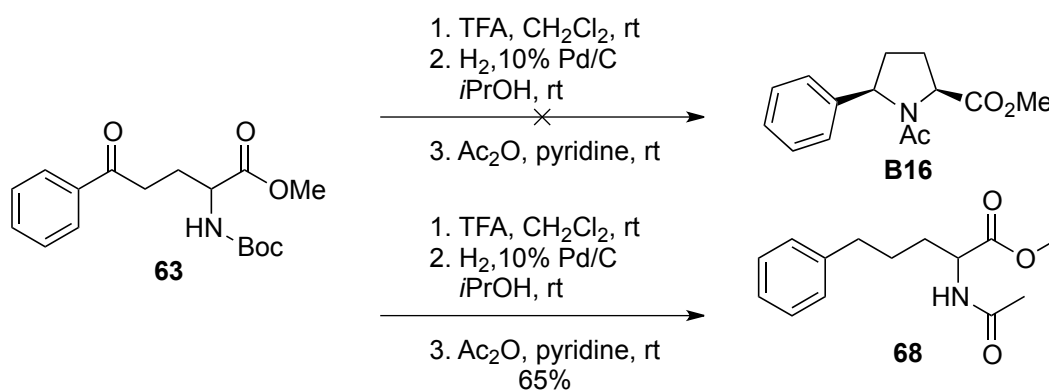


Scheme 3.35: Synthesis of methyl ester cis-64.

The synthesis of methyl ester *cis*-**64** was proven by ^1H NMR spectroscopy. In the ^1H NMR spectrum, the phenyl protons appeared at δ 7.54, 7.32 and 7.22. There was a

rotameric multiplet and double doublet (1H integration in total) at δ 4.99-4.97 and 4.35 which were assigned to the NCH. There were two rotameric singlets δ 1.41 and 1.14 (9H integration in total) due to the Boc group. The ^1H NMR spectroscopic data matched with those previously reported in the literature.⁵⁶

The ring-closing reaction to give methyl ester *cis*-**64** via a literature route⁵⁶ was successfully carried out. However, the yield was low. Therefore, an alternative literature route⁵⁵ was investigated. Boc deprotection and cyclisation of **63** with TFA in CH_2Cl_2 gave the crude imine. Subsequent hydrogenation of the crude imine with palladium on carbon should have given the free amine fragment, which was reacted with acetic anhydride in pyridine to give fragment **B16**. However, after purification by flash column chromatography, the desired acetamide fragment **B16** was not observed. Instead, ring-opening product acetamide **68** was isolated in 65% yield. Ring-opened acetamide **68** was presumably formed by benzylic C-N bond cleavage, due to over-reaction in hydrogenation.



Scheme 3.36: Synthesis of acetamide **68**.

The structure of ring-opened product acetamide **68** was proven by characterisation by the ^1H and ^{13}C NMR spectroscopy. In the ^1H NMR spectrum (Figure 3.10), there were the expected phenyl signals at δ 7.28, 7.19 and 7.15 and a broad doublet (1H

integration) at δ 5.94 due to the NH. There was a 1H integration multiplet at δ 4.67-4.62 which was assigned to the NCH. There was a 2H integration multiplet at δ 2.69-2.56 due to the CH₂ next to the phenyl group. There was a singlet (3H integration) at δ 2.01 which was due to the acetamide. The ¹³C NMR spectrum of **68** showed a carbonyl signal at δ 173.2 due to the methyl ester. There was a CH₃ signal at δ 52.1 which was assigned to the ester group. There was a CH₃ signal at δ 23.4 due to the acetamide group. The *m/z* value of **68** was measured by electrospray ionisation (ESI) mass spectrometry. In the ESI spectrum, the (M + Na)⁺ was at 272.1249 which compared well with the calculated C₁₄H₁₉NO₃ (M + Na)⁺ 272.1257. The spectroscopic data matched those reported in the literature.⁵⁸

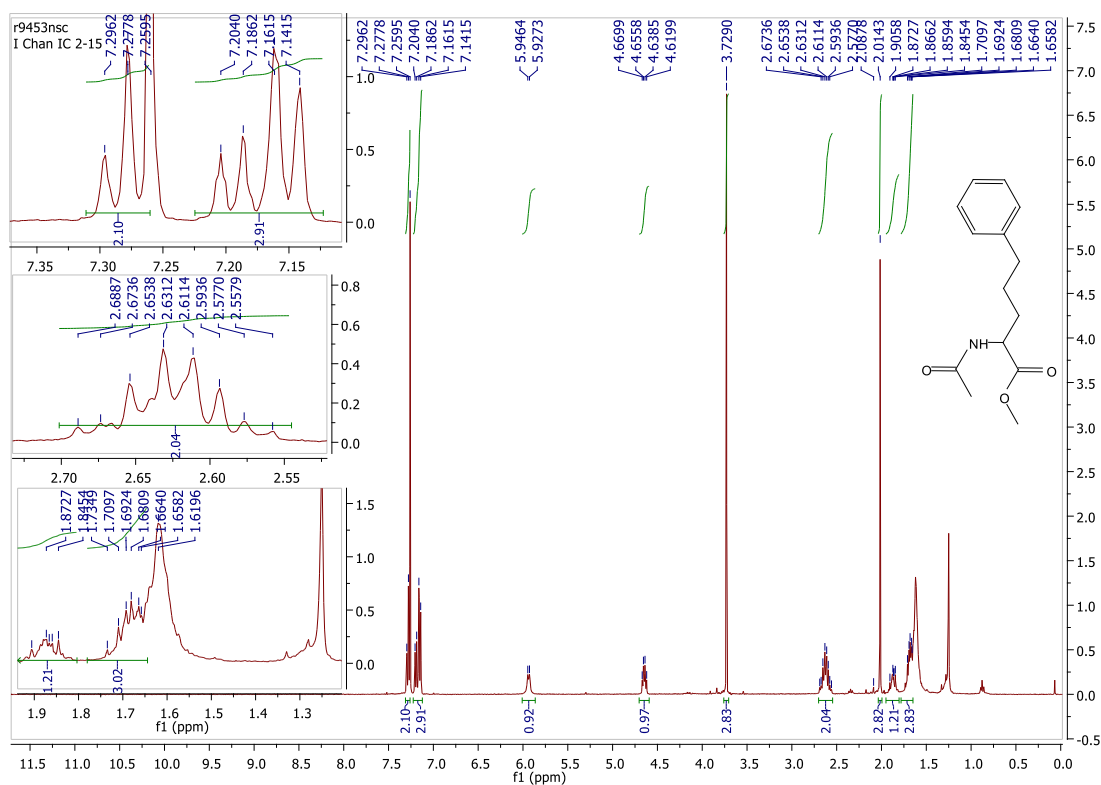
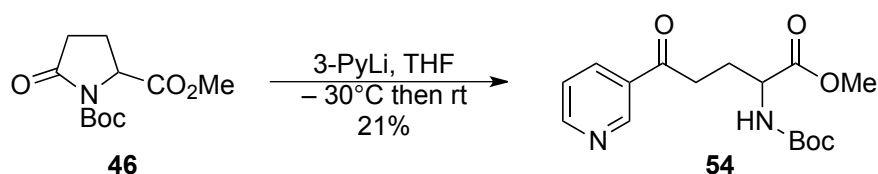


Figure 3.10: ¹H NMR spectrum of acetamide **68**.

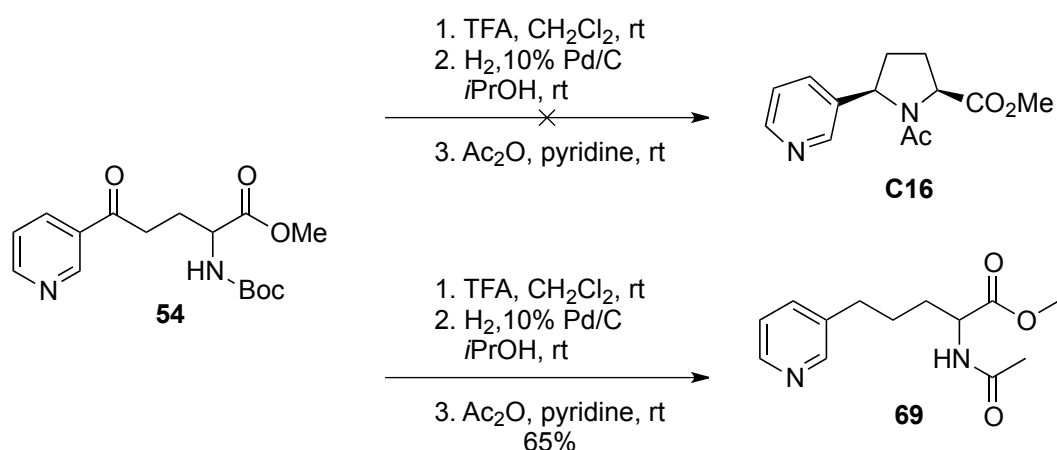
With this failed reaction, we investigated the analogous pyridine reaction. Instead of using a Grignard reagent as with the phenyl derivative, the use of 3-pyridinylithium was explored. 3-Pyridinylithium was formed by reacting 3-bromopyridine and *n*-BuLi in THF for 30 min, based on the procedure reported by Xu *et al.*⁵⁵ (see Scheme 3.29). Then, the 3-pyridinylithium was reacted with Boc protected methyl ester **46** in THF at $-30\text{ }^{\circ}\text{C}$. The resulting mixture was stirred at rt for 1 h. After aqueous work-up, the crude product was purified by flash column chromatography and a 21% yield of keto ester **54** was obtained (Scheme 3.37).



Scheme 3.37: Synthesis of keto ester 54.

The synthesis of keto ester **54** was confirmed by characterisation by ^1H and ^{13}C NMR spectroscopy. In the ^1H NMR spectrum, there were signals at δ 9.16, 8.79, 8.22 and 7.42 which were assigned to the protons in the pyridine group. There was a doublet (1H integration) at δ 5.15 due to the NH. There was a 3H integration singlet at δ 3.76 which was assigned to the protons in the ester group. The protons from the *tert*-butyl in the Boc group gave a 9H integration singlet at δ 1.40. The ^{13}C NMR spectrum of **54** showed a carbonyl signal at δ 197.8 due to the ketone. There were other carbonyl signals at δ 172.9 and 153.7, which were assigned to the ester and Boc group respectively. These spectroscopic data matched those reported in the literature.⁵⁵

The ring-closing reaction of keto ester **54** was carried out *via* a literature route⁵⁵ and using the same conditions as with phenyl derivative to give acetamide **69**. Boc deprotection and cyclisation of **54** with TFA in CH₂Cl₂ gave the crude imine. Subsequent hydrogenation of the crude imine with palladium on carbon and acetylation should have given the desired fragment **C16**. However, after purification by flash column chromatography, the ring-opened product acetamide **69** was isolated in 65% yield (Scheme 3.38). The result was the same as the phenyl series.



Scheme 3.38: Synthesis of acetamide **69**.

The structure of ring-opening product acetamide **69** was proven by characterisation by the ¹H and ¹³C NMR spectroscopy. In the ¹H NMR spectrum (Figure 3.10), there were the expected phenyl signals at δ 8.41-8.38, 7.45 and 7.19 and a multiplet (1H integration) at δ 6.39-6.29 due to the NH. There was a 1H integration multiplet at δ 4.65-4.55 which was assigned to the NCH. There was a 2H integration multiplet at δ 2.73-2.54 due to CH₂ next to the phenyl group. There was a singlet (3H integration) at δ 2.00 which was due to the acetamide. The ¹³C NMR spectrum of **69** showed a carbonyl signal at δ 173.1 due to the methyl ester. There was another carbonyl signal

at δ 170.0, which was assigned to the acetamide. There were five pyridine signals at δ 149.8, 147.5, 137.0, 126.0 (*ipso*) and 123.5. There was a CH₃ signal at δ 52.6 which was assigned to the ester group. There was a CH₃ signal at δ 23.2 due to the acetamide group. The *m/z* value of **69** was measured by electrospray ionisation (ESI) mass spectrometry. In the ESI spectrum, the (M + H)⁺ was at 251.1387 which compared well with the calculated C₁₃H₁₈N₂O₃ (M + H)⁺ 251.1390. The spectroscopic data was compared the phenyl derivative.

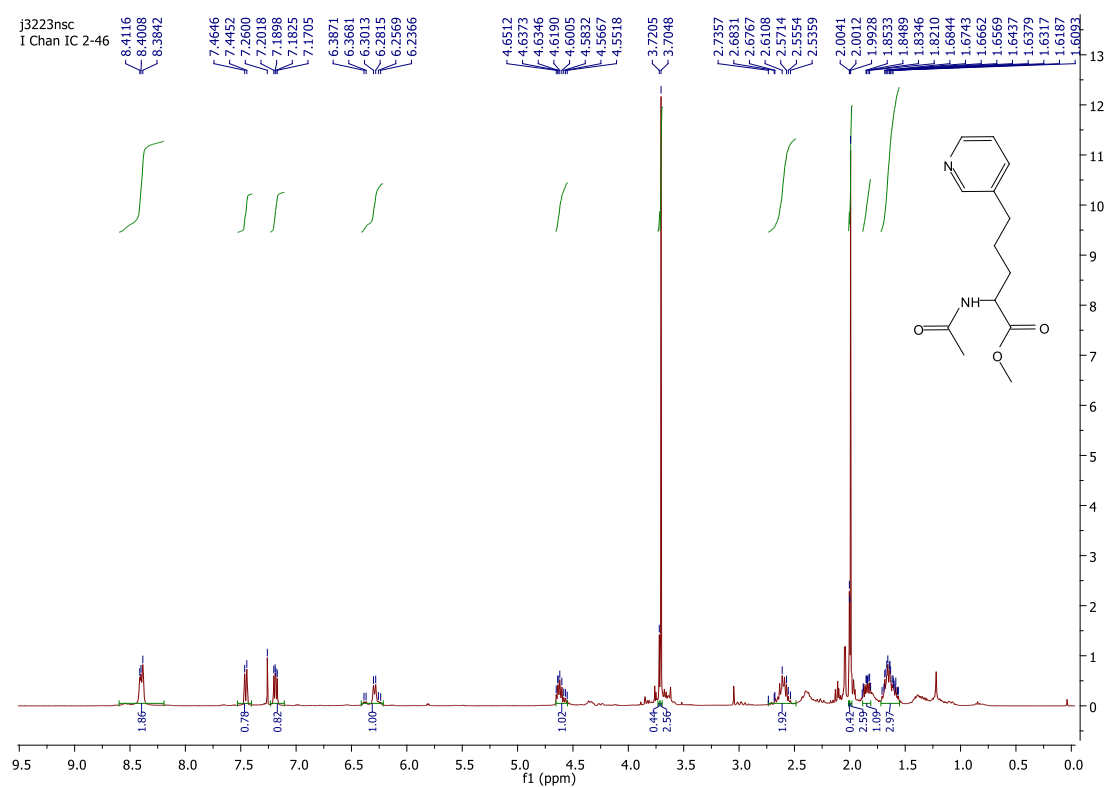
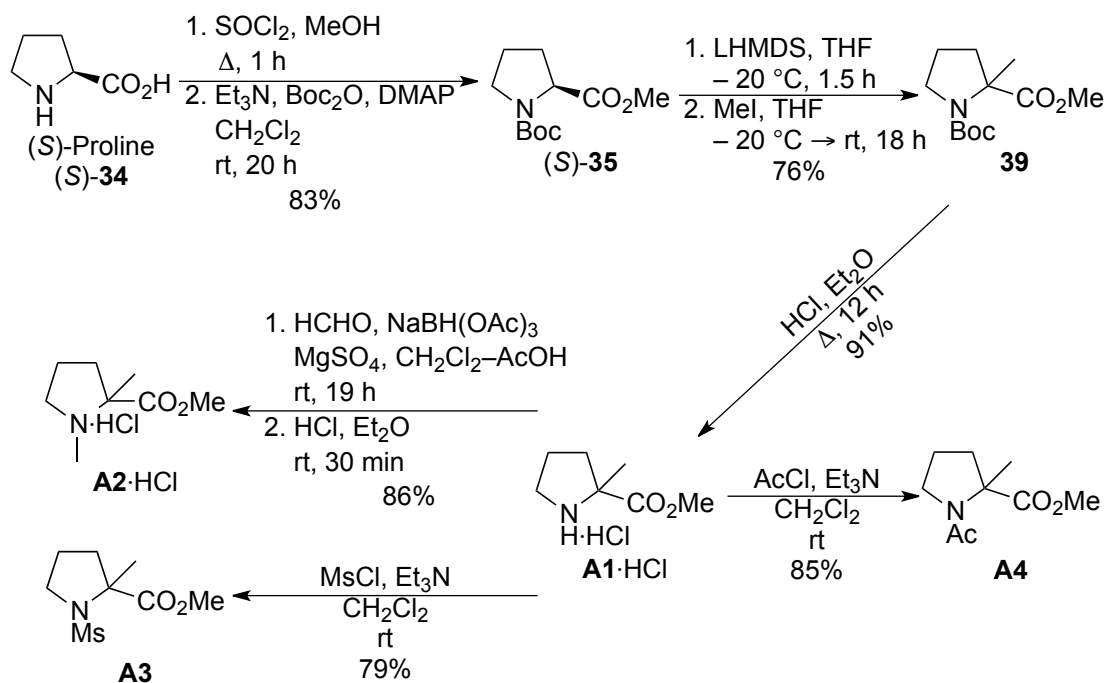


Figure 3.11: ¹H NMR spectrum of acetamide **69**.

Due to lack of time, no further studies of the synthesis of the 2,5-*cis*-disubstituted pyrrolidine fragments has been carried out.

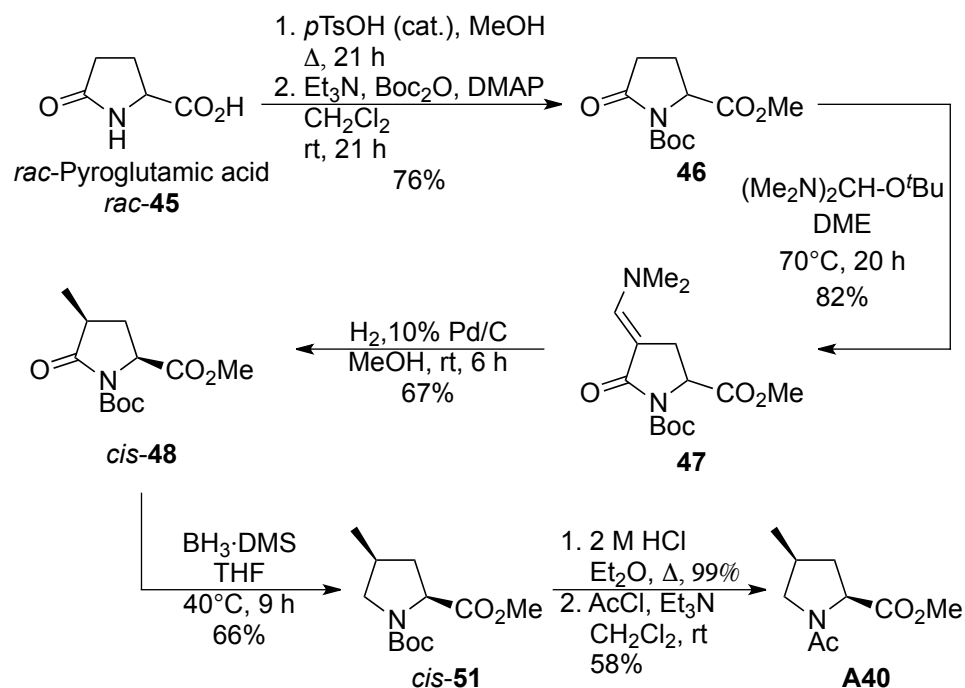
3.5 Conclusions and Future Work

First, we have successfully developed a synthetic route for the preparation of the geminal 2,2-disubstituted pyrrolidine fragments **A1-A4** from (*S*)-proline (**S-34**). The overall route is summarised in Scheme 3.39. The key intermediate was *N*-Boc methyl **39** which was prepared by enolate alkylation. Deprotection gave fragment **A1·HCl** and *N*-functionalisation gave fragment **A2·HCl** and **A3-4**.



Scheme 3.39: Synthetic route to fragments **A1·HCl**, **A2·HCl**, **A3** and **A4**.

Second, a route to 2,4-*cis*-disubstituted pyrrolidine fragment **A40** was developed (Scheme 3.40). The route started with *rac*-pyroglutamic acid *rac*-**45** and the key step was *cis*-stereoselective hydrogenation of enaminane **47**.



Scheme 3.40: Synthetic route to fragment A40.

Third, attempts to prepare 2,5-*cis*-disubstituted pyrrolidine fragments **G16** and **H16** were unsuccessful (Figure 3.12). The key issue was over-reduction in the hydrogenation step. Future work could involve the use of shorter hydrogenation reaction times or the use of NaBH₄ for the reaction.

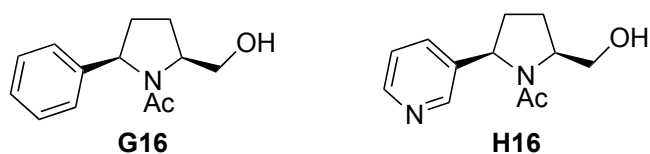


Figure 3.12: 2,5-*cis*-disubstituted pyrrolidine fragments **G16** and **H16**.

Other members in the group have synthesised all of the remaining pyrrolidine fragments with methyl and methyl ester substituents. Therefore, the future work should focus on the 11 aromatic pyrrolidine fragments identified in Chapter 2 (Figure 3.13).

Pervious work in the O'Brien group has developed a route⁵⁹ to 2,2-disubstituted pyrrolidine esters and this would be suitable for the synthesis of **B3**, **B4**, **C3**, **C4**, **H3** and **H4**. Routes to **G16** and **H16** would be based on that used in Section 3.4. Finally, a new route⁶⁰ to **G20** would need to be devised.

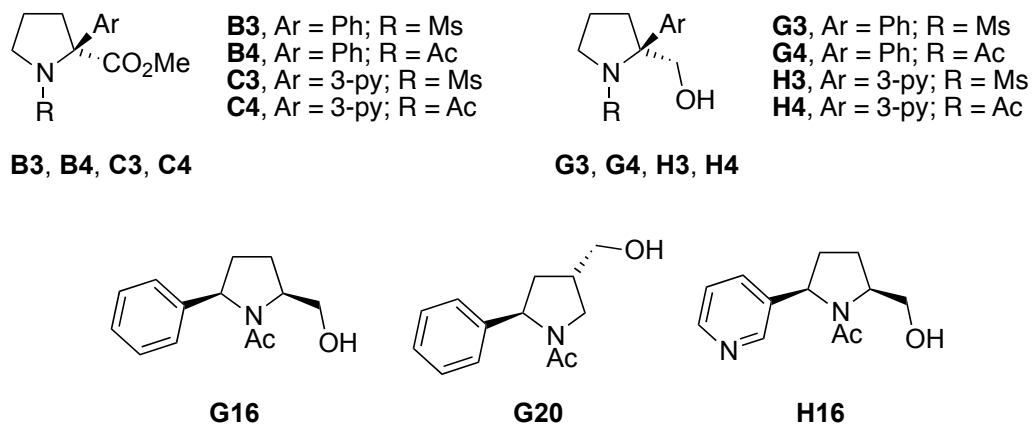


Figure 3.13: 11 selected aromatic pyrrolidine fragments.

Chapter 4: Experimental

4.1 General Procedures

4.1.1 Computational Methods

Shape analysis

A SMILES file containing the SMILES strings for all fragment compounds was generated using ChemDraw 12.0.

Three-dimensional structures were generated using Pipeline Pilot 8.5.0.200, 2011, Accelrys Software Inc. Generated conformations were used to generate the three Principal Moments of Inertia (I1, I2 and I3) which were then normalised by dividing the two lower values by the largest (I1/I3 and I2/I3) using Pipeline Pilot built-in components.

Principal moments of inertia (PMI) about the principal axes of a molecule were calculated based on the following rules (In Accelrys Software Inc. 2016):

1. The moments of inertia are computed for a series of straight lines through the centre of mass.
2. Distances are established along each line proportional to the reciprocal of the square root of I on either side of the centre of mass. The locus of these distances forms an ellipsoidal surface. The principal moments are associated with the principal axes of the ellipsoid.

The PMI plots were then generated with these data in Excel 2016.

Molecular properties

All physical properties in this study were calculated using Pipeline Pilot built-in algorithms.

Computational protocol

Prior to conformer generation a wash step was performed, which involved stripping salts and ionising the molecule at pH 7.4. Any stereocentre created here was left with undefined stereochemistry. SMILES strings were converted to their canonical representation. A list of allowed chirality at each centre is generated and a SMILES file with all possible stereoisomers was written. Conformers were generated using the BEST method in Catalyst using the rel option, run directly on the server and not through the built-in Conformation Generator component with a chosen maximum relative energy threshold of 20 kcal mol⁻¹, maximum of 255 conformers for each compound. Conformations were read, ones that cannot be represented by the canonical SMILES are discarded, with the remaining ones standardised to a single enantiomer. Duplicates were filtered with a RMSD threshold of 0.1. Minimisation with 200 steps of Conjugate Gradient minimisation with an RMS gradient tolerance of 0.1 was performed using the CHARMM forcefield with Momany-Rone partial charge estimation and a Generalised Born implicit solvent model. Duplicates were filtered again with a RMSD threshold of 0.1.

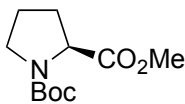
4.1.2 General Methods

All non-aqueous reactions were carried out under oxygen-free Ar or N₂. THF was freshly distilled from sodium and benzophenone. All solvents were purchased in Winchester quantities. Brine refers to a saturated solution. Water is distilled water.

Flash column chromatography was carried out using Fluka Chemie GmbH silica (220-440 mesh). Thin layer chromatography was carried out using commercially available Merck F254 aluminium backed silica plates. Proton (400 MHz) and carbon (100.6 MHz) NMR spectra were recorded on a Jeol ECX- 400 instrument using an internal deuterium lock. For samples recorded in CDCl₃, chemical shifts are quoted in parts per million relative to CHCl₃ (δ_{H} 7.26) and CDCl₃ (δ_{C} 77.0, central line of triplet). Carbon NMR spectra were recorded with broad band proton decoupling and assigned using DEPT, HMQC and HMBC experiments. Coupling constants (J) are quoted in Hertz. Melting points were carried out on a Gallenkamp melting point apparatus. Infrared spectra were recorded on a Perkin Elmer UATR Two FT-IR spectrometer. Absorption maxima (ν_{max}) of selected peaks are quoted to the nearest cm⁻¹. Electrospray high and low resonance mass spectra were recorded at room temperature on a Bruker Daltronics microTOF spectrometer. Selected mass-to-charge ratio peaks (m/z) are quoted in Daltons as a percentage of the base peak. Optical rotations were recorded at room temperature on a Jasco DIP-370 polarimeter (using sodium D line, 589 nm) and $[\alpha]_{\text{D}}$ given in units of 10⁻¹ deg cm³ g⁻¹. Chiral stationary phase HPLC was performed on an Agilent 1200 series chromatograph.

4.2 Experimental Procedures and Characterisation Data

(*S*)-1-*tert*-Butyl 2-methyl pyrrolidine-1,2-dicarboxylate (*S*)-35



(*S*)-35

Thionyl chloride (0.70 mL, 9.55 mmol, 1.1 eq) was added dropwise to a stirred solution of (*S*)-proline (*S*)-34 (1.00 g, 8.69 mmol, 1.0 eq) in MeOH (10 mL) at 0 °C under Ar. The resulting solution was stirred and heated at reflux for 1 h. After being allowed to warm to rt, the solvent was evaporated under reduced pressure to give the crude methyl ester. Et₃N (1.21 mL, 8.69 mmol, 1.0 eq) was added to a stirred solution of the crude methyl ester in CH₂Cl₂ (5 mL) at 0 °C under Ar. Then, a solution of Boc₂O (1.896 g, 8.69 mmol, 1.0 eq) and DMAP (50 mg, 0.409 mmol, 0.001 eq) in CH₂Cl₂ (5 mL) was added dropwise. The resulting solution was stirred at rt for 18 h. The solvent was evaporated under reduced pressure to give a wet solid. The wet solid was dissolved in Et₂O (10 mL) and the solution was washed with 1 M HCl_(aq) (2 × 5 mL) and saturated NaHCO_{3(aq)} (5 mL), dried (MgSO₄) and evaporated under reduced pressure to give the crude product. Purification by flash column chromatography on silica with 1:1 hexane–Et₂O as eluent gave methyl ester (*S*)-35 (1.22 g, 82% over 2 steps) as a pale yellow oil, *R*_F (1:1 hexane–Et₂O) 0.37; IR (ATR) 2976, 2881, 1747 (C=O, CO₂Me), 1695 (C=O, Boc), 1391, 1365, 1157, 1119, 772 cm⁻¹; ¹H NMR (400 MHz, CDCl₃) (60:40 mixture of rotamers) δ 4.28 (dd, *J* = 8.5, 3.0 Hz, 0.4H, NCHCO), 4.18 (dd, *J* = 8.5, 4.0 Hz, 0.6H, NCHCO), 3.68 (s, 3H, OMe), 3.54–3.31 (m, 2H, NCH), 2.24–2.10 (m, 1H, CH), 1.97–1.78 (m, 3H, CH), 1.42 (s, 3.6H, CMe₃), 1.37 (s, 5.4H, CMe₃); ¹³C NMR (101.6 MHz, CDCl₃) (rotamers) δ 173.7 (C=O, CO₂Me), 173.4 (C=O, CO₂Me), 154.7 (C=O, Boc), 153.3 (C=O, Boc), 79.94 (CMe₃), 79.88 (CMe₃), 59.0 (NCH), 58.6

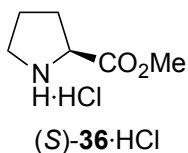
(NCH), 52.0 (OMe), 51.8 (OMe), 46.5 (NCH₂), 46.2 (NCH₂), 30.8 (CH₂), 29.8 (CH₂), 28.3 (CMe₃), 28.2 (CMe₃), 24.3 (CH₂), 24.0 (CH₂); MS (ESI) *m/z* 252 [(M + Na)⁺, 100], 196 [(M – CMe₃)⁺]; HRMS (ESI) *m/z* calcd for C₁₁H₁₉NO₄ (M + H)⁺ 252.1206, found 252.1211 (–1.8 ppm error). Spectroscopic data consistent with those reported in the literature.⁴⁰

Lab Book Reference: IC 1-16

The optical rotation was recorded on a different sample: [α]_D –57.0 (*c* 1.0 in CHCl₃) [lit.⁶¹, –54.5 (*c* 1.0, CHCl₃)]

Lab Book Reference: IC 2-7

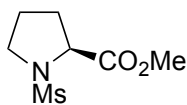
(S)-2-(Methoxycarbonyl) pyrrolidin-1-ium chloride (S)-36·HCl



Hydrogen chloride (19.2 mL of a 2.0 M solution in Et₂O, 38.38 mmol, 4.4 eq) was added dropwise to a stirred solution of the methyl ester (S)-35 (2.00 g, 8.723 mmol, 1.0 eq) in Et₂O (20 mL) at rt under Ar. The resulting mixture was stirred and heated at reflux for 68 h. Then, the solvent was evaporated under reduced pressure to give the pyrrolidine salt (S)-36·HCl (1.40 g, 97%) as a brown solid, *R_F* (100:9:1 CH₂Cl₂–MeOH–NH₄OH_(aq)) 0.63. ¹H NMR (400 MHz, CDCl₃) δ 10.61 (br s, 1H, NH), 9.07 (s, 1H, NH), 4.49 (br m, 1H, NCH), 3.90 (s, 3H, OMe), 3.64–3.53 (m, 2H, NCH), 3.11 (br. s, 1H, NCH), 2.47–2.40 (m, 1H, CH), 2.29–2.08 (m, 3H, CH). Spectroscopic data consistent with those reported in the literature.⁶²

Lab Book Reference: IC 1- 70

(S)-N-Methylsulfonyl-proline methyl ester (S)-37

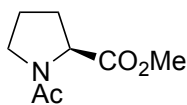


(S)-37

Methanesulfonyl chloride (1.1 mL, 13.95 mmol, 3.0 eq) was added dropwise to a stirred solution of the pyrrolidine salt (S)-36·HCl (770 mg, 4.468 mmol, 1.0 eq) and Et₃N (2 mL, 13.95 mmol, 3.0 eq) in CH₂Cl₂ (15 mL) at 0 °C under Ar. The resulting mixture was stirred at rt for 3 h. Water (50 mL) was added and the mixture was extracted with CH₂Cl₂ (3 × 50 mL). The combined organic extracts were dried (MgSO₄) and evaporated under reduced pressure to give the crude product. Purification by flash column chromatography with 10:1 CH₂Cl₂–MeOH as eluent gave the sulfonamide (S)-37 (329 mg, 34%) as brown oil, *R_F* (100:9:1 CH₂Cl₂–MeOH–NH₄OH_(aq)) 0.20; IR (ATR) 2927, 2851, 1740 (C=O, CO₂Me), 1652 (C=O, C(O)Me), 1438, 1143, 1020, 797 cm⁻¹; ¹H NMR (400 MHz, CDCl₃) δ 4.47-4.42 (m, 1H, NCHCO₂Me), 3.71 (s, 3H, OMe), 3.54-3.39 (m, 2H, NCH), 2.97 (s, 3H, SO₂Me), 2.30-2.21 (m, 1H, CH), 2.07-1.93 (m, 3H, CH); ¹³C NMR (101.6 MHz, CDCl₃) δ 173.0 (C=O, CO₂Me), 60.5 (NCH), 52.5 (OMe), 47.8 (NCH₂), 39.1 (SO₂Me), 31.0 (CH₂), 25.0 (CH₂); MS (ESI) *m/z* 230 [(M + Na)⁺, 100]; HRMS (ESI) *m/z* calcd for C₇H₁₃NO₄S (M + Na)⁺ 230.0457, found 230.0454 (+1.4 ppm error); [α]_D -80.2 (*c* 1.0 in CHCl₃) [lit.⁴², -83.6 (*c* 1.1, CHCl₃)]. Spectroscopic data consistent with those reported in the literature.⁴²

Lab Book Reference: IC 1-79

Methyl 1-acyl-2-methylpyrrolidine-2-carboxylate (*S*)-**38**

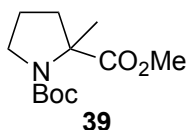


(*S*)-**38**

Acetyl chloride (258 μ L, 3.623 mmol, 3.0 eq) was added dropwise to a stirred solution of the pyrrolidine salt (*S*)-**36**·HCl (200 mg, 1.208 mmol, 1.0 eq) and Et₃N (505 μ L, 3.623 mmol, 3.0 eq) in CH₂Cl₂ (4 mL) at rt under Ar. The resulting mixture was stirred at rt for 21 h. Water (10 mL) was added and the mixture was extracted with CH₂Cl₂ (3 \times 10 mL). The combined organic extracts were dried (MgSO₄) and evaporated under reduced pressure to give the crude product. Purification by flash column chromatography with 100:10 CH₂Cl₂–MeOH as eluent gave acetamide (*S*)-**38** (110 mg, 53%) as a pale yellow oil, R_F (10:1 CH₂Cl₂–MeOH) 0.44; IR (ATR) 2958, 1740 (C=O, CO₂Me), 1617 (C=O, acetamide), 1079, 751 cm⁻¹; ¹H NMR (400 MHz, CDCl₃) (80:20 mixture of rotamers) δ 4.45 (dd, J = 8.5, 3.5 Hz, 0.8H, NCH), 4.35 (dd, J = 8.5, 2.5, 0.2H, NCH), 3.72 (s, 0.6H, OMe), 3.68 (s, 2.4H, OMe), 3.65–3.44 (m, 2H, NCH), 2.30–1.86 (m, 4H, NCH), 2.06 (s, 2.4H, C(O)Me), 1.94 (s, 0.6H, C(O)Me); ¹³C NMR (101.6 MHz, CDCl₃) δ 172.9 (C=O, CO₂Me), 169.6 (C=O, acetamide), 58.6 (NCH), 52.3 (OMe), 47.8 (NCH₂), 29.5 (CH₂), 24.8 (CH₂), 22.3 (acetamide); MS (ESI) m/z 194 [(M + Na)⁺], 172 [(M + H)⁺]; HRMS (ESI) m/z calcd for C₈H₁₃NO₃ (M + Na)⁺ 194.0788, found 194.0790 (–0.5 ppm error), (M + H)⁺ 172.0968, found 172.0963 (+3.5 ppm error); [α]_D –89.3 (c 1.0 in CHCl₃). Spectroscopic data consistent with those reported in the literature.⁴³

Lab Book Reference: IC 1-71

1-*tert*-Butyl 2-methyl 2-methylpyrrolidine-1,2-dicarboxylate 39

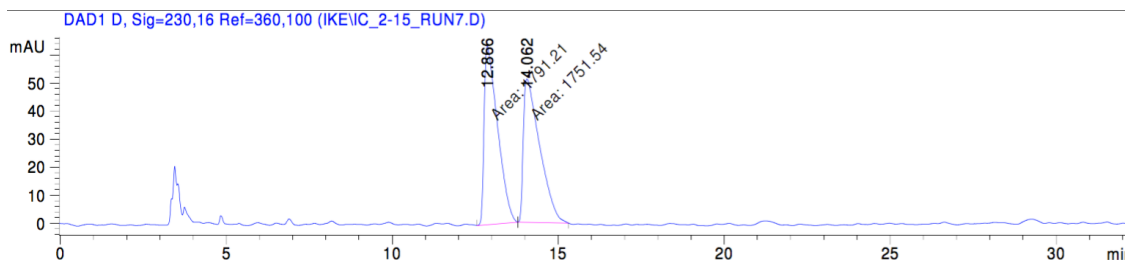


Lithium bis(trimethylsilyl)amide (12.2 mL of a 1 M solution in THF, 12.21 mmol, 1.4 eq) was added dropwise to a stirred solution of (*S*)-**35** (2.00 g, 8.72 mmol, 1.0 eq) in THF (20 mL) at $-20\text{ }^{\circ}\text{C}$ under Ar. The resulting mixture was stirred at $-20\text{ }^{\circ}\text{C}$ for 1.5 h. Then, methyl iodide (760 μL , 12.21 mmol, 1.4 eq) was added. After being allowed to warm to rt, the resulting mixture was stirred at rt for 18 h. Saturated $\text{NH}_4\text{Cl}_{(\text{aq})}$ (20 mL) was added and the mixture was extracted with EtOAc ($3 \times 20\text{ mL}$). The combined organic extracts were washed with brine ($3 \times 20\text{ mL}$), dried (MgSO_4) and evaporated under reduced pressure to give the crude product. Purification by flash column chromatography on silica with 3:1 hexane–EtOAc as eluent gave methylated product **39** (1.62 g, 76%, 51:49 er by CSP-HPLC) as a pale yellow oil, R_F (1:1 hexane–EtOAc) 0.56; IR (ATR) 2976, 2877, 1742 (C=O, CO_2Me), 1694 (C=O, Boc), 1386, 1366, 1160, 1135, 773 cm^{-1} ; ^1H NMR (400 MHz, CDCl_3) (70:30 mixture of rotamers) δ 3.69 (s, 3H, OMe), 3.57-3.39 (m, 2H, NCH), 2.18-2.05 (m, 1H, CH), 1.93-1.76 (m, 3H, CH), 1.52 (s, 0.9H, CMe), 1.47 (s, 2.1H, CMe), 1.40 (s, 2.7H, CMe_3), 1.37 (s, 6.3H, CMe_3); ^{13}C NMR (101.6 MHz, CDCl_3) (rotamers) δ 175.4 (C=O, CO_2Me), 175.2 (C=O, CO_2Me), 154.0 (C=O, Boc), 153.6 (C=O, Boc), 79.9 (CMe_3), 79.5 (CMe_3), 65.2 (CMe), 64.8 (CMe), 52.21 (OMe), 52.16 (OMe), 48.0 (NCH₂), 47.8 (NCH₂), 40.2 (CH₂), 39.2 (CH₂), 28.5 (CMe_3), 28.3 (CMe_3), 23.4 (CH₂), 23.2 (CH₂), 22.9 (CMe), 22.3 (CMe); MS (ESI) m/z 252 [$(\text{M} + \text{Na})^+$, 100], 196 [$(\text{M} - \text{CMe}_3)^+$]; HRMS (ESI) m/z calcd for $\text{C}_{12}\text{H}_{21}\text{NO}_4$ ($\text{M} + \text{Na})^+$ 266.1363, found 266.1362 (+0.9) ppm error); $[\alpha]_D$

-0.97 (*c* 1.0 in CHCl₃). Spectroscopic data consistent with those reported in the literature.³⁹

Lab Book Reference: IC 1-23

The CSP-HPLC was recorded on a different sample: Chiralpak® ID (95:5 hexane-*i*-PrOH, 1 mL min⁻¹) 12.9 min and 14.1 min.



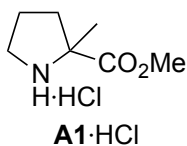
Signal 4: DAD1 D, Sig=230,16 Ref=360,100

Peak #	RetTime [min]	Type	Width [min]	Area [mAU*s]	Height [mAU]	Area %
1	12.866	MM	0.4688	1791.20947	63.67430	50.5599
2	14.062	MM	0.5709	1751.53662	51.13630	49.4401

Totals : 3542.74609 114.81060

Lab Book Reference: IC 2-12

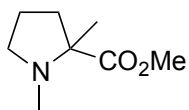
Methyl 2-methylpyrrolidinium chloride-2-carboxylate **A1**·HCl



Hydrogen chloride (22.6 mL of a 2.0 M solution in Et₂O, 44.13 mmol, 4.4 eq) was added dropwise to a stirred solution of the methyl ester **39** (2.44 g, 10.28 mmol, 1.0 eq) in Et₂O (20 mL) at rt under Ar. The resulting mixture was stirred and heated at reflux for 23 h. Then, the solvent was evaporated under reduced pressure to give the pyrrolidine salt **A1**·HCl (1.75 g, 97%) as a brown solid, mp 86-94 °C (lit.,⁶³ 106-108 °C); *R_F* (100:9:1 CH₂Cl₂-MeOH-NH₄OH_(aq)) 0.67; IR (ATR) 3387 (NH), 2919, 2744, 2508, 1741 (C=O, CO₂Me), 1585, 1440, 1290, 1214, 1129, 985, 886, 763 cm⁻¹; ¹H NMR (400 MHz, CDCl₃) δ 10.69 (s, 1H, NH), 9.47 (s, 1H, NH), 3.90 (s, 3H, OMe), 3.68-3.58 (m, 2H, NCH), 2.48-2.42 (m, 1H, CH), 2.25-1.94 (m, 3H, CH), 1.96 (s, 3H, CMe); ¹³C NMR (101.6 MHz, CD₃OD) δ 172.6 (C=O), 70.1 (CMe), 54.4 (OMe), 46.5 (NCH₂), 36.5 (CH₂), 27.8 (CH₂), 21.6 (CMe); MS (ESI) *m/z* 144 [M⁺, 100]; HRMS (ESI) *m/z* calcd for C₇H₁₄NO₂ M⁺ 144.1019, found 144.1020 (+0.3 ppm error). Spectroscopic data consistent with those reported in the literature.⁴⁵

Lab Book Reference: IC 1-46

Attempted synthesis of methyl 1,2-dimethylpyrrolidine-2-carboxylate **A2**

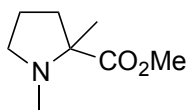


A2

Sodium bis(trimethylsilyl)amide (535 μL of a 2 M solution in THF, 1.07 mmol, 2.5 eq) was added dropwise to a stirred solution of pyrrolidine salt **A1** $\cdot\text{HCl}$ (77 mg, 0.428 mmol, 1.0 eq) in THF (4.3 mL) at $-78\text{ }^\circ\text{C}$ under Ar. The resulting solution was stirred at $-78\text{ }^\circ\text{C}$ for 30 min. Then, methyl iodide (53 μL , 0.8566 mmol, 2.0 eq) was added. After being allowed to warm to rt, the resulting solution was stirred at rt for 15 h. Water (5 mL) was added and the mixture was extracted with EtOAc ($3 \times 5\text{ mL}$). The combined organic extracts were washed with brine ($3 \times 5\text{ mL}$), dried (MgSO_4) and evaporated under reduced pressure to give the crude product. Purification by flash column chromatography on silica with 200:9:1 $\text{CH}_2\text{Cl}_2\text{-MeOH-NH}_4\text{OH}_{(\text{aq})}$ as eluent gave no identifiable products.

Lab Book Reference: IC 1-21

Attempted synthesis of methyl 1,2-dimethylpyrrolidine-2-carboxylate **A2**

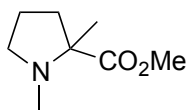


A2

10% Pd/C (20.1 mg, 0.1886 mmol, 0.27 eq) and 37% aqueous formaldehyde solution (60 μ L, 0.7682 mmol, 1.1 eq) were added to a stirred solution of pyrrolidine salt **A1**·HCl (100 mg, 0.6984 mmol, 1.0 eq) in MeOH (7 mL) at rt under Ar. Then, the reaction flask was evacuated under reduced pressure and back-filled with Ar three times. After a final evacuation, a balloon of H₂ was attached and the reaction mixture was stirred vigorously at rt under H₂ for 23 h. Then, the solids were removed by filtration through Celite[®] and washed with MeOH (20 mL). The filtrate was evaporated under reduced pressure to give the crude product which contained starting material and methylamine **A2** (by ¹H NMR spectroscopy). Purification by flash column chromatography on silica with 200:9:1 CH₂Cl₂–MeOH–NH₄OH_(aq) as eluent gave no identifiable products.

Lab Book Reference: IC 1-29

Methyl 1,2-dimethylpyrrolidine-2-carboxylate **A2**



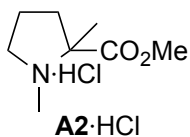
A2

37% aqueous formaldehyde solution (1.78 mL, 22.04 mmol, 10.0 eq) and MgSO_4 (1.3 mg, 9.240 mmol, 4.2 eq) were added to a stirred solution of pyrrolidine salt **A1**·HCl (396 mg, 2.20 mmol, 1.0 eq) in CH_2Cl_2 -AcOH (4:1, 11 mL) at 0 °C under Ar. Then, $\text{NaBH}(\text{OAc})_3$ (1.4 g, 6.613 mmol, 3.0 eq) was added and the resulting mixture was stirred at rt for 21 h. Saturated $\text{NH}_4\text{OH}_{(\text{aq})}$ (5 mL) was added and the mixture was extracted with CH_2Cl_2 (3×5 mL). The combined organic extracts were dried (MgSO_4) and evaporated under reduced pressure to give the crude product. Purification by flash column chromatography on silica with 200:9:1 CH_2Cl_2 -MeOH- $\text{NH}_4\text{OH}_{(\text{aq})}$ as eluent gave methylamine **A2** (25 mg, 7%) as a yellow oil, R_F (100:9:1 CH_2Cl_2 -MeOH- $\text{NH}_4\text{OH}_{(\text{aq})}$) 0.48; $^1\text{H NMR}$ (400 MHz, CDCl_3) δ 3.68 (s, 3H, OMe), 2.87-2.84 (m, 2H, NCH), 2.30 (s, 3H, NMe), 2.24-2.14 (m, 1H, CH), 1.91-1.68 (m, 3H, CH), 1.26 (s, 3H, CMe).

Methylamine **A2** was shown to be volatile so care is needed during the rotary evaporation.

Lab Book Reference: IC 1-45

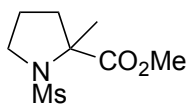
Methyl 1,2-dimethylpyrrolidine-2-carboxylate hydrochloride **A2**·HCl



37% aqueous formaldehyde solution (1.13 mL, 13.87 mmol, 10.0 eq) and MgSO₄ (708 mg, 5.87 mmol, 4.2 eq) were added to a stirred solution of pyrrolidine salt **A1**·HCl (200 mg, 1.387 mmol, 1.0 eq) in CH₂Cl₂–AcOH (4:1, 10 mL) at 0 °C under Ar. Then, NaBH(OAc)₃ (882 mg, 4.161 mmol, 3.0 eq) was added and the resulting mixture was stirred at rt for 21 h. Saturated NH₄OH_(aq) (20 mL) was added and the mixture was extracted with CH₂Cl₂ (3 × 5 mL). The combined organic extracts were dried (MgSO₄). Hydrogen chloride (3.47 mL of a 2.0 M solution in Et₂O, 6.94 mmol, 5.0 eq) was added to the filtrate. The resulting solution was stirred at rt for 30 min. The solvent was evaporated under reduced pressure to give the methylamine salt **A2**·HCl (205 mg, 86%) as a yellow oil, *R_F* (100:9:1 CH₂Cl₂–MeOH–NH₄OH_(aq)) 0.44; IR (ATR) 3405 (NH), 2957, 2465, 1738 (C=O), 1448, 1286, 1215, 1118, 976, 729, 484 cm⁻¹; ¹H NMR (400 MHz, CD₃OD) δ 3.87 (s, 3H, OMe), 3.88-3.83 (m, 1H, NCH), 3.71-3.76 (m, 1H, NCH), 2.90 (s, 3H, NMe), 2.38-2.21 (m, 3H, CH), 2.10-2.00 (m, 1H, CH) 1.61 (s, 3H, CMe); ¹³C NMR (101.6 MHz, CD₃OD) δ 172.1 (C=O), 73.7 (NCMe), 55.5 (NCH₂), 54.5 (OMe), 49.8 (CH₂), 36.6 (NMe), 21.3 (CMe), 17.1 (CH₂); MS (ESI) *m/z* 158 [M⁺, 100]; HRMS (ESI) *m/z* calcd for C₇H₁₆NO₂ M⁺ 158.1176, found 158.1172 (+2.6 ppm error).

Lab Book Reference: IC 1-52

Methyl 1-methylsulfonamide-2-methylpyrrolidine-2-carboxylate **A3**

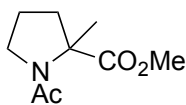


A3

Methanesulfonyl chloride (0.5 mL, 573.8 mmol, 3.0 eq) was added dropwise to a stirred solution of pyrrolidine salt **A1**·HCl (300 mg, 1.670 mmol, 1.0 eq) and Et₃N (0.5 mL, 5.010 mmol, 3.0 eq) in CH₂Cl₂ (6 mL) at rt under Ar. The resulting mixture was stirred at rt for 18 h. Water (20 mL) was added and the mixture was extracted with CH₂Cl₂ (3 × 20 mL). The combined organic extracts were dried (MgSO₄) and evaporated under reduced pressure to give the crude product. Purification by flash column chromatography with 10:1 CH₂Cl₂–MeOH as eluent gave sulfonamide **A3** (293 mg, 79%) as an off-white solid, mp 67-72 °C; *R_F* (100:9:1 CH₂Cl₂–MeOH–NH₄OH_(aq)) 0.61; IR (ATR) 3004, 2972, 1721 (C=O), 1443, 1319, 1140, 1087, 1008, 897, 777, 733 cm⁻¹; ¹H NMR (400 MHz, CDCl₃) δ 3.70 (s, 3H, OMe), 3.52-3.44 (m, 2H, NCH), 2.92 (s, 3H, SO₂Me), 2.23-2.14 (m, 1H, CH), 2.00-1.89 (m, 3H, CH), 1.61 (s, 3H, CMe); ¹³C NMR (101.6 MHz, CDCl₃) δ 174.6 (C=O), 68.7 (NCMe), 52.6 (OMe), 48.8 (NCH₂), 40.1 (CH₂), 39.6 (SO₂Me), 24.6 (CMe), 23.4 (CH₂); MS (ESI) *m/z* 244 [(M + Na)⁺, 100]; HRMS (ESI) *m/z* calcd for C₈H₁₅NO₄S (M + Na)⁺ 244.0614, found 244.0614 (0.0 ppm error).

Lab Book Reference: IC 1-82

Methyl 1-acyl-2-methylpyrrolidine-2-carboxylate **A4**

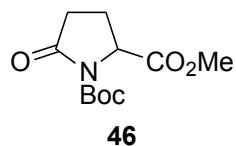


A4

Acetyl chloride (0.24 mL, 3.340 mmol, 3.0 eq) was added dropwise to a stirred solution of the pyrrolidine salt **A1**·HCl (200 mg, 1.113 mmol, 1.0 eq) and Et₃N (0.47 mL, 3.340 mmol, 3.0 eq) in CH₂Cl₂ (4 mL) at rt under Ar. The resulting mixture was stirred at rt for 23 h. Water (20 mL) was added and the mixture was extracted with CH₂Cl₂ (3 × 20 mL). The combined organic extracts were dried (MgSO₄) and evaporated under reduced pressure to give the crude product. Purification by flash column chromatography with 100:10 CH₂Cl₂–MeOH as eluent gave acetamide **A4** (175 mg, 85%) as a pale yellow oil, *R_F* (200:9:1 CH₂Cl₂–MeOH–NH₄OH_(aq)) 0.36; IR (ATR) 2952, 2876, 2508, 1736 (C=O, CO₂Me), 1641 (C=O, acetamide), 1410, 1283, 1135, 869 cm⁻¹; ¹H NMR (400 MHz, CDCl₃) δ 3.69 (s, 3H, OMe), 3.65-3.54 (m, 2H, NCH), 2.15 (ddd, 1H, *J* = 12.0, 9.0, 7.0 Hz, CH), 2.00 (s, 3H, C(O)Me), 2.64-1.95 (m, 2H, CH), 1.87 (ddd, 1H, *J* = 12.0, 6.0, 6.0 Hz, CH), 1.54 (s, 3H, *CMe*); ¹³C NMR (101.6 MHz, CDCl₃) δ 174.7 (C=O, CO₂Me), 168.9 (C=O, acetamide), 65.6 (NCMe), 52.5 (NCH₂), 49.0 (OMe), 38.8 (CH₂), 24.0 (CH₂), 23.1 (C(O)Me), 21.7 (*CMe*); MS (ESI) *m/z* 208 [(M + Na)⁺, 100]; HRMS (ESI) *m/z* calcd for C₉H₁₅NO₃ (M + Na)⁺ 208.0944, found 208.0947 (–1.1 ppm error).

Lab Book Reference: IC 1-86

1-*tert*-Butyl 2-methyl 5-oxopyrrolidine-1,2-dicarboxylate **46**

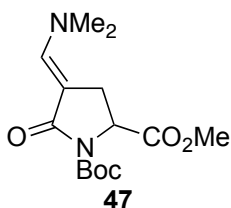


p-Toluenesulfonic acid monohydrate (884 mg, 4.64 mmol, 0.03 eq) was added a stirred solution of *rac*-pyroglutamic acid *rac*-**45** (20.0 g, 154.9 mmol, 1.0 eq) in MeOH (300 mL) at rt under Ar. The resulting solution was stirred and heated at reflux for 24 h. The mixture was then allowed to cool to rt and the solvent was evaporated under reduced pressure to give the crude methyl ester. Et₃N (23.8 mL, 170.4 mmol, 1.1 eq) was added to a stirred solution of the crude methyl ester in CH₂Cl₂ (5 mL) at rt under Ar. Then, a solution of Boc₂O (37.2 g, 170.4 mmol, 1.1 eq) and DMAP (1.892 g, 170.4 mmol, 1.1 eq) in CH₂Cl₂ (142 mL) were added dropwise. The resulting mixture was stirred at rt for 23 h. The solvent was evaporated under reduced pressure to give a wet solid. Saturated NH₄Cl_(aq) (80 mL) was added and the mixture was extracted with EtOAc (3 × 40 mL). The combined organic extracts were dried (MgSO₄) and evaporated under reduced pressure to give the crude product. Purification by flash column chromatography on silica with 4:1 hexane–EtOAc as eluent gave methyl ester **46** (28.5 g, 76%) as a pale yellow oil, *R*_F (1:1 hexane–EtOAc) 0.26; IR (ATR) 2980, 2878, 1789 (C=O, CO₂Me), 1746 (C=O), 1714 (C=O), 1369, 1256, 1146, 843, 729 cm⁻¹; ¹H NMR (400 MHz, CDCl₃) δ 4.60 (dd, *J* = 9.5, 3.0 Hz, 1H, NCH), 3.77 (s, 3H, OMe), 2.61 (ddd, *J* = 17.5, 10.0, 10.0 Hz, 1H, CH), 2.47 (ddd, *J* = 13.0, 10.0, 10.0 Hz, 1H, CH), 2.06–1.99 (m, 2H, CH), 1.47 (s, 9H, CMe₃); ¹³C NMR (101.6 MHz, CDCl₃) δ 173.2 (C=O), 171.8 (C=O), 149.2 (C=O, Boc), 83.6 (CMe₃), 58.8 (NCH), 52.5 (OMe), 31.1 (CH₂), 27.8 (CMe₃), 21.4 (CH₂); MS (ESI) *m/z* 266 [(M + Na)⁺, 100];

HRMS (ESI) m/z calcd for $C_{11}H_{17}NO_5$ (M + Na)⁺ 266.0999, found 266.0986 (+4.7 ppm error). Spectroscopic data consistent with those reported in the literature.⁵¹

Lab Book Reference: IC 2-22

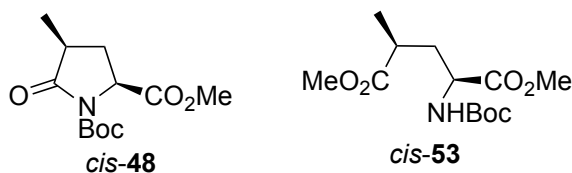
1-*tert*-Butyl 2-methyl 4-((dimethylamino)methylene)-5-oxopyrrolidine-1,2-dicarboxylate 47



tert-Butoxy bis(dimethylamino)methane (575 μ L, 2.79 mmol, 1.5 eq) was added to a stirred solution of methyl ester **46** (452 mg, 1.86 mmol, 1.0 eq) in DME (2 mL) at rt under Ar. The resulting solution was stirred and heated at reflux for 20 h. The solvent was then evaporated under reduced pressure. Hexane (200 mL) was added and the solids were removed by filtration through filter paper. The filtrate was evaporated under reduced pressure to give the enaminone **47** (453 mg, 82%) as yellow solid, mp 127-129 $^{\circ}$ C (lit., mp 124–127 $^{\circ}$ C⁶⁴) R_F (1:1 hexane–EtOAc) 0.01; IR (ATR) 2990, 2956, 2815, 1960, 1757 (C=O), 1740 (C=O), 1677 (C=O), 1607 (C=C), 1440, 1374, 1366, 1308, 1250, 1152, 1110, 1015, 843, 771, 737, 457 cm^{-1} ; ^1H NMR (400 MHz, CDCl_3) δ 7.11 (s, 1H, C=CH), 4.60 (dd, $J = 11.0, 4.0$ Hz, 1H, NCH), 3.73 (s, 3H, OMe), 3.23 (dd, $J = 14.0, 11.0$ Hz, 1H, CH) 3.00 (s, 6H, NMe_2), 2.87 (dd, $J = 14.0, 4.0$ Hz, 1H, CH), 1.47 (s, 9H, CMe_3). ^{13}C NMR (101.6 MHz, CDCl_3) δ 172.9 (C=O), 169.6 (C=O), 150.6 (C=O), 146.6 (NCH=C), 91.0 (NCH=C), 82.4 (CMe_3), 56.1 (NCH), 52.5 (OMe), 42.1 (CH_2), 28.2 (CMe_3), 26.4 (CH_2); MS (ESI) m/z 321 [(M + Na)⁺, 100], 299 [(M + H)⁺, 100]; HRMS (ESI) m/z calcd for $\text{C}_{14}\text{H}_{22}\text{N}_2\text{O}_5$ (M + Na)⁺ 321.1421, found 321.1413 (+2.0 ppm error). Spectroscopic data consistent with those reported in the literature.⁵¹

Lab Book Reference: IC/1/31

1-*tert*-Butyl 2-methyl 4-methyl-5-oxopyrrolidine-1,2-dicarboxylate *cis*-48 and dimethyl-*N*-*tert*-butoxycarbonyl-4-methylglutamate *cis*-53

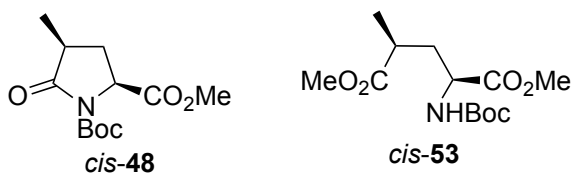


10% Pd/C (125 mg, 0.118 mmol, 0.14 eq) was added to a stirred solution of enaminone **47** (250 mg, 0.839 mmol, 1.0 eq) in MeOH (2 mL) at rt under Ar. Then, the reaction flask was evacuated under reduced pressure and back-filled with Ar three times. After a final evacuation, a balloon of H₂ was attached and the reaction mixture was stirred vigorously at rt under H₂ for 16 h. Then, the solids were removed by filtration through Celite[®] and washed with MeOH (20 mL). The filtrate was evaporated under reduced pressure to give the crude product. Purification by flash column chromatography on silica with 4:1 hexane–Et₂O as eluent gave methyl pyroglutamate *cis*-**48** (112 mg, 52%) as a pale yellow oil, *R*_F (4:1 hexane–EtOAc) 0.1; IR (ATR) 1759 (C=O, CO₂Me), 1678 (C=O, Boc), 1609 cm⁻¹; ¹H NMR (400 MHz, CDCl₃) δ 4.49 (dd, *J* = 4.5, 4.5 Hz, 1H, NCH), 3.77 (s, 3H, OMe), 2.67-2.49 (m, 2H, CH), 1.64-1.61 (m, 2H) 1.49 (s, 9H, CMe₃), 1.25 (d, *J* = 7.0 Hz, 1H, NCOCHMe); ¹³C NMR (101.6 MHz, CDCl₃) δ 175.8 (C=O), 172.2 (C=O), 149.6 (C=O, Boc), 83.8 (CMe₃), 57.5 (NCH), 52.7 (OMe), 37.7 (CHMe), 29.9 (CH₂), 28.0 (CMe₃), 16.3 (CHMe); MS (ESI) *m/z* 280 [(M + Na)⁺, 100]; HRMS (ESI) *m/z* calcd for C₁₂H₁₉NO₅ (M + Na)⁺ 280.1155, found 280.1145 (+3.2 ppm error) and dimethyl ester *cis*-**53** (101 mg, 47%) as a colourless oil, *R*_F (4:1 hexane–EtOAc) 0.2; IR (ATR) 3364 (NH), 2977, 1713 (C=O), 1514, 1437, 1366, 1158, 1061, 859, 780 cm⁻¹; ¹H NMR (400 MHz, CDCl₃) 4.98 (d, *J* = 9.0 Hz, 1H, NH), 4.32 (ddd, *J* = 9.0, 9.0, 5.0 Hz, 1H, NHCH), 3.70 (s, 3H, OMe), 3.64 (s, 3H, OMe), 2.54

(ddq, $J = 7.0, 7.0, 7.0$ Hz, 1H, *CHMe*), 2.00 (ddd, $J = 12.0, 8.0, 4.0$ Hz, 1H, CH), 1.89-1.83 (m, 1H, CH), 1.40 (s, 9H, CMe_3), 1.19 (d, $J = 8.0$ Hz, 3H, *NCOCHMe*); ^{13}C NMR (101.6 MHz, $CDCl_3$) δ 176.7 (C=O), 173.1 (C=O), 155.6 (C=O, Boc), 80.1 (CMe_3), 52.5 (OMe), 51.9 (OMe), 36.4 (CH), 36.0 (CH), 28.4 (CMe_3), 17.3 (*CHMe*); MS (ESI) m/z 312 [(M + Na) $^+$, 100]; HRMS (ESI) m/z calcd for $C_{13}H_{23}NO_6$ (M + Na) $^+$ 312.1418, found 312.1423 (-2.0 ppm error). Spectroscopic data consistent with those reported in the literature.^{51,54}

Lab Book Reference: IC 1-33

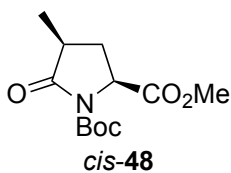
1-*tert*-Butyl 2-methyl 4-methyl-5-oxopyrrolidine-1,2-dicarboxylate *cis*-48 and dimethyl 2-((*tert*-butoxycarbonyl)amino)-4-methylpentanedioate *cis*-53



10% Pd/C (125 mg, 0.118 mmol, 0.14 eq) was added to a stirred solution of enaminone **47** (250 mg, 0.839 mmol, 1.0 eq) in MeOH (2 mL) at rt under Ar. Then, the reaction flask was evacuated under reduced pressure and back-filled with Ar three times. After a final evacuation, a balloon of H₂ was attached and the reaction mixture was stirred vigorously at rt under H₂ for 6 h. Then, the solids were removed by filtration through Celite[®] and washed with MeOH (20 mL). The filtrate was evaporated under reduced pressure to give the crude product. Purification by flash column chromatography on silica with 4:1 hexane–Et₂O as eluent gave methyl pyroglutamate *cis*-**48** (148 mg, 67%) as a pale yellow oil, *R_F* (4:1 hexane–EtOAc) 0.1, and dimethyl ester *cis*-**53** (24 mg, 10%) as a colourless oil, *R_F* (4:1 hexane–EtOAc) 0.2.

Lab Book Reference: IC 1-63

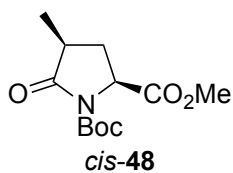
1-*tert*-Butyl 2-methyl 4-methyl-5-oxopyrrolidine-1,2-dicarboxylate *cis*-48



10% Pd/C (50 mg, 47.0 μmol , 0.14 eq) was added to a stirred solution of enaminone **47** (100 mg, 0.335 mmol, 1.0 eq) in *i*-PrOH–MeOH (2:1, 4 mL) at rt under Ar. Then, the reaction flask was evacuated under reduced pressure and back-filled with Ar three times. After a final evacuation, a balloon of H₂ was attached and the reaction mixture was stirred vigorously at rt under H₂ for 22 h. Then, solids were removed by filtration through Celite[®] and washed with *i*-PrOH (20 mL). The filtrate was evaporated under reduced pressure to give the crude product. Purification by flash column chromatography on silica with 4:1 hexane–Et₂O as eluent gave methyl pyroglutamate *cis*-**48** (45 mg, 74%) as a pale yellow oil, *R*_F (4:1 hexane–EtOAc) 0.1.

Lab Book Reference: IC 1-56

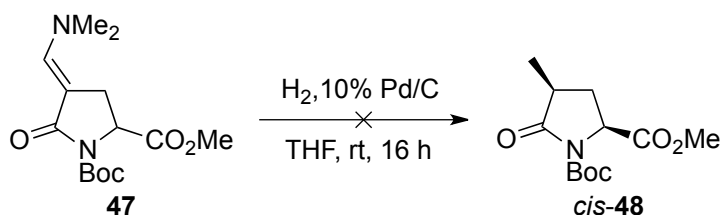
1-*tert*-Butyl 2-methyl 4-methyl-5-oxopyrrolidine-1,2-dicarboxylate *cis*-48



10% Pd/C (134.4 mg, 0.126 mmol, 0.05 eq) was added to a stirred solution of enaminone **47** (700 mg, 2.35 mmol, 1.0 eq) in *i*-PrOH (4 mL) at rt under Ar. Then, the reaction flask was evacuated under reduced pressure and back-filled with Ar three times. After a final evacuation, a balloon of H₂ was attached and the reaction mixture was stirred vigorously at rt under H₂ for 71 h. Then, the solids were removed by filtration through Celite[®] and washed with *i*-PrOH (20 mL). The filtrate was evaporated under reduced pressure to give the crude product. Purification by flash column chromatography on silica with 4:1 hexane–Et₂O as eluent gave methyl pyroglutamate *cis*-**48** (423 mg, 74%) as a pale yellow oil, *R*_F (4:1 hexane–EtOAc) 0.1.

Lab Book Reference: IC 2-21

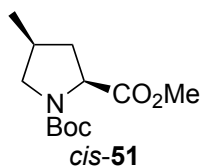
Attempted synthesis of 1-*tert*-butyl 2-methyl 4-methyl-5-oxopyrrolidine-1,2-dicarboxylate *cis*-48



10% Pd/C (125 mg, 0.118 mmol, 0.14 eq) was added to a stirred solution of enaminone **47** (250 mg, 0.839 mmol, 1.0 eq) in THF (2 mL) at rt under Ar. Then, the reaction flask was evacuated under reduced pressure and back-filled with Ar three times. After a final evacuation, a balloon of H₂ was attached and the reaction mixture was stirred vigorously at rt under H₂ for 16 h. Then, the solids were removed by filtration through Celite[®] and washed with MeOH (20 mL). The filtrate was evaporated under reduced pressure to give the crude product which contained none of the desired product (by ¹H NMR spectroscopy).

Lab Book Reference: IC 1-37

1-*tert*-Butyl 2-methyl 4-methylpyrrolidine-1,2-dicarboxylate *cis*-51

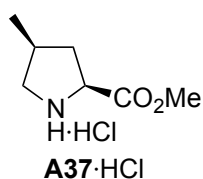


BH₃·DMS (0.49 mL of a 2 M solution in THF, 0.972 mmol) was added dropwise to a stirred solution of methyl pyroglutamate *cis*-48 (125 mg, 0.486 mmol, 1.0 eq.) in THF (4 mL) at rt under Ar. The resulting solution was stirred and heated at reflux for 9 h. The solvent was evaporated under reduced pressure to give a wet solid. EtOAc (20 mL) was added and washed with H₂O (20 mL). The aqueous layer was extracted with EtOAc (3 × 10 mL). The combined organic layers were dried (MgSO₄) and evaporated under reduced pressure to give the crude product. Purification by flash column chromatography on silica with 3:2 hexane–Et₂O as eluent gave methyl ester *cis*-51 (78 mg, 66%) as a pale yellow oil, *R*_F (1:1 hexane–EtOAc) 0.6; IR (ATR) 2977, 2931, 2851, 1742 (C=O, CO₂Me), 1694 (C=O, Boc), 1393, 1367, 1256, 1169, 994, 906 cm⁻¹; ¹H NMR (400 MHz, CDCl₃) (60:40 mixture of rotamers) δ 4.25 (dd, *J* = 8.0, 8.0 Hz, 0.4H, NCH), 4.19 (dd, *J* = 9.0, 8.0 Hz, 0.6H, NCH), 3.75–3.64 (m, 1H, NCH), 3.73 (s, 1.2H, OMe), 3.72 (s, 1.2H, OMe), 2.98 (dd, *J* = 10.0, 10.0 Hz, 1H, NCH), 2.38 (dddd, *J* = 19.0, 13.0, 6.0 Hz, 1H, CH), 2.29–2.15 (m, 1H, CH), 1.61–1.50 (m, 2H, CH), 1.45 (s, 3.6H, CMe₃), 1.40 (s, 5.4H, CMe₃), 1.06 (d, *J* = 6.5 Hz, 1.8H, CHMe), 1.04 (d, *J* = 6.5 Hz, 1.2H, CHMe); ¹³C NMR (101.6 MHz, CDCl₃) (rotamers) δ 173.9 (C=O), 173.7 (C=O), 154.3 (C=O, Boc), 153.6 (C=O, Boc), 79.9 (CMe₃), 79.9 (CMe₃), 59.8 (NCH), 59.3 (NCH), 53.8 (NCH₂), 53.3 (NCH₂), 52.2 (CHMe), 52.0 (CHMe), 39.0 (CH₂), 38.1 (CH₂), 33.3 (CH), 32.7 (CH), 28.5 (CMe₃), 28.3 (CMe₃), 17.07 (CHMe), 16.95 (CHMe); MS (ESI) *m/z* 266 [(M + Na)⁺, 100]; *m/z* calcd for C₁₂H₂₁NO₅ (M +

Na)⁺ 266.1363, found 266.1370 (−2.6 ppm error). Spectroscopic data consistent with those reported in the literature.⁵³

Lab Book Reference: IC 1-64

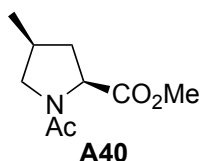
2-(Methoxycarbonyl)-4-methylpyrrolidin-1-ium chloride **A37**·HCl



Hydrogen chloride (1.78 mL of a 2.0 M solution in Et₂O, 3.563 mmol, 4.4 eq) was added dropwise to a stirred solution of methyl ester *cis*-**51** (2.44 g, 10.28 mmol, 1.0 eq) in Et₂O (20 mL) at rt under Ar. The resulting mixture was stirred and heated at reflux for 17 h. Then, the solvent was evaporated under reduced pressure to give the crude pyrrolidine salt **A37**·HCl (1.4 mg, 99%) as a brown oil, *R*_F (100:9:1 CH₂Cl₂–MeOH–NH₄OH_(aq)) 0.55; ¹H NMR (400 MHz, CD₃OD) δ 4.43 (dd, *J* = 10.0, 8.0 Hz, 1H, NCH), 3.84 (s, 3H, OMe), 3.48 (dd, *J* = 11.0, 8.0 Hz, 1H, CH₂), 2.88 (dd, *J* = 11.0, 8.0 Hz, 1H, CH), 2.61–2.54 (m, 1H, CH) 2.52–2.42 (m, 1H, CH), 1.72–1.65 (m, 1H, CH), 1.12 (d, *J* = 6.5 Hz, 3H, CHMe); ¹³C NMR (101.6 MHz, CD₃OD) δ 170.6 (C=O), 60.8 (NCH), 53.9 (NCH₂), 53.1 (OMe), 37.3 (CHMe), 34.4 (CH₂), 16.7 (CHMe).

Lab Book Reference: IC 1-75

Methyl 1-acetyl-4-methylpyrrolidine-2-carboxylate **A40**

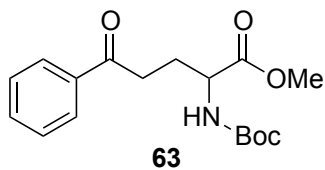


Acetyl chloride (0.24 mL, 3.340 mmol, 3.0 eq) was added dropwise to a stirred solution of the crude pyrrolidine salt **A37**·HCl (200 mg, 1.113 mmol, 1.0 eq) and Et₃N (0.47 mL, 3.340 mmol, 3.0 eq) in CH₂Cl₂ (1 mL) at rt under Ar. The resulting mixture was stirred at rt for 4 h. Water (20 mL) was added and the mixture was extracted with CH₂Cl₂ (3 × 20 mL). The combined organic extracts were dried (MgSO₄) and evaporated under reduced pressure to give the crude product. Purification by flash column chromatography with 10:1 CH₂Cl₂–MeOH as eluent gave the acetamide **A40** (175 mg, 85%) as a pale yellow oil, *R_F* (100:9:1 CH₂Cl₂–MeOH–NH₄OH_(aq)) 0.59; IR (ATR) 2957, 2875, 1740 (C=O, CO₂Me), 1644 (C=O acetamide), 1417, 1197, 1174, 1026, 877, 800, 626., 597, 504 cm⁻¹; ¹H NMR (400 MHz, CDCl₃) (80:20 mixture of rotamers) δ 4.35 (dd, *J* = 8.0, 8.0 Hz, 0.8H, NCH), 4.05 (dd, *J* = 8.0, 8.0 Hz, 0.2H, NCH), 3.77 (s, 2.4H, OMe), 3.76 (s, 0.6H, OMe), 3.72-3.66 (m, 1H, NCH), 3.18 (dd, *J* = 8.0, 8.0 Hz, 0.8H, NCH), 2.96 (dd, *J* = 8.0, 8.0 Hz, 0.2H, NCH), 2.44-2.30 (m, 2H, CH), 2.07 (s, 2.4H, C(O)Me), 1.93 (s, 0.6H, C(O)Me), 1.57-1.51 (m, 0.8H, CH), 1.29-1.25 (m, 0.2H, CH), 1.10 (d, *J* = 8.0 Hz, 2.4H, CHMe), 1.05 (d, *J* = 8.0 Hz, 0.6H, CHMe); ¹³C NMR (101.6 MHz, CDCl₃) (rotamers) δ 173.2 (C=O, CO₂Me), 173.1 (C=O, CO₂Me), 169.7 (C=O, Ac), 169.2 (C=O, Ac), 60.3 (NCH), 59.3 (NCH), 55.0 (OMe), 53.4 (NCH₂), 52.7 (NCH₂), 52.3 (NCH₂), 39.6 (CHMe), 37.6 (CHMe), 33.9 (CH₂), 31.9 (CH₂), 22.4 (Me, Ac), 21.4 (Me, Ac), 17.0 (CHMe); MS (ESI) *m/z* 208 [(M + Na)⁺, 100]; HRMS (ESI) *m/z* calcd for C₉H₁₅NO₃ (M + Na)⁺ 208.0944, found

208.0942 (−1.1 ppm error). Spectroscopic data consistent with those reported in the literature.⁴³

Lab Book Reference: IC 1-86

Methyl 2-((*tert*-butoxycarbonyl)amino)-5-oxo-5-phenylpentanoate **63**

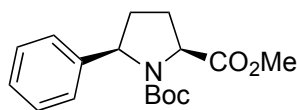


PhMgCl (0.822 mL of a 3.0 M solution in Et₂O, 2.466 mmol, 1.2 eq) was added dropwise to a stirred solution of pyroglutamate methyl ester **46** (500 mg, 2.055 mmol, 1.0 eq) in THF (6 mL) at –30 °C under Ar. The resulting mixture was stirred at rt for 30 h. Saturated NH₄Cl_(aq) (0.1 mL) was added the solvent was evaporated under reduced pressure to give a wet solid. The wet solid was dissolved in CH₂Cl₂–saturated NH₄Cl_(aq) (1:1, 16 mL) and extracted with CH₂Cl₂ (3 × 3 mL). The combined organic layers were washed with saturated NaHCO_{3(aq)} (8 mL), dried (MgSO₄) and evaporated pressure to give the crude product. Purification by flash column chromatography with 1:0-2:1 hexane–EtOAc as eluent keto ester **63** (502 mg, 76%) as a white solid. mp 83–86 °C (lit.,⁶⁵ 109 °C); *R*_F (1:1 hexane–EtOAc) 0.63; IR (ATR) cm^{–1} 3365 (NH), 2981, 2967, 2944, 2892, 1737 (C=O, CO₂Me), 1681 (C=O, COAr), 1670 (C=O, Boc), 1599, 1582, 1514, 1449, 1349, 1163, 1044, 888, 851, 740, 686, 558 cm^{–1}; ¹H NMR (400 MHz, CDCl₃) δ 7.95 (d, *J* = 7.5 Hz, 2H, Ph), 7.57 (t, *J* = 7.5 Hz, 1H, Ph), 7.46 (dd, *J* = 7.5, 7.5 Hz, 2H, Ph), 5.16 (d, *J* = 7.0 Hz, 1H, NH), 4.42–4.37 (m, NCH), 3.75 (s, 3H, OMe), 3.18–3.00 (m, 2H, CH), 2.36–2.27 (m, 1H, CH), 2.17–2.06 (m, 1H, CH), 1.42 (s, 9H, CMe₃); ¹³C NMR (101.6 MHz, CDCl₃) δ 199.0 (C=O, PhCO), 173.1 (C=O, CO₂Me), 155.6 (C=O, Boc), 136.8 (CH, *ipso*-Ph), 133.4 (Ph), 128.8 (Ph), 128.2 (Ph), 80.2 (CMe₃), 53.2 (OMe), 52.6 (NCH), 34.7 (CH₂), 28.4 (CMe₃), 27.1 (CH₂); MS (ESI) *m/z* 344 [(M + Na)⁺], 288 [(M – CMe₃)⁺]; HRMS (ESI) *m/z* calcd for C₁₇H₂₃NO₅ (M

+ Na)⁺ 344.1468, found 344.1463 (+1.0 ppm error). Spectroscopic data consistent with those reported in the literature.⁵⁶

Lab Book Reference: IC 1-9

1-*tert*-Butyl 2-methyl 5-phenylpyrrolidine-1,2-dicarboxylate *cis*-64



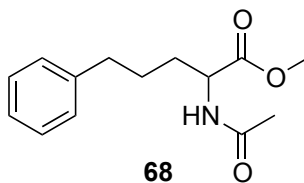
cis-64

TFA (0.95 mL, 12.45 mmol, 20 eq) was added to a stirred solution of keto ester **63** (200 mg, 0.6223 mmol 1.0 eq) in CH₂Cl₂ (6 mL) at rt under Ar. The resulting solution was stirred at rt for 20 h. The solvent was evaporated under reduced pressure to give an orange oil. CH₂Cl₂ (5 mL) was added to the orange oil and the solvent was evaporated under reduced pressure to give the crude product. The addition of CH₂Cl₂ and evaporation was repeated four more time to give the crude imine (298 mg) as an orange oil. NaBH₄ (44.72 mg, 1.182 mmol, 1.9 eq) was add portionwise to a stirred solution of the crude imine in MeOH (5 mL) at 0 °C under Ar. The resulting solution was stirred at rt for 21 h. The solvent was evaporated under reduced pressure. Then, MeOH (4 × 5 mL) was added and the and solvent was evaporated under reduced pressure to give the crude amine. The addition of MeOH and evaporation was repeated three more time to give the crude amine (330 mg). Boc₂O (204 mg, 0.9334 mmol, 1.5 eq), Et₃N (0.07 mL, 0.9334 mmol, 1.5eq) and DMAP (8 mg, 0.0622 mmol, 0.1 eq) were added to a stirred solution of the crude amine in CH₂Cl₂ (17 mL) at rt under Ar. The resulting mixture was stirred at rt for 65 h. Saturated NH₄Cl_(aq) (20 mL) was added and mixture was extracted with CH₂Cl₂ (3 × 20 mL). The combined organic extracts were dried (MgSO₄) and evaporated under reduced pressure to give the crude product. Purification by flash column chromatography on silica with 400:9:1 CH₂Cl₂–MeOH–NH₄OH_(aq) as eluent gave methyl ester *cis*-**64** (46 mg, 24%) as an orange oil, *R*_F (200:9:1 CH₂Cl₂–MeOH–NH₄OH_(aq)) 0.79; IR (ATR) 2952, 1732 (C=O), 1604, 1493, 1450, 1367, 1155, 1120, 912, 883, 756, 700, 545 cm⁻¹; ¹H NMR (400 MHz, CDCl₃)

(60:40 mixture of rotamers) δ 7.54 (d, $J = 7.5$ Hz, 2H, Ph), 7.32 (dd, $J = 7.5, 7.5$ Hz, 2H, Ph), 7.22 (t, $J = 7.5$ Hz, 1H, Ph), 4.99-4.97 (m, 0.4H, NCH), 4.74 (dd, 0.6H $J = 7.0, 7.0$ Hz, NCH), 4.49 (dd, $J = 8.0, 4.5$ Hz, 0.4H, CH), 4.35 (dd, $J = 7.5, 7.5$ Hz, 0.6H, CH), 3.81 (s, 3H, OMe), 2.36-2.28 (m, 1H, CH), 2.25-2.16 (m, 1H, CH), 2.11-1.92 (m, 2H, CH), 1.41 (s, 3.6H, CMe₃), 1.14 (s, 5.4H, CMe₃); MS (ESI) m/z 328 [(M + Na)⁺]; HRMS (ESI) m/z calcd for C₁₇H₂₃NO₄ (M + Na)⁺ 328.1519, found 328.1525 (+2.8 ppm error). Spectroscopic data consistent with those reported in the literature.⁵⁶

Lab Book Reference: IC 2-4

Methyl 2-acetamido-5-phenylpentanoate **68**

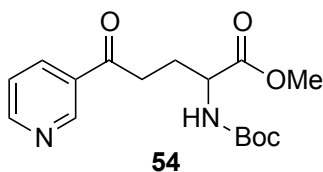


TFA (0.95 mL, 12.45 mmol, 20 eq) was added to a stirred solution of keto ester **63** (200 mg, 0.6223 mmol, 1.0 eq) in CH₂Cl₂ (6 mL) at rt under Ar. The resulting solution was stirred at rt for 20 h. The solvent was evaporated under reduced pressure to give an orange oil. CH₂Cl₂ (5 mL) was added to the orange oil and the solvent was evaporated under reduced pressure to give the crude product. The addition of CH₂Cl₂ and evaporation was repeated four more time to give the crude imine (294 mg) as an orange oil. 10% Pd/C (125 mg, 0.118 mmol, 0.08 eq) was added to a stirred solution of crude imine in *i*-PrOH (1 mL) at rt under Ar. Then, the reaction flask was evacuated under reduced pressure and back-filled with Ar three times. After a final evacuation, a balloon of H₂ was attached and the reaction mixture was stirred vigorously at rt under H₂ for 23 h. Then, the solids were removed by filtration through Celite[®] and washed with *i*-PrOH (10 mL). The filtrate was evaporated under reduced pressure to give the crude amine (198 mg). Ac₂O (0.18 mL, 1.867 mmol, 3.0 eq) and DMAP (23 mg, 0.1867 mmol, 0.1 eq) were added to a stirred solution of the crude amine in pyridine (0.15 mL, 1.867 mmol, 3.0 eq) at rt under Ar. The solution was stirred at rt for 2.5 h. Water (40 mL) was added and the mixture was extracted with CH₂Cl₂ (3 × 10 mL). The combined organic extracts were dried (MgSO₄) and evaporated under reduced pressure to give the crude product. Purification by flash column chromatography on silica with 100:9:1 CH₂Cl₂-MeOH-NH₄OH_(aq) as eluent gave acetamide **68** (100 mg, 65%) as an orange oil, *R*_F (100:9:1 CH₂Cl₂-MeOH-NH₄OH_(aq)) 0.43; IR (ATR) 3281

(NH), 3027, 2951, 2861, 1741 (C=O, CO₂Me), 1652 (C=O, acetamide), 1543, 1436, 1373, 1207, 1169, 1127, 1030, 735, 699, 593, 524, 495 cm⁻¹; ¹H NMR (400 MHz, CDCl₃) δ 7.28 (dd, *J* = 7.5, 7.5 Hz, 2H, Ph), 7.19 (d, *J* = 7.5 Hz, 1H, Ph), 7.15 (d, *J* = 7.5 Hz, 2H, Ph), 5.94 (br d, *J* = 8.0 Hz, 1H, NH), 4.67-4.62 (m, 1H, NCH), 3.73 (s, 3H, OMe), 2.69-2.56 (m, 2H, ArCH₂), 2.01 (s, 3H, C(O)Me), 1.91-1.85 (m, 1H, CH), 1.71-1.66 (m, 2H, CH); ¹³C NMR (101.6 MHz, CDCl₃) δ 173.2 (C=O, CO₂Me), 169.9 (C=O, acetamide), 141.7 (*ispo*-Ph), 128.5 (Ph), 126.1 (Ph), 52.6 (NCH), 52.1 (OMe), 29.9 (CH₂), 27.7 (CH₂), 23.4 (C(O)Me); MS (ESI) *m/z* 272 [(M + Na)⁺]; HRMS (ESI) *m/z* calcd for C₁₄H₁₉NO₃ (M + Na)⁺ 272.1257, found 272.1249 (+2.9 ppm error). Spectroscopic data consistent with those reported in the literature.⁵⁸

Lab Book Reference: IC 2-15

Methyl 2-((*tert*-butoxycarbonyl)amino)-5-oxo-5-(pyridin-3-yl)pentanoate **54**

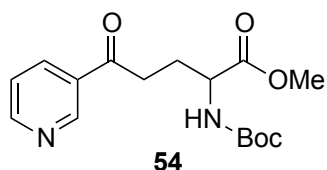


A solution of 3-bromopyridine (223 μL , 2.261 mmol, 1.1 eq) in Et_2O (1.73 mL) was added dropwise to a stirred solution of *n*-BuLi (1.13 mL of a 2 M solution in hexane, 2.261 mmol, 1.1 eq) in Et_2O (5.1 mL) at -78°C under Ar. The resulting yellow slurry was stirred at -78°C for 30 min. Then, a solution of pyroglutamate methyl ester **46** (500 mg, 2.055 mmol, 1.0 eq) in THF– Et_2O (1:1, 2.88 mL) was added dropwise. The resulting mixture was stirred at -78°C for 1 h. The reaction mixture was poured into H_2O (5 mL) and extracted with Et_2O (3×5 mL). The combined organic layers were dried (MgSO_4) and evaporated under reduced pressure to give the crude product. Purification by flash column chromatography on silica with 7:3 CH_2Cl_2 – EtOAc as eluent gave keto ester **54** (119 mg, 18%) as a white solid, mp 86 – 92°C (lit.,⁵⁵ 90 – 92°C); R_F (200:9:1 CH_2Cl_2 – MeOH – $\text{NH}_4\text{OH}_{(\text{aq})}$) 0.43; IR (ATR) 3230 (NH), 3006, 2984, 2951, 1749, (C=O, CO_2Me), 1699 (C=O, COAr), 1682 (C=O, Boc), 1588, 1539, 1364, 1303, 1160, 1012, 979, 700 cm^{-1} ; ^1H NMR (400 MHz, CDCl_3) δ 9.16 (d, $J = 2.0$ Hz, 1H, CH, Ar), 8.79 (d, $J = 4.0$ Hz, 1H, Ar), 8.22 (br d, $J = 8.0$ Hz, 1H, Ar), 7.42 (dd, $J = 8.0, 4.0$ Hz, 1H, Ar), 5.15 (d, $J = 7.5$ Hz, 1H, NH), 4.43–4.38 (m, 1H, NCH), 3.76 (s, 3H, OMe), 3.20–3.02 (m, 2H, CH), 2.37–2.35 (m, 1H, CH), 2.12–2.03 (m, 1H, CH), 1.40 (s, 9H, CMe_3); ^{13}C NMR (101.6 MHz, CDCl_3) δ 197.8 (C=O, COAr), 172.9 (C=O, CO_2Me), 153.7 (C=O, Boc), 149.7 (Ar), 135.5 (Ar), 132.4 (*ipso*-Ar), 123.8 (Ar), 80.3 (CMe_3), 52.9 (OMe), 52.6 (CH), 34.9 (CH_2), 28.4 (CMe_3), 26.9 (CH_2); MS (ESI) m/z 345 [(M + Na)⁺], 323 [(M + H)⁺]; HRMS (ESI) m/z calcd for $\text{C}_{17}\text{H}_{23}\text{NO}_5$ (M + Na)⁺

345.1421, found 345.1412 (+2.7 ppm error). Spectroscopic data consistent with those reported in the literature.⁵⁵

Lab Book Reference: IC 2-31

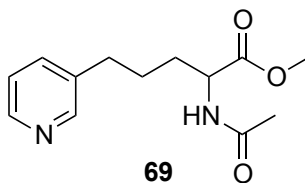
Methyl 2-((tert-butoxycarbonyl)amino)-5-oxo-5-(pyridin-3-yl)pentanoate **54**



A solution of 3-bromopyridine (3.24 mL, 33.68 mmol, 2.2 eq) in Et₂O (16 mL) was added dropwise to a stirred solution of *n*-BuLi (21.05 mL of a 1.6 M solution in hexane, 33.68 mmol, 2.2 eq) in Et₂O (40 mL) at -78 °C under Ar. The resulting yellow slurry was stirred at -78 °C for 30 min. Then, a solution of pyroglutamate methyl ester **46** (3.724 g, 15.31 mmol, 1.0 eq) in THF-Et₂O (1:1, 18.3 mL) was added dropwise. The resulting mixture was stirred at -78 °C for 1 h. The reaction mixture was poured into H₂O (35 mL) and extracted with Et₂O (3 × 35 mL). The combined organic layers were dried (MgSO₄) and evaporated under reduced pressure to give the crude product. Purification by flash column chromatography on silica with 7:3 CH₂Cl₂-EtOAc as eluent gave keto ester **53** (1.028 g, 21%) as a white solid.

Lab Book Reference: IC 2-41

Methyl 2-acetamido-5-(pyridin-3-yl)pentanoate **69**



TFA (2.38 mL, 31.02 mmol, 20 eq) was added to a stirred solution of keto ester **54** (500 mg, 1.551 mmol, 1.0 eq) in CH₂Cl₂ (16 mL) at rt under Ar. The resulting solution was stirred at rt for 3.5 h. The solvent was evaporated under reduced pressure to give an orange oil. CH₂Cl₂ (16 mL) was added to the orange oil and the solvent was evaporated under reduced pressure to give the crude product. The addition of CH₂Cl₂ and evaporation was repeated four more time to give the crude imine (780 mg) as an orange oil. 10% Pd/C (394 mg, 3.704 mmol, 1.07 eq) was added to a stirred solution of crude imine in *i*-PrOH (21 mL) at rt under Ar. Then, the reaction flask was evacuated under reduced pressure and back-filled with Ar three times. After a final evacuation, a balloon of H₂ was attached and the reaction mixture was stirred vigorously at rt under H₂ for 5.3 h. Then, the solids were removed by filtration through Celite[®] and washed with *i*-PrOH (16 mL). The filtrate was evaporated under reduced pressure to give the crude amine (520 mg). Ac₂O (0.72 mL, 7.608 mmol, 3.0 eq) and DMAP (3.1 mg, 0.0254 mmol, 0.1 eq) were added to a stirred solution of the crude amine in pyridine (1.9 mL) at rt under Ar. The solution was stirred at rt for 7 h. Water (30 mL) was added and the mixture was extracted with CH₂Cl₂ (3 × 40 mL). The combined organic extracts were dried (MgSO₄) and evaporated under reduced pressure to give the crude product. Purification by flash column chromatography on silica with 100:9:1 CH₂Cl₂-MeOH-NH₄OH_(aq) as eluent gave acetamide **69** (100 mg, 65%) as an orange oil. *R*_F (100:9:1 CH₂Cl₂-MeOH-NH₄OH_(aq)) 0.43; IR (ATR) 3281 (NH), 3027,

2951, 2861, 1741 (C=O, CO₂Me), 1652 (C=O, acetamide), 1543, 1497, 1436, 1373, 1267, 1207, 1169, 1127, 1030, 735, 699, 593, 524, 495 cm⁻¹; ¹H NMR (400 MHz, CDCl₃) δ 8.41-8.38 (m, 2H, CH, Ar), 7.45 (d, *J* = 8.0 Hz, 1H, Ar), 7.19 (dd, *J* = 8.0, 5.0 Hz, 1H, Ar), 6.39-6.24 (m, 1H, NH), 4.65-4.55 (m, 1H, NCH), 3.70 (s, 3H, OMe), 2.73-2.54 (m, 2H, CH₂), 2.00 (s, 3H, C(O)Me), 2.90-1.76 (m, 2H, CH₂); ¹³C NMR (101.6 MHz, CDCl₃) δ 173.1 (C=O, CO₂Me), 170.0 (C=O, acetamide), 149.8 (Ar), 147.5 (Ar), 137.0 (Ar), 136.0 (*ipso*-Ar), 123.5 (Ar), 52.6 (OMe), 51.9 (NCH), 32.5 (CH₂), 32.3 (CH₂), 26.9 (CH₂), 23.2 (C(O)Me); MS (ESI) *m/z* 251 [(M + H)⁺]; HRMS (ESI) *m/z* calcd for C₁₃H₁₈N₂O₃ (M + H)⁺ 251.1390, found 251.1387 (+1.3 ppm error).

Lab Book Reference: IC 2-42

Abbreviations

Ac	Acetyl
ALARM	A la assay to detect reactive molecules
Aq	Aqueous
Ar	Aromatic ring
ATP	Adenosine triphosphate
BACE1	Beta-secretase 1
Br	Broad
B-Raf	v-Raf murine sarcoma viral oncogene homolog B
ChoK α	Choline Kinase
cIAP1	Cellular inhibitor of apoptosis protein-1
cm ⁻¹	Wavenumber
CS	Preclinical candidate selection
CSK	C-Src Tyrosine Kinase
d	Doublet
Da	Dalton
DMAP	4-Dimethylaminopyridine
DME	Dimethoxyethane
DMSO	Dimethylsulfoxide
DOS	Diversity oriented synthesis
Eq	Equivalents
ESI	Electrospray ionisation
Et ₂ O	Diethyl ether
EtOAc	Ethyl acetate

FBDD	Fragment-based drug discovery
FBLG	Fragment-based lead generation
FBS	Fragment-based screening
FDA	Food and drug administration
FGFR1	Fibroblast growth factor receptor 1
FL	Fragment library
Fsp ³	Fraction sp ³
FTIH	first time in human
g	Gram(s)
h	Hour(s)
H bond	Hydrogen bond
HAC	Heavy atom count
HBD	Hydrogen bond donor(s)
HBA	Hydrogen bond acceptor(s)
HCHO	Formaldehyde
HRMS	High resolution mass spectrometry
HTS	High throughput screening
Hz	Hertz
IAP	Inhibitor of apoptosis
<i>i</i> -PrOH	Isopropyl alcohol
J	Coupling constant in Hz
kcal mol ⁻¹	Kilocalories per mole
LC-MS	Liquid chromatography–mass spectrometry
LE	Ligand efficiency

LHMDS	Lithium bis(trimethylsilyl)amide
m	Multiplet
M	Molar
<i>m/z</i>	Mass to charge ratio
M+	Molecular ion
Me	Methyl
mg	Milligrams
μM	Micromolar
mL	Millilitre(s)
mmol	Millimole(s)
μmol	Micromole(s)
MMP-13	Matrix metalloproteinase 13
MS	Mass spectrometry
Ms	Sulfonamide
MW	Molecular weight
NaHMDS	Sodium bis(trimethylsilyl)amide
nM	Nanomolar
NMR	Nuclear Magnetic Resonance
NPR	Normalised PMI ratio
NROT(s)	Number of rotational bond(s)
P1	Phase 1
P2	Phase 2
PAINS	Pan-assay interference compounds
PBF	Plane of Best Fit

Pd/C	Palladium on carbon
Ph	Phenyl
PIM1	Proto-oncogene serine/threonine-protein kinase
PMI	Principal moment of inertia
POC	Proof-of-concept trials
PPI	Protein-protein interaction
ppm	Parts per million
PSA	Polar surface area
Py	Pyridine
q	Quartet
RF	Retention Factor
rt	Room temperature
t	Triplet
TBAF	Tetra- <i>n</i> -butylammonium
TBDMSCl	<i>tert</i> -Butyldimethylsilyl chloride
TEMPO	(2,2,6,6-Tetramethylpiperidin-1-yl)oxyl
TFA	Trifluoroacetic acid
THF	Tetrahydrofuran
s	Singlet
SAR	Structure-activity relationships
SMILES	Simplified molecular-input line-entry system
SPR	Surface plasmon resonance
XIAP	X-linked inhibitor of apoptosis protein

References

- (1) Rees, D. C.; Rees, D. C.; Congreve, M.; Congreve, M.; Murray, C. W.; Murray, C. W.; Carr, R.; Carr, R. *Nat. Rev. Drug Discov.* **2004**, *3*, 660.
- (2) Carr, R. A. E.; Congreve, M.; Murray, C. W.; Rees, D. C. *Drug Discov. Today* **2005**, *10*, 987.
- (3) Murray, C. W.; Rees, D. C. *Nat. Chem.* **2009**, *1*, 187.
- (4) Erlanson, D. A.; Fesik, S. W.; Hubbard, R. E.; Jahnke, W.; Jhoti, H. *Nat. Rev. Drug Discov.* **2016**, *15*, 605.
- (5) Bollag, G.; Hirth, P.; Tsai, J.; Zhang, J.; Ibrahim, P. N.; Cho, H.; Spevak, W.; Zhang, C.; Zhang, Y.; Habets, G.; Burton, E. A.; Wong, B.; Tsang, G.; West, B. L.; Powell, B.; Shellooe, R.; Marimuthu, A.; Nguyen, H.; Zhang, K. Y. J.; Artis, D. R.; Schlessinger, J.; Su, F.; Higgins, B.; Iyer, R.; D'Andrea, K.; Koehler, A.; Stumm, M.; Lin, P. S.; Lee, R. J.; Grippo, J.; Puzanov, I.; Kim, K. B.; Ribas, A.; McArthur, G. A.; Sosman, J. A.; Chapman, P. B.; Flaherty, K. T.; Xu, X.; Nathanson, K. L.; Nolop, K. *Nature* **2010**, *467*, 596.
- (6) Souers, A. J.; Levenson, J. D.; Boghaert, E. R.; Ackler, S. L.; Catron, N. D.; Chen, J.; Dayton, B. D.; Ding, H.; Enschede, S. H.; Fairbrother, W. J.; Huang, D. C. S.; Hymowitz, S. G.; Jin, S.; Khaw, S. L.; Kovar, P. J.; Lam, L. T.; Lee, J.; Maecker, H. L.; Marsh, K. C.; Mason, K. D.; Mitten, M. J.; Nimmer, P. M.; Oleksijew, A.; Park, C. H.; Park, C.-M.; Phillips, D. C.; Roberts, A. W.; Sampath, D.; Seymour, J. F.; Smith, M. L.; Sullivan, G. M.; Tahir, S. K.; Tse, C.; Wendt, M. D.; Xiao, Y.; Xue, J. C.; Zhang, H.; Humerickhouse, R. a; Rosenberg, S. H.; Elmore, S. W. *Nat. Med.* **2013**, *19*, 202.
- (7) Zech, S. G.; Kohlmann, A.; Zhou, T.; Li, F.; Squillace, R. M.; Parillon, L. E.;

- Greenfield, M. T.; Miller, D. P.; Qi, J.; Thomas, R. M.; Wang, Y.; Xu, Y.; Miret, J. J.; Shakespeare, W. C.; Zhu, X.; Dalgarno, D. C. *J. Med. Chem.* **2016**, *59*, 671.
- (8) Taylor, S. J.; Abeywardane, A.; Liang, S.; Muegge, I.; Padyana, A. K.; Xiong, Z.; Hill-Drzewi, M.; Farmer, B.; Li, X.; Collins, B.; Li, J. X.; Heim-Riether, A.; Proudfoot, J.; Zhang, Q.; Goldberg, D.; Zuvela-Jelaska, L.; Zaher, H.; Li, J.; Farrow, N. A. *J. Med. Chem.* **2011**, *54*, 8174.
- (9) Winneroski, L. L.; Schiffler, M. A.; Erickson, J. A.; May, P. C.; Monk, S. A.; Timm, D. E.; Audia, J. E.; Beck, J. P.; Boggs, L. N.; Borders, A. R.; Boyer, R. D.; Brier, R. A.; Hudziak, K. J.; Klimkowski, V. J.; Garcia Losada, P.; Mathes, B. M.; Stout, S. L.; Watson, B. M.; Mergott, D. J. *Bioorg. Med. Chem.* **2015**, *23*, 3260.
- (10) Hann, M. M.; Leach, A. R.; Harper, G. *J. Chem. Inf. Comput. Sci.* **2001**, *41*, 856.
- (11) Leach, A. R.; Hann, M. M. *Current Opinion in Chemical Biology*. 2011, pp 489–496.
- (12) Fink, T.; Raymond, J. L. *J. Chem. Inf. Model.* **2007**, *47*, 342.
- (13) Fischer, M.; Hubbard, R. E. *Mol. Interv.* **2009**, *9*, 22.
- (14) Murray, C. W.; Rees, D. C. *Angew. Chemie - Int. Ed.* **2016**, *55*, 488.
- (15) Park, Sheldon; Mann, Jasdeep; Li, N. *Chem. Eng. Process Tech.* **2013**, 1004.
- (16) Lipinski, C. a; Lombardo, F.; Dominy, B. W.; Feeney, P. J. *Adv. Drug Deliv. Rev.* **1997**, *23*, 3.
- (17) Congreve, M.; Carr, R.; Murray, C.; Jhoti, H. *Drug Discov. Today* **2003**, *8*, 876.

- (18) Baell, J.; Walters, M. A. *Nature* **2014**, *513*, 481.
- (19) Baell, J. B.; Holloway, G. A. *J. Med. Chem.* **2010**, *53*, 2719.
- (20) Mashalidis, E. H.; Śledź, P.; Lang, S.; Abell, C. *Nat. Protoc.* **2013**, *8*, 2309.
- (21) Huth, J. R.; Mendoza, R.; Olejniczak, E. T.; Johnson, R. W.; Cothron, D. A.; Liu, Y.; Lerner, C. G.; Chen, J.; Hajduk, P. J. *J. Am. Chem. Soc.* **2005**, *127*, 217.
- (22) Seidler, J.; McGovern, S. L.; Doman, T. N.; Shoichet, B. K. *J. Med. Chem.* **2003**, *46*, 4477.
- (23) Bollag, G.; Tsai, J.; Zhang, J.; Zhang, C.; Ibrahim, P.; Nolop, K.; Hirth, P. *Nat. Rev. Drug Discov.* **2012**, *11*, 873.
- (24) Tsai, J.; Lee, J. T.; Wang, W.; Zhang, J.; Cho, H.; Mamo, S.; Bremer, R.; Gillette, S.; Kong, J.; Haass, N. K.; Sproesser, K.; Li, L.; Smalley, K. S. M.; Fong, D.; Zhu, Y.-L.; Marimuthu, A.; Nguyen, H.; Lam, B.; Liu, J.; Cheung, I.; Rice, J.; Suzuki, Y.; Luu, C.; Settachatgul, C.; Shellooe, R.; Cantwell, J.; Kim, S.-H.; Schlessinger, J.; Zhang, K. Y. J.; West, B. L.; Powell, B.; Habets, G.; Zhang, C.; Ibrahim, P. N.; Hirth, P.; Artis, D. R.; Herlyn, M.; Bollag, G. *Proc. Natl. Acad. Sci. U. S. A.* **2008**, *105*, 3041.
- (25) Chessari, G.; Buck, I. M.; Day, J. E. H.; Day, P. J.; Iqbal, A.; Johnson, C. N.; Lewis, E. J.; Martins, V.; Miller, D.; Reader, M.; Rees, D. C.; Rich, S. J.; Tamanini, E.; Vitorino, M.; Ward, G. A.; Williams, P. A.; Williams, G.; Wilsher, N. E.; Woolford, A. J. A. *J. Med. Chem.* **2015**, *58*, 6574.
- (26) Lovering, F.; Bikker, J.; Humblet, C. *J. Med. Chem.* **2009**, *52*, 6752.
- (27) Ritchie, T. J.; Macdonald, S. J. F. *Drug Discov. Today* **2009**, *14*, 1011.
- (28) Aldeghi, M.; Malhotra, S.; Selwood, D. L.; Chan, A. W. E. *Chem. Biol. Drug*

- Des.* **2014**, *83*, 450.
- (29) Meyer, a Y. *J. Comput. Chem.* **1986**, *7*, 144.
- (30) Sauer, W. H. B.; Schwarz, M. K. *J. Chem. Inf. Comput. Sci.* **2003**, *43*, 987.
- (31) Firth, N. C.; Brown, N.; Blagg, J. J. *J. Chem. Inf. Model.* **2012**, *52*, 2516.
- (32) Beckmann, H. S. G.; Nie, F.; Hagerman, C. E.; Johansson, H.; Tan, Y. S.; Wilcke, D.; Spring, D. R. *Nat. Chem.* **2013**, *5*, 861.
- (33) Hajduk, P. J.; Galloway, W. R. J. D.; Spring, D. R. *Nature* **2011**, *470*, 42.
- (34) Galloway, W. R. J. D.; Isidro-Llobet, A.; Spring, D. R. *Nat. Commun.* **2010**, *1*, 1.
- (35) Hung, A. W.; Ramek, A.; Wang, Y.; Kaya, T.; Wilson, J. A.; Clemons, P. A.; Young, D. W. *Proc. Natl. Acad. Sci.* **2011**, *108*, 6799.
- (36) Morley, A. D.; Pugliese, A.; Birchall, K.; Bower, J.; Brennan, P.; Brown, N.; Chapman, T.; Drysdale, M.; Gilbert, I. H.; Hoelder, S.; Jordan, A.; Ley, S. V.; Merritt, A.; Miller, D.; Swarbrick, M. E.; Wyatt, P. G. *Drug Discov. Today* **2013**, *18*, 1221.
- (37) Tran, N. C.; Dhondt, H.; Flipo, M.; Deprez, B.; Willand, N. *Tetrahedron Lett.* **2015**, *56*, 4119.
- (38) Fuller, N.; Spadola, L.; Cowen, S.; Patel, J.; Schönherr, H.; Cao, Q.; McKenzie, A.; Edfeldt, F.; Rabow, A.; Goodnow, R. *Drug Discov. Today* **2016**, *21*, 1272.
- (39) Kelleher, F.; Kelly, S.; Watts, J.; McKee, V. *Tetrahedron* **2010**, *66*, 3525.
- (40) Kelleher, F.; Kelly, S.; McKee, V. *Tetrahedron* **2007**, *63*, 9235.
- (41) Confalone, P. N.; Huie, E. M.; Ko, S. S.; Cole, G. M. *J. Org. Chem.* **1988**, *53*, 482.

- (42) Vakarov, S. A.; Gruzdev, D. A.; Chulakov, E. N.; Sadretdinova, L. S.; Ezhikova, M. A.; Kodess, M. I.; Levit, G. L.; Krasnov, V. P. *Chem. Heterocycl. Compd.* **2014**, *50*, 838.
- (43) Hinderaker, M. M. P.; Raines, R. T. R. *Protein Sci.* **2003**, *12*, 1188.
- (44) Seebach, D.; Schweizer, W. B. *J. Am. Chem. Soc.* **1983**, *105*, 5390.
- (45) Su, B.; Deng, M.; Wang, Q. *European J. Org. Chem.* **2013**, *1*, 1979.
- (46) Ege, M.; Wanner, K. T. *Org. Lett.* **2004**, *6*, 3553.
- (47) Aurelio, L.; Box, J. S.; Brownlee, R. T. C.; Hughes, A. B.; Sleeb, M. M. *J. Org. Chem.* **2003**, *68*, 2652.
- (48) Yempalla, K. R.; Munagala, G.; Singh, S.; Magotra, A.; Kumar, S.; Rajput, V. S.; Bharate, S. S.; Tikoo, M.; Singh, G. D.; Khan, I. A.; Vishwakarma, R. A.; Singh, P. P. *ACS Med. Chem. Lett.* **2015**, *6*, 1041.
- (49) Del Valle, J. R.; Goodman, M. *J. Org. Chem.* **2003**, *68*, 3923.
- (50) Shoulders, M. D.; Hodges, J. A.; Raines, R. T. *J. Am. Chem. Soc.* **2006**, *128*, 8112.
- (51) Coudert, E.; Acher, F.; Azerad, R. *Synthesis* **1997**, *1997*, 863.
- (52) Gu, Z.-Q.; Li, M. *Tetrahedron Lett.* **2003**, *44*, 3203.
- (53) Belema, M.; Hewawasam, P. Google Patents 2012.
- (54) Ardá, A.; G. Soengas, R.; Nieto, M. I.; Jiménez, C.; Rodríguez, J. *Org. Lett.* **2008**, *10*, 2175.
- (55) Xu, Y.; Choi, J.; Isabel Calaza, M.; Turner, S.; Rapoport, H. *J. Org. Chem.* **1999**, *64*, 4069.
- (56) Scharnagel, D.; Prause, F.; Kaldun, J.; Haase, R. G.; Breuning, M. *Chem. Commun. (Camb)*. **2014**, *50*, 6623.

- (57) Banfi, L.; Basso, A.; Guanti, G.; Riva, R. *Tetrahedron* **2006**, *62*, 4331.
- (58) Elaridi, J.; Patel, J.; Jackson, W. R.; Robinson, A. J. *J. Org. Chem.* **2006**, *71*, 7538.
- (59) Sheikh, N. S.; Leonori, D.; Barker, G.; Firth, J. D.; Campos, K. R.; Meijer, A. J. H. M.; O'Brien, P.; Coldham, I. *J. Am. Chem. Soc.* **2012**, *134*, 5300.
- (60) En, D.; Zou, G. F.; Guo, Y.; Liao, W. W. *J. Org. Chem.* **2014**, *79*, 4456.
- (61) Saito, Y.; Ouchi, H.; Takahata, H. *Tetrahedron* **2006**, *62*, 11599.
- (62) Ness, K. A.; Eddie, S. L.; Higgins, C. A.; Templeman, A.; D'Costa, Z.; Gaddale, K. K. D.; Bouzzaoui, S.; Jordan, L.; Janssen, D.; Harrison, T.; Burkamp, F.; Young, A.; Burden, R.; Scott, C. J.; Mullan, P. B.; Williams, R. *Bioorg. Med. Chem. Lett.* **2015**, *25*, 5642.
- (63) Lewis, A.; Ryan, D.; Gani, D. *J. Chem. Soc., Perkin Trans. 1* **1998**, 3767.
- (64) Dieterich, P.; Young, D. W. *Org. Biomol. Chem.* **2006**, *4*, 1492.
- (65) Van Esseveldt, B. C. J.; Van Delft, F. L.; De Gelder, R.; Rutjes, F. P. J. T. *Org. Lett.* **2003**, *5*, 1717.